UNIVERSITY OF NAPLES FEDERICO II

SCHOOL OF MATHEMATICS, PHYSICS AND NATURAL SCIENCES

PHD IN CHEMICAL SCIENCES, CYCLE XXV

ZIEGLER-NATTA CATALYSTS: MECHANISTIC STUDY *VIA* HIGH THROUGHPUT SCREENING METHODOLOGIES

LUCA RONGO

SUPERVISOR

PROF. VINCENZO BUSICO

ASSESSOR

PROF. GIOVANNI TALARICO

COORDINATOR

PROF. LUCIO PREVITERA

Table of contents

Chapter 1. General Introduction

1.1. Scope and Objectives

The industrial production of isotactic polypropylene (iPP) based materials, including the homopolymer, 'random' copolymers, and reactor blends of homopolymer and ethylene/propylene 'rubber' ('impact' PP), has more than doubled in the last 10 years, from about 25 Mt/y in 2000 to over 50 Mt/y in 2010 (Figure 1.1).[1] Behind this extraordinary performance there was no step change in science or technology, but 'just' a steady and patient day-by-day improvement, that is the kind of progress that in too many occasions nowadays is arrogantly labeled as 'incremental', and taken as an indication of maturity (an antonym of 'innovation'). As a matter of fact, the more iPP comes out of the plants, the less academia looks at how to make it better as something worthy of further research, and the leading scientific journals a subject of interest to their 'broad readership'.

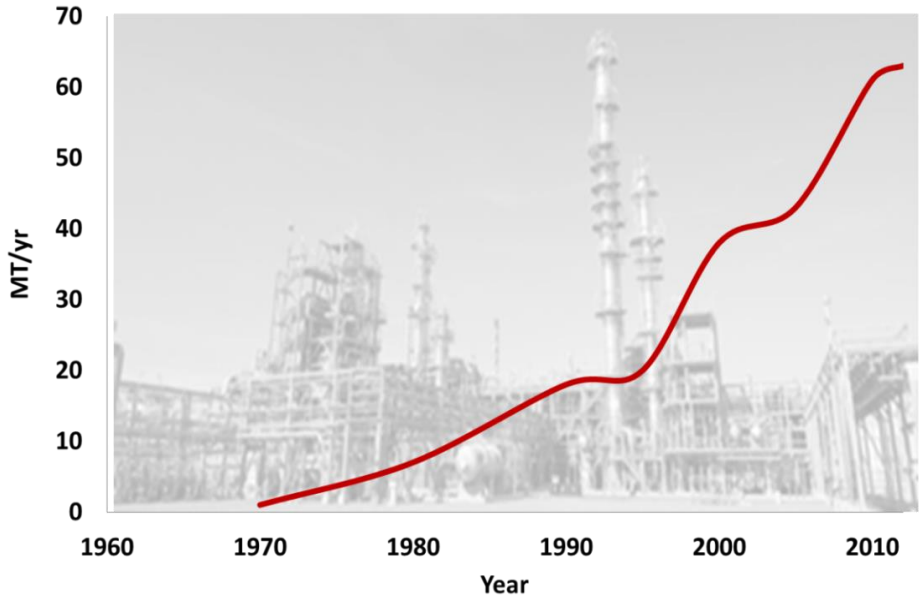

Figure 1.1. Global installed production capacity of iPP based materials (1970-2012).[1]

Our view is different, and in fact this thesis is a re-visitation of industrial High-Yield Ziegler-Natta catalysts (HY-ZNCs) for iPP[2,3], with focus on their structure, and the thermodynamic and kinetic aspects of their chemical reactivity. The general aim was to improve the understanding of, and

control over, active site structure and behavior. The main asset for the latter objective was the use of proper electron donor (Lewis base, LB) molecules, adsorbing on the active surfaces and playing the function that in molecular catalysis pertains to the ancillary ligand(s). Industry has been working on that for decades, primarily with a trial-and-error approach[2,3]; an important element of novelty of this thesis is that we wanted to hit the target 'by design', that is through the use of predictive models (albeit not necessarily of 'white-box' type).

Unquestionably, there is an elegant beauty in molecular propene polymerization catalysts[4] that no heterogeneous ZN system can exhibit as yet. The precise design of an ancillary ligand framework 'dressing' a transition metal center in view of a specific function, which is at the heart of the concept of tailor-made polymers[5], is thus far unique to metallocene[4] and post-metallocene[5] catalytic species. On the other hand, elegant and beautiful creations are often delicate and demanding as well, which are not the most obvious qualifications for a heavy-duty job. In fact, for catalysts like for humans, haute-couture and prêt-a-porter –not to speak of tech-wear– are different worlds in practically all respects. Continuing with the metaphor, it should be rather obvious that there is no conflict between such worlds, each offering opportunities and challenges, but also that the idea to convert all of them into a single one (which in the case of iPP found some credit in the 1990s) is –euphemistically– naïve, as Figure 1.2 (showing 2005 data which are still representative of the present-day situation[6]) clearly demonstrates.

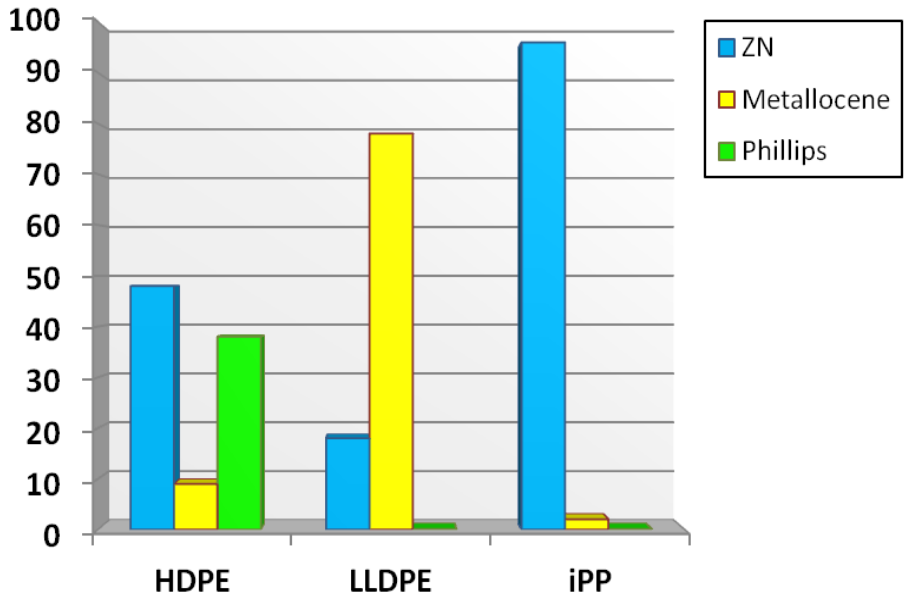

Figure 1.2. Polyolefin catalyst market share (2005 data; courtesy of N. Friederichs).

A rightful question is what made us confident to impact on a field that had been intensively cultivated for some 40 years (60 if one includes first-generation $TiCl_3$-based catalysts) with limited human resources (one single PhD project at a small academic group) and in a short time frame (3 years). The answer is that, for the first time ever in academic environment, in our study we made systematic and intensive use of state-of-the-art High-Throughput-Experimentation (HTE) tools and methods.[7] In a preliminary analysis, indeed, we identified three main hurdles in the investigation of HY-ZNCs evidently calling for HTE:

i) their complex formulation, with several chemical constituents interacting extensively between them[2,3] and with ubiquitous impurities such as water and oxygen, and ultimately giving rise to nano-structured particles with ill-defined active surfaces, difficult to characterize even with the most advanced surface science and spectroscopic techniques;
ii) the extreme reactivity, and the high sensitivity to preparation and use protocols, which complicates the acquisition of structural and polymerization data, and makes it questionable to compare data generated by different groups;
iii) the delicate technology issues related with handling and use under industrially relevant conditions, difficult to face in an academic laboratory and –even– in industry under (semi-)batch operation conditions.

As a matter of fact, looking at the past[2,3] we concluded that progress in the field mainly came from the slow accumulation of empirical knowledge at the various individual players (primarily petrochemical and/or polyolefin companies), with limited cross-fertilization and a marginal contribution of theoretical understanding. In the latter respect, ironically, even the few scientific models claimed to have inspired the development of novel systems or parts thereof on a rational basis[8] turned out to be flawed at a later stage[9], which implies that serendipity was behind those achievements too.

In the laboratory hosting the present thesis, a comprehensive state-of-the-art HTE workflow specifically conceived for investing olefin polymerization catalysis has been implemented starting from the second half of 2006.[10] The workflow includes two powerful platforms: one (Freeslate [former Symyx] Extended Core Module, XCM™) for parallel organic and organometallic synthesis; another (Freeslate [former Symyx] Parallel Pressure Reactor, PPR48) for parallel catalyst screening under industrially relevant conditions. Both platforms are integrally contained in a glove-box environment, and can run robotically a very large number of experiments (typically between 24

and 96 per day) in small scale (1-20 mL working volumes), with fully automated protocols and on-line individual reaction monitoring and control. As we shall see in more detail in Chapter 2, an extensive benchmarking project demonstrated that, despite the miniaturization, the results generated by said platforms are –at least trend-wise– representative of those obtained with much larger semi-batch industrial reaction units. Downstream to the platforms and fully integrated with them are fast analytical tools which accommodate without bottlenecks the throughput of catalysts and polymers for the necessary characterizations; specially notable are a Freeslate Rapid-GPC setup, and a Bruker Avance III 400 ^{13}C NMR spectrometer equipped with a high-temperature cryoprobe and a pre-heated robotic sample-changer, both ensuring an individual PP sample analysis time below 30 min, hence adequate to the throughput of the PPR. Therefore, in principle, some 50 catalyst systems (and the polymers thereof) can be prepared and fully characterized every day.

Importantly, the reproducibility and reliability inherent in robotic operation inside a glove-box make the results of a quality suited to input databases for Quantitative Structure-Properties Relationship (QSAR) analysis, which can be built up at an unprecedentedly high size and speed. Making use of this infrastructure, we launched a thorough investigation of industrial HY-ZNCs for iPP, with the objectives declared at the beginning of this section and starting practically from scratch. In other words, we re-examined all steps between precatalyst preparation and polymer production, generating our own experimental database on the HTE platforms, and feeding the results into suitable 'white-box' or 'black-box' models, without disregarding previous knowledge[2,3], but at the same time always giving us the benefit of doubt.

Three further assets greatly contributed to the project. One is the long-standing tradition of our research group (Laboratory of Stereoselective Polymerizations, LSP; www.lsp.unina.it) in the chemical investigation of catalytic olefin polymerization; this can be traced back to the pioneering schools of Paolo Corradini and Adolfo Zambelli (the two Natta associates who elucidated, respectively, the crystal structure and the chain microstructure of iPP). Another is our association with Sabic (a world-leading polyolefin producer), in the framework of a bilateral research agreement with its Competence Center of Geleen (The Netherlands). In our opinion, investigating HY-ZNCs without collaborating with an industrial polyolefin producer is like studying the theory of driving a car without practicing; moreover, something that should always be kept in mind is that high-throughput requires high-input, and the support of a large company supplying the hundreds of chemicals necessary to sustain a serious HTE screening is, if not indispensable, certainly very

useful. Last but not least is the backing of LSP computational chemists, who carried out in recent years, partly under the umbrella of the Dutch Polymer Institute (DPI, Eindhoven, The Netherlands; www.polymers.nl), a parallel investigation of HY-ZNCs by means of state-of-the-art Quantum Mechanics methods; this provided an invaluable theoretical background to our experimental observations, pointing out gross inconsistencies in the previous literature, and building up a new and more adequate theoretical interpretation frame.

Throughout this dissertation, we will assume that the fundamentals of catalytic olefin polymerization (poly-insertion) are known. Several books[3,5,11-13] and reviews[2,14,15] covered the subject exhaustively, and readers who are not familiar with the topic are referred to that literature. While recognizing their tremendous importance for application, in the present work we did not cover physical and process engineering issues, not strictly functional to our objectives.

1.2. HY-ZNCs for iPP 'in a Pill'[2,3]

In the vast majority of cases, a modern HY-ZNC system for iPP consists of a solid precatalyst of composition $MgCl_2$/$TiCl_4$/Internal Donor (ID), and a soluble AlR_3/External Donor (ED) cocatalyst (activator).

One way to prepare the precatalyst is (i) intensively milling $MgCl_2$, $TiCl_4$ and the ID, or $MgCl_2$ and the ID alone followed by impregnation of the solid with neat or concentrated $TiCl_4$ at high temperature; and (ii) removing the excess $TiCl_4$ and ID by hot-washing with hydrocarbons. Precatalysts prepared in this way typically contain 1-2% by weight of Ti and 5-10% by weight of ID. The commonly accepted interpretation of this protocol is that $TiCl_4$ adsorbs strongly on certain sites of the $MgCl_2$ surface, stabilized and possibly modulated by the ID, and then remains firmly bound at those sites during subsequent washing, activation and catalysis. The pitfall of said preparation is that it does not give control on precatalyst morphology. More recent preparation routes start from soluble or low-melting $MgCl_2$ precursors (e.g. MgR_2, or $MgCl_2$/alcohol adducts). With the aid of emulsion, spray-drying or spray-cooling technologies, the removal of the organic phase by reaction with excess $TiCl_4$ at high temperature in the presence of the ID (or a precursor to it) ends up with precatalysts featuring highly porous secondary particles with well-controlled spherical morphology; these are aggregates of billions of primary $MgCl_2$/$TiCl_4$/ID nano-particles of

lower size, and therefore with higher Ti and ID contents (up to 5 and 20% by weight, respectively), but otherwise similar to those obtained by physical methods.

It is generally believed that $MgCl_2$ acts as an inert carrier for $TiCl_4$, from which the catalytic species form by reaction with the AlR_3 activator via alkylation and reduction, mainly to the Ti(III) oxidation state. The additional fundamental role of AlR_3 as a scavenger of ubiquitous impurities (in general, molecules containing heteroatoms, including water and oxygen, lethal to the highly oxophilic Ti species) is unquestioned; other functions, on the other hand, such as a direct interaction with the active Ti species, have been proposed considering the massive adsorption of Al-containing species on the solid phase, but did not find unanimous consensus. The ID and ED, in turn, chemisorb on coordinatively unsaturated $MgCl_2$ surfaces, thus lowering surface energy and stabilizing primary precatalyst particles down to a very small size (a pre-requisite for a compact matrix like $MgCl_2$ to achieve a high specific surface area). Although the details are still partly controversial, it is widely accepted that LB molecules co-adsorbed in the vicinity of inherently chiral but otherwise too sterically open surface Ti complexes provide the necessary hindrance for the transition metal centers to effectively discriminate the two enantiofaces of the prochiral propene molecules at the insertion step. This role is undeniable and crucial, as is demonstrated by the fact that practically all aspects of the catalytic performance depend on the specific nature of the LBs present in the system (Table 1.1). With reference to the table, it is worthy to recall here that all ZNCs are 'multi-sited', that is feature multiple classes of active species differing –inter alia– in selectivity and molar mass capability. As far as the former aspect is concerned, even the best industrial systems contain active species yielding low amounts of PP of comparatively low degree of stereoregularity, conventionally defined 'atactic' (but actually a combination of poorly isotactic and moderately syndiotactic sequences). The relative amount of this by-product can be quantified by means of solvent fractionation (e.g. dissolution in hot xylene followed by fractional precipitation, or extraction by boiling heptane); the percentage by weight of the insoluble 'isotactic' PP fraction (e.g. the polymer part that re-precipitates from xylene solution at room temperature, or does not dissolve in boiling heptane) is usually defined 'Index of Isotacticity' (I.I.), and is dramatically enhanced by proper ID/ED combinations. LBs also impact on PP molar mass, shifting it to higher average values, and modulating its distribution, always broader than a Schultz-Flory function (M_w/M_n = 2.0) by an extent depending on the specific ID/ED pair used.

Table 1.1. Typical formulations and performance of HY-ZNCs for iPP.

Internal Donor, ID	External Donor, ED	Productivity [(a)]	I.I.	M_w/M_n
Aromatic monoester (e.g. ethylbenzoate)	Aromatic monoester (e.g. methyl-*p*-toluate)	0.5	>95	5-7
Aromatic diester (e.g. dibutyl-*o*-phthalate)	Alkoxysilane (e.g. $R^1R^2Si(OMe_2)$)	1-2	>97	5-7
2,2'-dialkyl-1,3-dimethoxypropane	Alkoxysilane (e.g. $R^1R^2Si(OMe_2)$)	>2	>97	3-5
Aliphatic diester (e.g. dialkylsuccinate)	Alkoxysilane (e.g. $R^1R^2Si(OMe_2)$)	1-2	>98	>7

[(a)] 10^3 Kg(PP) g(Ti)$^{-1}$

1.3. A Critical Survey of the Literature on HY-ZNCs

1.3.1. Sources

This section is a brief survey of the literature on HY-ZNCs for iPP and related systems, as available when we started this work. Apart from monographic articles in encyclopedias[2], the last comprehensive effort to review the subject dates back to 1996, with a competent book originating from inside a major polyolefin company.[3] More recently (2008), a book describing in general the progress of industrial polyolefin catalysis, including molecular catalysts on supports and polyethylene based materials, dedicated a chapter to HY-ZNCs for iPP.[5] Two highly cited reviews on PP microstructure, also interpreted as a catalyst 'fingerprint' and as such representing an important source of mechanistic information on the catalytic species, appeared in *Chem Rev.* (2000)[4] and *Progr. Polym. Sci.* (2001)[15]; the former was almost entirely dedicated to metallocene-PP, whereas the latter covers ZN-iPP including the latest models of active sites. The stream of original papers and industrial patents on ZNCs has never dried out (Figure 1.3)[1], and their overall number is countless; on the other hand, the vast majority are of rather limited use due to narrow scope and/or repetitive character. In the following, we will focus on the comparatively few

experimental and theoretical publications which left a clear mark in the field, by introducing solid facts or widespread models (in the latter case irrespective of whether or not these have been abandoned at a later stage in favor of new ones).

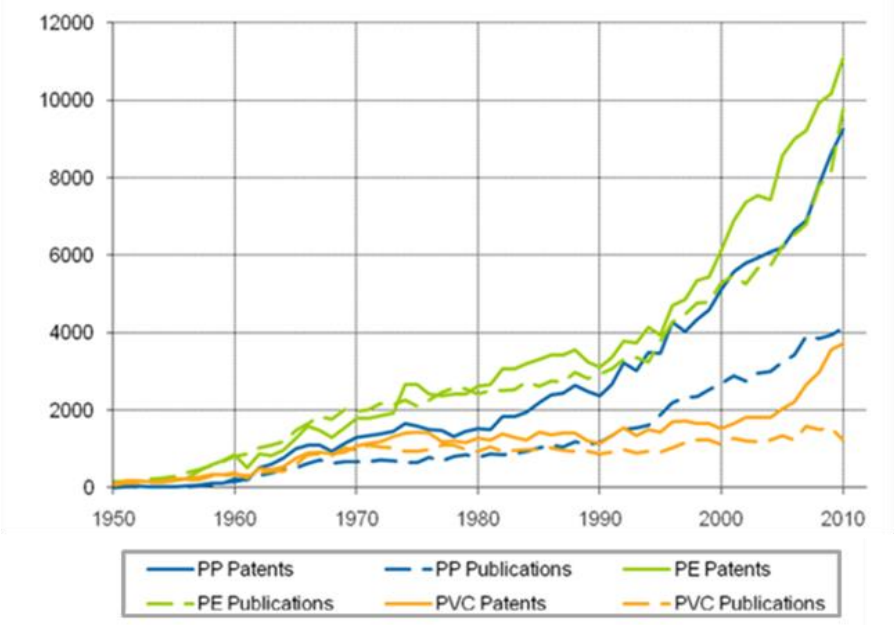

Figure 1.3. Trends of scientific publication and industrial patent outputs for polyolefins and other large volume plastics (1950-2010).[1]

1.3.2. Surface Science and Spectroscopic Studies

The number of direct experimental observations of ZN precatalysts is limited. These solids are extremely reactive, and the possibility that the active Ti represents only a small fraction of the total amount is unquestionably a serious deterrent (vide infra).

In what is possibly the most relevant surface science experiment, Magni and Somorjai studied the interaction of $TiCl_4$ with $MgCl_2$ films epitaxially grown on a gold support.[16] They found that at low temperature (<110 K) $TiCl_4$ binds only weakly and is completely removed again on evacuation. If, on the other hand, after condensing $TiCl_4$ on $MgCl_2$ the temperature is first raised to 300 K and then high vacuum is applied, part of $TiCl_4$ is now strongly bound and requires heating to the sublimation temperature of $MgCl_2$ to be removed. The amount of this $TiCl_4$ was estimated as corresponding roughly to 1-2% by weight of Ti, that is close to that found in actual catalysts. The authors ascribed the strong binding to incorporation into the 'bulk' of $MgCl_2$, without going into details nor discussing the implications for catalysis.

Based on High-Resolution TEM images (Figure 1.4), Terano reported that small particles in 'activated' crystalline $MgCl_2$ samples exhibit, in addition to the basal 001 planes, two kinds of lateral terminations, namely 'atomically flat' 110-type planes and 'atomically rough' planes perpendicular to the former.[17] The adsorption of $TiCl_4$ on $MgCl_2$ severely distorts the crystals and makes their surfaces 'no longer atomically flat planes'.[17]

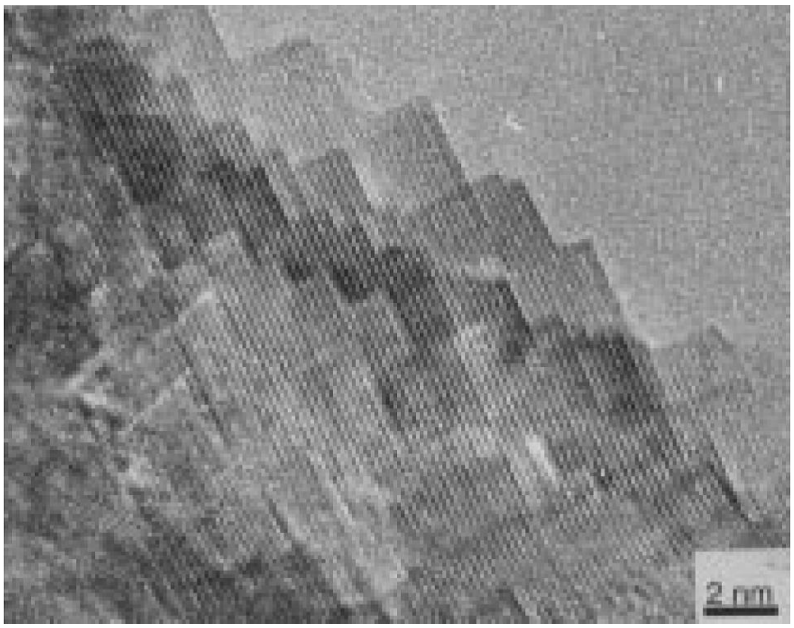

Figure 1.4. HR-TEM image of an 'activated' crystalline $MgCl_2$ sample.[17]

Recent vibrational spectroscopic studies by Zerbi concluded that the surface Ti species in HY-ZNCs are most likely octahedral $TiCl_4$ units bound to 4-coordinated Mg (e.g., on $MgCl_2$(110) or equivalent surfaces).[18]

Interesting information came from Electron Microscopy observations. In particular, independent studies by Oleshko[19] and Thüne[20] demonstrated that crystalline $MgCl_2$ domains, along with regions characterized by extensive disorder, are present in samples obtained from precursor $MgCl_2$.nROH adducts[21] (Figure 1.5). This seems to confirm that, in spite of the different morphology, the structure of physically and chemically activated HY-ZNCs is basically the same. Ref. 19 includes an interesting in-situ kinetic study concluding that the observed initial average growth rate of PP particles (~0.2 nm s^{-1}) is roughly 6 orders of magnitude lower than that theoretically allowed by the collision theory; this suggests that most surface Ti species would be (temporarily?) hindered by some physical or chemical barrier. We will come back to this point later.

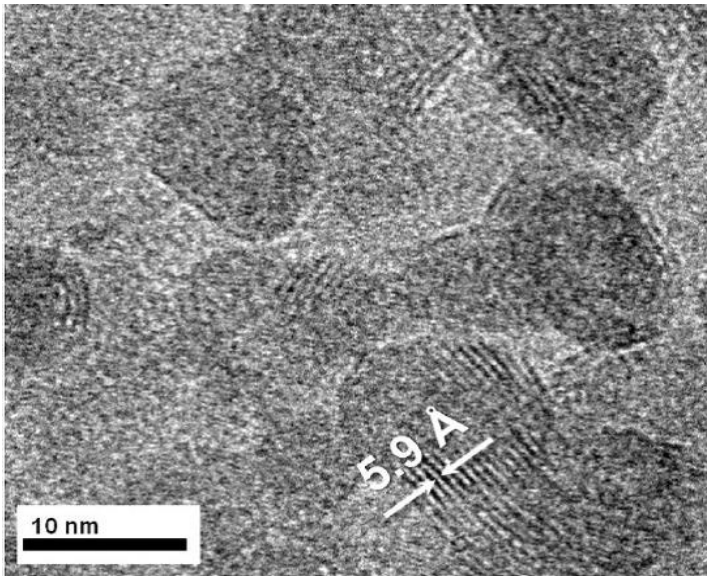

Figure 1.5. TEM image of an $MgCl_2$ film spin-coated from an ethanol solution at 30°C. The observed spacing of 0.59 nm is typical of the layer structure of crystalline $MgCl_2$.[20]

1.3.3. The Crystallochemical Modeling Approach

HY-ZNCs for iPP are a direct derivation of those discovered in the laboratories of Giulio Natta at the Milan Polytechnic in 1954, featuring $TiCl_3$ in one of its 'violet' crystalline modifications with a layer structure (α, γ, δ) as the solid precatalyst.[11,22] Natta had received a solid education in X-ray and electron diffraction, and Paolo Corradini (one of his most brilliant co-workers) was in turn an X-ray crystallographer; this was fortunate, because the intuition that the structure of the catalytic species in those systems is related with that of the crystal surfaces, determined in turn by the structure of the bulk, was basically correct, and prompted scientists of the caliber of Corradini, Bassi and Allegra to investigate the polymorphism of $TiCl_3$, discover the 'violet' modifications with a layered structure[22], and highlight the chirality of the Ti centers in the octahedral cavities of the structural layers, including those on the crystal edges (Figure 1.6[23]). Thus, the much higher stereoselectivity in propene polymerization of these modifications, compared with the 'brown' polymorph with fibrillar structure and non-chiral Ti[22] originally obtained by Ziegler, found an immediate and convincing explanation. On the other hand, in the following years the concept was probably over-emphasized, and ultimately slowed somehow the understanding of later catalyst generations with much smaller primary particles.

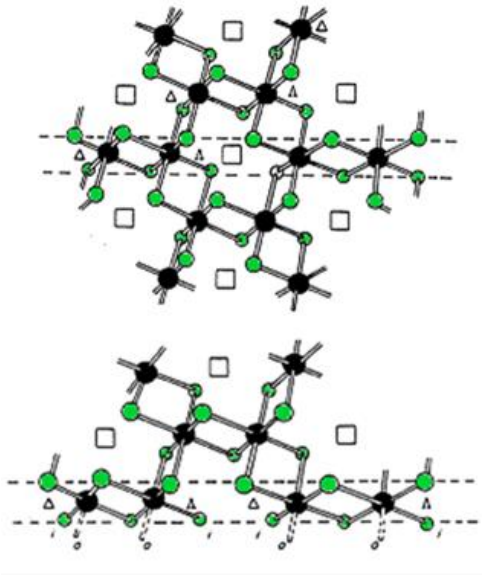

Figure 1.6. Schematic representation of a 'violet' $TiCl_3$ structural layer, before (*top*) and after (*bottom*) being cut along the (110) crystallographic direction. The Δ or Λ chirality of the stereogenic Ti centers is explicitly indicated, as well as the 'inward' ('*i*') or 'outward' ('*o*') orientation of the exposed coordination sites of the edge Ti atoms with respect to the layer interior.

At the end of the 1960s, seminal papers by Cossee and Arlman[24,25] proposed that the active sites in 'violet' $TiCl_3$ are located on the thin, coordinatively unsaturated side faces of the platelet-like crystals, and put explicitly in relation the chirality of the surface Ti atoms with the stereoselectivity in propene polymerization. With a few additions, Cossee's mechanism of isotactic chain propagation (Figure 1.7) is still regarded as a sound and solid interpretation of the polymerization process, and since it carries over to modern $MgCl_2$-supported catalysts we introduce it here.

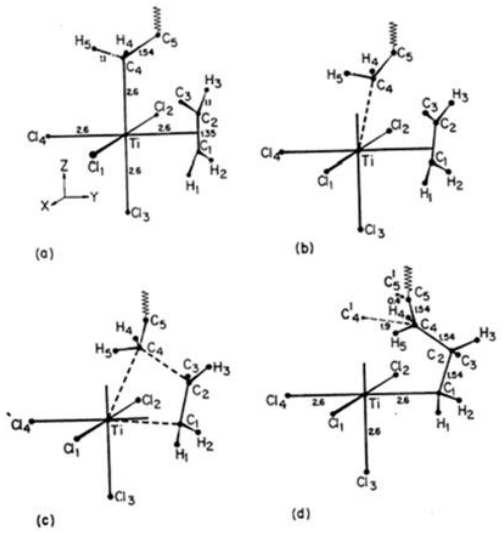

Figure 1.7. Propene insertion path into the Ti-Polymeryl bond of a model ZN catalytic species on the edge of a 'violet' $TiCl_3$ crystal, as proposed by Cossee.[25]

In brief, its key points are as follows:

i) As noted before, the Ti atoms in the bulk of 'violet' $TiCl_3$ crystals are chiral; indeed, each of them is bonded to three neighboring ones by pairs of bent Cl bridges, which results in an octahedral tris-chelate coordination with local C_2 symmetry and Δ or Λ configuration (Figure 1.6-top).

ii) Plausible lateral terminations of the structural layers are obtained by breaking one out of the three bridge pairs (e.g., parallell to the (110) or (100) crystallographic directions; Fig. 1.6-bottom and 1.7-a,b). This exposes linear racemic arrays of enantiomorphous Ti centers with two *cis* bridge pairs directed toward the crystal interior, and one 'dangling' terminal Cl left from the third broken bridge pair ensuring electroneutrality.

iii) The active species form by metathesis with the Al-alkyl activator, which replaces the unbridged Cl with an alkyl (R) group. Propene can coordinate at the remaining empty site of the octahedron, and insert into the Ti-R bond in a chain migratory fashion (Figure 1.7-c,d).

iv) The insertion is enantioselective due to non-bonded contacts at the inherently chiral active Ti centers, with opposite monomer enantiofaces preferred at active centers of opposite configuration ('enantiomorphic-sites control').

Point ii has been recently re-confirmed by periodic DFT-D calculations on α- and γ-$TiCl_3$ model lattices.[26] The hypothesis of a migratory insertion (point iii), which is now a milestone in organometallic chemistry, was based by Cossee on the assumption of the least nuclear motion, as can be clearly seen in Figure 1.7-c,d; his intuition was proved conclusively in 1987, with the discovery of C_s-symmetric *ansa*-metallocene catalysts for syndiotactic propene polymerization.[27] The main limitation of the construction was that the detailed origin of the selectivity, and in particular the steric contacts involved in the chiral recognition of propene (point iv), were not identified. However, the first ^{13}C NMR characterizations of the polymers in the mid-1970s confirmed the postulated 1,2 insertion regiochemistry, and demonstrated the site-controlled origin of the isotactic stereoselectivity.[28]

A few years later, Molecular Mechanics models by Corradini and co-workers highlighted the key role of the growing chain as a messenger transferring the chiral information from the Ti center to the incoming monomer via non-bonded contacts between the methyl group of the latter and the first chain C-C bond (Figure 1.8).[23,29,30] A compelling demonstration of this model came –again– from ^{13}C NMR analysis, in this case of the polymer chain ends. In fact, Zambelli found that for highly isotactic-selective ZNCs (including early $MgCl_2$-supported ones) the enantioselectivity of 1,2

propene insertion into initial Ti-[^{13}C-labeled]-R bonds is different from that of the subsequent ones: he observed no enantioselectivity for insertion into a Ti-$^{13}CH_3$ bond, and only partial (~80%) enantioselectivity for that into a Ti-$^{13}CH_2$-CH_3 bond, whereas the following propagation steps were almost completely enantioselective.[31] These findings highlighted the steric requirements for the asymmetric induction, and proved –in particular– that for the onset of the stereocontrol the alkyl group bound to Ti needs to be a 'chain', i.e. consist of at least two C atoms and preferably more. Incidentally, this conclusion, known as 'growing chain orientation mechanism of stereocontrol', holds for a variety of stereoselective olefin polymerization catalysts, including Group 4 *ansa*-metallocenes of various symmetries with chirotopic sites.[32]

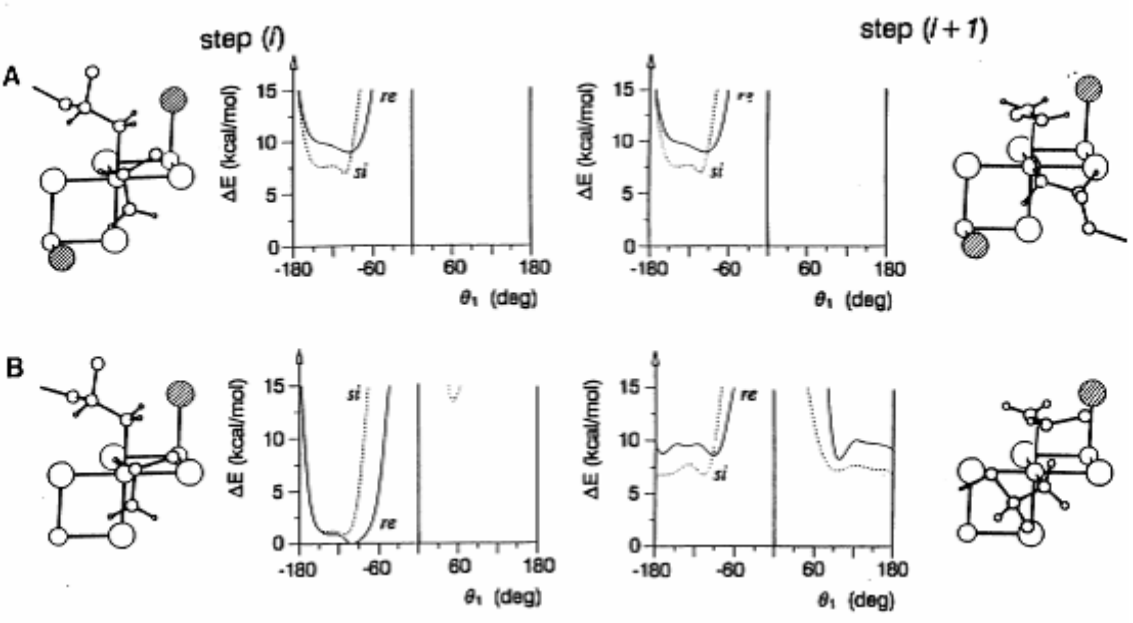

Figure 1.8. MM models of active sites on (110) (A) and (100) (B) lateral terminations of a 'violet' $TiCl_3$ structural layer.[30] The situations marked as (*i*) and (*i*+1) correspond to two consecutive 1,2 propene pre-insertion intermediates, in the hypothesis of a chain migratory insertion mechanism under 'Kinetic Quench' regime. In both cases, the active species has a Δ configuration; the local symmetry is C_2 for species A, C_1 for species B. The authors' educated guess, based on the MM calculations (see internal energy maps aside), was that propene insertion at both homotopic sites of species A would be enantioselective, because non-bonded interactions between the nearest-in-space surface Cl atom (striped in the drawings) and the growing polymer chain constrain the latter into a chiral orientation, which in turn slows propene insertion with the enantioface orienting the methyl group *syn* to the first chain C-C bond; therefore, chain propagation is *isotactic*. On the other hand, the lack of one of said two Cl atoms next to species B results into a loss of enantioselectivity at step (*i*+1); this would yield a *hemi-isotactic* chain propagation.

As is well-known, the main drawback of $TiCl_3$-based catalysts was the low yield, resulting into non-negligible residual amounts of acidic Ti-Cl bonds in the polymer, which had to be subjected to

energy and cost intensive processes of catalyst de-ashing.[2,3] Supporting the active Ti species on an inert matrix, thus increasing the productivity referred to Ti, looked like an obvious solution to the problem. However, we have seen before that in 'violet' $TiCl_3$ the bulk of the crystal is not an innocent self-support, because its structure determines that of the catalytic surfaces, and in particular the stereogenic environment of the exposed Ti centers. As a matter of fact, when typical supports like calcined silica or alumina were impregnated with $TiCl_4$ and reacted with Al-alkyls for Ti alkylation/reduction, the results were very poor (at most moderate activity in the polymerization of ethene, low or no activity and no stereoselecivity in that of propene).[2,3] The breakthrough came serendipitously when highly active catalysts for ethene polymerization were obtained by supporting $TiCl_4$ on MgO; it did not take too long to realize that (a) $TiCl_4$ chlorinates MgO ending up with $MgCl_2/TiCl_4$ adducts, and (b) $MgCl_2$ has a layer structure very similar to that of 'violet' $TiCl_3$ (i.e. stacked Cl-Mg-Cl 'sandwiches' with all octahedral cavities in between the two Cl planes occupied by Mg).[2,3]

Using authentic $MgCl_2$ as the support led to even better catalysts for polyethylene, whereas the performance for polypropylene was ambivalent: high productivity (>150 kg of polymer per gram of Ti) but poor stereoselectivity (less than 40% 'isotactic' polymer). However, the addition of proper LBs to catalyst formulation (Table 1.1), as components of the solid precatalyst ('Internal Donor', ID) or complexed with the Al-alkyl ('External Donor', ED), improved both the productivity (up to 2 tons of polymer per gram of Ti, or even more in special cases) and the stereoselectivity (>95% 'isotactic' polymer).[2,3]

The aforementioned similarity in crystal structure between $MgCl_2$ and 'violet' $TiCl_3$, and the observation of X-ray crystallinity in the first $MgCl_2/TiCl_4$(/ID) precatalysts, prompted many to extend to HY-ZNCs the crystallochemical approach used by Cossee and Arlman for $TiCl_3$. The starting assumption was that $TiCl_4$ chemisorption can only take place at the coordinatively unsaturated side faces of the platelet-like $MgCl_2$ crystals. According to Giannini[33] and Corradini[34], the most plausible terminations of $MgCl_2$ structural layers are 100 (exposing penta-coordinated Mg atoms) and 110 (exposing tetra-coordinated Mg atoms). In particular, a pioneering paper by Corradini and co-workers[34] proposed that stereoselective active species would result from the epitaxial chemisorption of $TiCl_4$ in the form of dinuclear Ti_2Cl_8 adducts on 100 terminations (Figure 1.9-a), followed by alkylation and reduction by AlR_3; the close similarity in the local coordination environment of Ti between these model species and authentic edges of 'violet' $TiCl_3$ structural layers (Figure 1.6) is certainly impressive. Sterically more open (albeit chiral) non-stereoselective

active species, on the other hand, would form by mononuclear epitaxial $TiCl_4$ chemisorption on 110 terminations (Figure 1.9-b); this undesired case was postulated to be largely prevented by the addition of a suitable ID, which would bind to the highly Lewis-acidic tetra-coordinated Mg atoms more strongly than $TiCl_4$.[34] According to this model, an ID able to chelate the doubly unsaturated Mg on $MgCl_2$(110) would be specially effective in the modification of HY-ZNCs; 1,3-dimethoxypropane IDs, introduced in the 1990s, were actually claimed to have been 'designed' on purpose.[8,35]

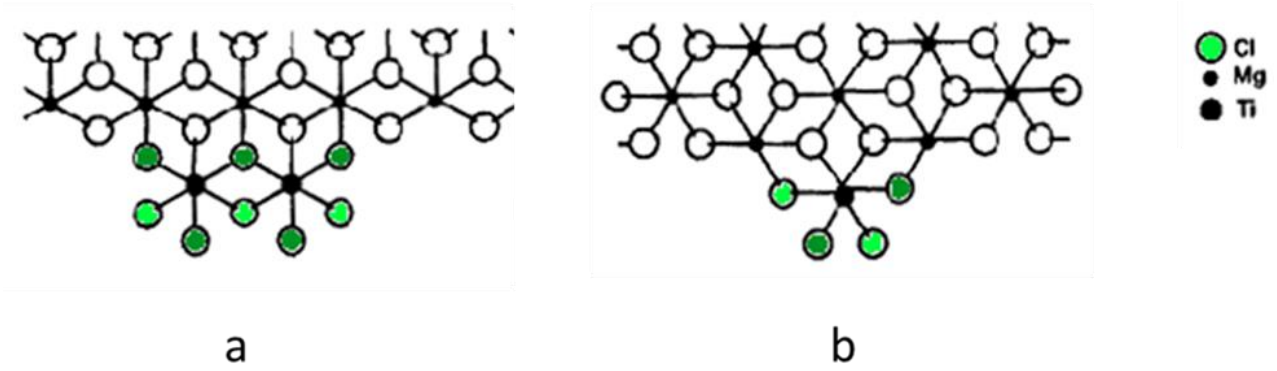

Figure 1.9. Models of (a) dinuclear Ti_2Cl_8 adducts on $MgCl_2$(100) terminations and (b) mononuclear $TiCl_4$ adducts on $MgCl_2$(110) terminations resulting from epitaxial $TiCl_4$ chemisorption.[34]

The interaction of the surface $TiCl_4$ adducts with the AlR_3 cocatalyst is known to result into their alkylation and reduction to Ti(III) and –in part– Ti(II).[2,3,36] A common assumption is that the active state in propene polymerization is Ti(III), similar to the case of first-generation $TiCl_3$-based catalysts.[2,3] As a matter of fact, there is no evidence suggesting the presence of cationic Ti(IV) active species (just to mention one, methylalumoxane (MAO) is not a suitable cocatalyst), and over-reduction to Ti(II) is associated with a loss of catalytic activity. Several papers reported that a very significant fraction of the Ti(III) species in HY-ZNCs are ESR-silent[37], which calls for some kind of aggregation, but not necessarily for the formation of dinuclear Ti(III) species with paired 3d electrons. Ti(II)-based species were claimed to be active primarily in ethene poly-insertions[13]; the latter claim, however, conflicts with the reported invariance of the average comonomer reactivity ratios with increasing reaction time in batch experiments[38], in spite of the progressive increase in the relative amount of Ti(II) in the catalyst pointed out by redox titrations.[36] On the other hand, evidence that, in a proper context, Ti(II) species can be active for both ethene and propene poly-insertions has been reported, e.g. by Albizzati.[39] Overall, the question is still open.

Some IDs, and in particular aromatic mono-esters (e.g. ethylbenzoate) and diesters (e.g. dialkyl-*ortho*-phthalates), also react irreversibly with AlR_3, and are largely extracted from the solid catalyst during polymerization.[40,41] In the absence of a proper ED replacing the ID on catalyst surface (another mono-ester for ethylbenzoate, an alkoxysilane for a phthalate), this results into a severe loss of stereoselectivity.[40] Catalysts including IDs which are unreactive to AlR_3 (e.g. 1,3-dimethoxy-propanes), on the other hand, can feature a high stereoselectivity also without the addition of an ED.[35] The simple hypothesis that $TiCl_4$ and the ID are located on different $MgCl_2$ crystal terminations, as originally proposed by Corradini et al.[34], does not provide an easy explanation for these observations. The same authors, therefore, proposed that:

i) dinuclear $Ti_2Cl_{2n-x}R_x$ species (n = 4 or 3) on $MgCl_2$(100) can split into mononuclear ones, an entropy driven process requiring a higher surface occupation (one $Ti_2Cl_{2n-x}R_x$ species covering three Mg atoms, two $TiCl_{n-x}R$ species covering four);

ii) the mononuclear adducts are non-chiral and non-stereoselective, which can explain the loss of catalyst stereoselectivity;

iii) adding an ED would be functional to increase the surface coverage of $MgCl_2$(100) terminations, thus keeping the surface Ti species into the more compact dinuclear stereoselective form.[34]

1.3.4. Quantum Mechanics Modeling

The mechanistic construction described in the previous section was largely accepted for at least two decades (1980-2000), and culminated with the disclosure of 1,3-dimethoxypropane IDs.[8] Several facts, however, called for a critical revision.

On the modeling side, flaws in the Molecular Mechanics (MM) conclusions became apparent as soon as the progress in Quantum Mechanics (QM) made it possible to approach large and complex systems like ZN surfaces with Density Functional Theory (DFT) applications. Until the late 1980s, MM was the only available computational tool in such cases; unfortunately, it cannot evaluate transition states, and in those early days, even when applied to ground states, the rather poor definition of geometries and potentials to be used in calculations on organometallic systems made it little more than a digital version of stick-and-ball hard models. With this we do not intend to diminish the value of the MM approach to ZNCs[23,29,30], which rather demonstrated that limitations in tools can be overcome by means of intuition and imaginative thinking; as a matter of fact,

Corradini's 'growing chain orientation mechanism of stereocontrol' was an outcome of those pioneering studies, and remains a milestone, in general, for stereoselective olefin polymerizations.[32] On the other hand, quantitative evaluations of insertion barriers (and other important reactive events), as well as absolute and relative estimates of surface and adsorbate stabilities for all aforementioned crystallochemical models were –at most– educated guesses.

This being said, it is also important to realize that a rigorous QM treatment is still unfeasible for large systems (with more than 10-20 atoms, indicatively), and therefore approximations like DFT are required. The latter can work extremely well with systems featuring localized bonds, but has serious drawbacks whenever medium and long-range interactions are important; this is obviously the case, in general, for crystals.[9] It may be worthy to recall at this stage that standard DFT methods do not include dispersion forces, and whenever such forces are non-negligible, semi-empirical ad-hoc corrections must be introduced in the calculations (so-called DFT-D approach). Very recently, new generations of functionals covering medium and long-range correlations have been implemented, some specifically for use with crystals, and seem to perform rather well[9], but their adoption is not yet widespread. Another extremely important issue is the choice of basis sets, which must be expertly pondered, and can otherwise lead to wildly scattered results for systems containing atoms with highly delocalized electrons (e.g. Cl).[9] Unfortunately, in the last 10-15 years many DFT studies of HY-ZNCs have been published without a serious analysis of the aforementioned aspects, which means that their results are potentially –if not likely– flawed.

An extreme case history is that of $TiCl_4$ adsorption on given $MgCl_2$ crystal terminations, studied computationally by several groups and ending up with totally different conclusions. On the one hand, Martinsky found that adsorption of both mono-nuclear $TiCl_4$ on $MgCl_2$(110) and dinuclear Ti_2Cl_8 on $MgCl_2$(100) is strong,[42] which would be consistent with the classical view of competing 'selective' and 'non-selective' Ti sites formation proposed by Corradini. Opposite results were obtained by Ziegler, who concluded that there are **no** stable chemisorption sites for $TiCl_4$ on $MgCl_2$ (!)[43], and proposed that Ti would bind in reduced form (although the nature of the process and the necessary reductant were not declared). In between these two extremes are studies by Parrinello,[44] Cavallo,[45] Zakharov,[46] Taniike[47] and others. Notably, most said studies did not consider adsorption entropy in the calculations.

DFT investigations of LB adsorption give a similarly controversial picture. Several studies have been reported on the binding to small $MgCl_2$ clusters (often unrealistic as being not allowed to relax) of

typical IDs and EDs featuring an organic framework with two electron-donating O atoms. These confirmed that, when in bidentate coordination, molecules with a comparatively short O∧O spacer (such as dialkoxysilanes and 1,3-dimethoxypropanes) have a preference for 4-coordinated Mg (e.g. on $MgCl_2$(110) terminations), whereas binding to two neighboring 5-coordinated Mg atoms (e.g. on $MgCl_2$(104) terminations) is also an option for molecules with a longer O∧O spacer (such as dialkyl-*ortho*-phthalates and dialkylsuccinates).[48] A wider search in the conformational space, however, provided additional and conflicting information. Parrinello, in particular, was the first to point out, with extensive periodic Car-Parrinello simulations, that a dibutyl-*ortho*-phthalate molecule on $MgCl_2$(110) favors monodentate over bidentate coordination, due to a mismatch between the crystal lattice dimensions and the carbonyl O∧O distance needed for an effective bite.[44c]

The first DFT-D studies explicitly addressing all 'technical' aspects of the calculations and therefore ending up with best-in-class predictions came from inside the research group hosting the present thesis. In particular, an investigation of neat $MgCl_2$ led the authors to conclude that well-formed α-$MgCl_2$ crystals should only feature basal planes and lateral terminations with 5-coordinated Mg (104 or equivalent; Figure 1.10).[49] Surfaces exposing 4-coordinated Mg (110 or equivalent) are appreciably (albeit not prohibitively) higher in energy, and should at most constitute a small minority.[49,50] On the other hand, not surprisingly, the latter surfaces turned out to bind LBs much more strongly[50], which favors their formation in $MgCl_2$/LB adducts[20,51] (e.g. $MgCl_2$.nROH, $MgCl_2$.nH_2O; studies on model adducts with industrially relevant ID and ED molecules are currently in progress[52]). $TiCl_4$ chemisorption was also found to be much stronger (and possibly to occur exclusively) on 110-type faces (Figure 1.11).[9] All this evidently calls for a major revision of the crystallochemical models.

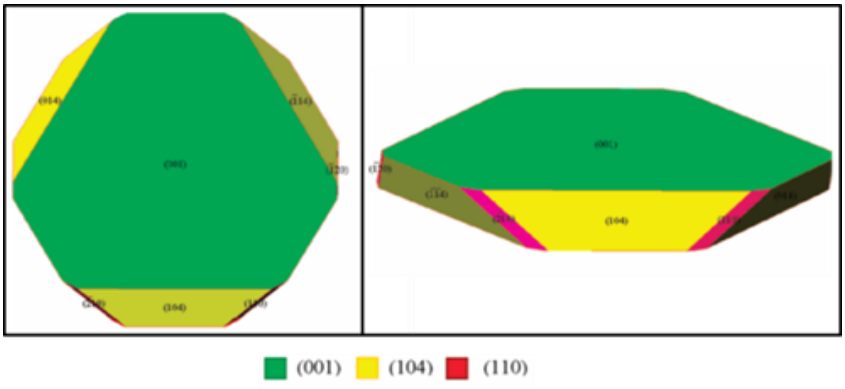

Figure 1.10. Models of well-formed neat $MgCl_2$ crystals mainly featuring 104-type lateral terminations, according to DFT-D estimates of surface energy.[50]

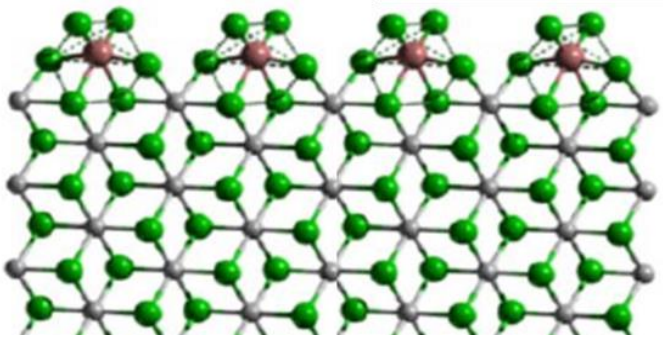

Figure 1.11. Mononuclear epitaxial $TiCl_4$ chemisorption on $MgCl_2(110)$ terminations, according to state-of-the-art DFT-D calculations.[9]

Other important aspects of HY-ZNCs can be looked at by DFT. In particular, a recent paper by Cavallo[53] investigated the mechanism of [Mg]Ti(IV)/[Mg]Ti(III) reduction/alkylation, and concluded that the process likely entails a first homolytic cleavage of a 'dangling' [Mg]Ti(IV)-Cl bond by AlR_3, yielding $AlR_3Cl^{\cdot}$ and a [Mg]Ti(III)Cl_3(☐) species (☐ = coordination vacancy); the latter would then undergo Cl/R metathesis with a second molecule of AlR_3, yielding AlR_2Cl and [Mg]Ti(III)Cl_2R(☐), which can enter the classical monomer coordination/insertion Cossee-type mechanism (Figure 1.12).

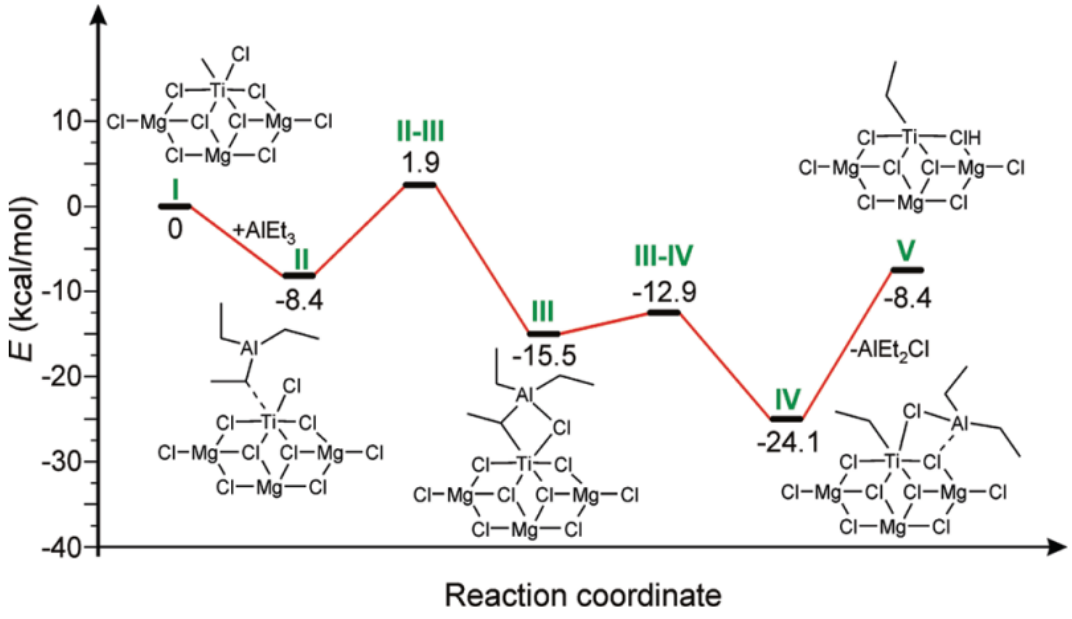

Figure 1.12. DFT-calculated pattern of Cl/R metathesis for a model [Mg]Ti(III)Cl_3(☐) species with $AlEt_3$ (☐ = coordination vacancy).[53]

1.3.5. Active site 'fingerprinting' from PP microstructure

The idea that a synthetic polymer chain is a tape where the history of the polymerization process is permanently encrypted, and that therefore the statistical analysis of polymer microstructure can be a precious source of mechanistic information, is almost as old as polymer science.[15] For heterogeneous ZN catalysis, however, this indirect method of investigating the catalytic species is particularly useful because it selects by definition the information coming from the active sites, whereas all conceivable direct methods have the drawback that they consider the total population of Ti species, only a small fraction of which seems to be catalytically active.[15] That this is indeed the case has been found in the vast majority of active site counts based on quenched-flow[54] or radioactive labeling[55] methods. Although these results may be questioned, for kinetic reasons (e.g., slow initiation) and/or because the underlying chemistry has not been fully worked out, simple calculations confirm the conclusion. A modern HY-ZNC typically yields some 20 kg of PP per g of catalyst at 70-80°C with an average residence time of 2 h.[2,3] For a Ti content of 2.5 wt.-% and a PP M_n of 50 kDa, this corresponds to 0.52 mmol of Ti yielding 0.40 mol of PP chains. Knowing that the growth time of an individual PP chain is <<1 s[54], the utilization of Ti then is <<10%. Whether this means that much less than 10% of Ti is involved in the reaction, or that each Ti center is active for much less than 10% of the time, are two plausible limiting hypotheses, the unknown reality probably lying somewhere in between. In all cases, though, it is clear that drawing conclusions on the nature of the active sites based on the results of surface science or spectroscopic measurements is questionable.

The first attempts to 'read the tape' for PP were made with ^{1}H NMR already in the 1960s, but it was only with the development of ^{13}C NMR in the following decades that significant applications aimed at active site 'fingerprinting' were reported.[15] These can range from very basic to highly sophisticated, and all have their merits. A simple but very important piece of information is the factual observation that catalyst stereoselectivity is exquisitely sensitive to the structure of the individual ID and ED molecules used to modify the active surfaces. As a matter fact, the integration of preparative Temperature Rising Elution Fractionation (prep-TREF) and routine ^{13}C NMR analysis of the eluted fractions at pentad level demonstrated that the degree of stereoregularity of the 'isotactic' PP fraction produced with HY-ZNCs is (much) higher when LBs are used, compared with the case of a LB-free catalyst (Figure 1.13).[56] Clearly, this points to the fact that LB molecules and active Ti species are co-adsorbed nearby at non-bonded contact. It is surprising that such a

straightforward and compelling evidence was disregarded as a dis-proof to the model in Figure 1.9.[34]

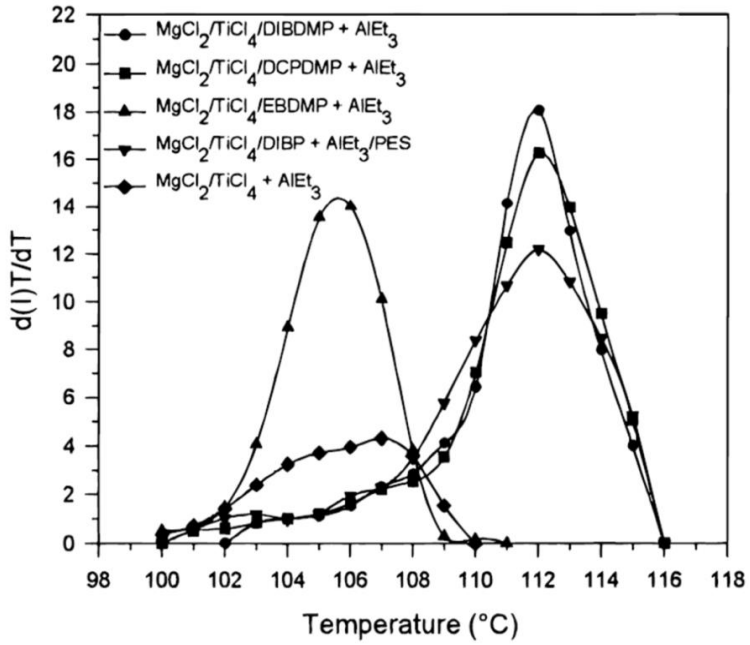

Figure 1.13. Temperature Rising Elution Fractionation (TREF) profiles of iPP samples prepared with a variety of HY-ZNCs.[56] Higher values of ^{13}C NMR degree of isotacticity turned out to be the main reason for the shift of a given elution curve to higher T values.

The quantitative statistical analysis of stereosequence distribution of ZN-PP in terms of multi-sited stochastic models, on the other hand, is a difficult and delicate exercise requiring very high resolution (up to the level of the steric nonads), to avoid over-fitting with the complex multi-site chain propagation models necessary to reproduce the ^{13}C NMR results.[15] The PP obtained with HY-ZNCs indeed is a mixture of stereosequences (or possibly whole chains) ranging from almost ideally isotactic to predominantly syndiotactic, passing through poorly isotactic ('isotactoid') ones. LBs have a profound impact on the relative abundance and also –to some extent– the degree of stereoregularity of the various types of stereosequences; in particular, many ID/ED pairs (Table 1.1) can suppress almost entirely the generation of stereosequences other than highly isotactic.[2,3,15] A few ones, on the other hand, enhance the formation of syndiotactic sequences.[57] The following general facts must be noted (Figure 1.14)[15]:

(i) The microstructure of the isotactic and isotactoid sequences is clearly indicative of a stereocontrol traceable primarily to the inherent chirality of the catalytic species (…*mmmm**rr**mmmm*… stereodefects). For the isotactoid sequences, however, the distribution of

configurations deviates from the classical Bernoullian (0-order Markovian) statistics normally observed in case of enantiomorphic-sites control; in particular, consecutive stereodefects are almost absent (experimental fraction of …*mmmm**rmr**mmmm*… sequences well below the calculated one).

(ii) The microstructure of the syndiotactic sequences is compatible with the hypothesis of chain-end control (…*rrrr**m**rrrr*… sequences largely prevailing over *rrrr**mm**rrrr*… ones).

(iii) No truly atactic sequences have ever been observed.

(iv) The different types of stereosequences can be part of individual stereoblock macromolecules (e.g., isotactic/syndiotactic, isotactic/isotactoid).

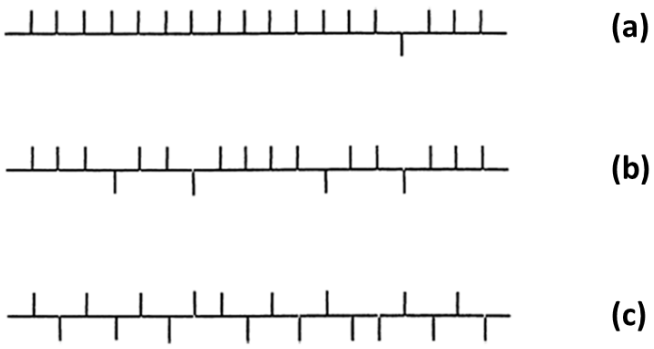

Figure 1.14. Adapted Fischer projections of isotactic (a), 'isotactoid' (b), and syndiotactic (c) sequences/stereoblocks as identified in PP samples made with ZNCs.[15,57]

The last point, originally based on indirect evidence provided by solvent fractionation experiments, was very recently re-confirmed by means of Adsorption Liquid Chromatography.[58]

It seems reasonable to assume that such a diversity in the polymerization products originates from a corresponding differentiation in the structure of the catalytic species, as is also suggested by the rather broad polymer molar mass distributions ($M_w/M_n > 2.0$).[2,3] On the other hand, the observed behavior is not unique to $TiCl_4$ on $MgCl_2$(/LB), because the very same three types of stereosequences are also present in PP samples produced with a variety of other Ti-based ZN catalysts, including $TiCl_3/AlR_{3-x}Cl_x$ ones.[15]

To reconcile all of the above findings, at the end of the 1990s Busico formulated a dynamic three-site model for HY-ZNCs in which the catalytic species, assumed to be in the Ti(III) oxidation state, all have the Ti center in a single octahedral and chiral coordination environment, which can occur

however in three basic variants depending on whether or not the first-neighbor surface Mg or Ti atom on either side exhibits a coordination vacancy (Figure 1.15).[57] In the classical models of Cossee and Arlman[24,25], subsequently elaborated by Corradini[30,32,34], the ligands that in Figure 1.15 are generically denoted as **L1** and **L2**, whose presence is crucial for the onset of the stereoselectivity in propene insertion according to the growing chain orientation mechanism (Figure 1.8), are supposed to be Cl atoms. Based on experimental and computational evidence, Busico suggested instead that a larger moiety is necessary for a high regio- and stereoselectivity, and that this is most likely a LB molecule.[15,57] The model ascribes isotactic propagation to catalytic species of type **C1** in Figure 1.15 (with no surface vacancy, and both active sites under strong steric pressure), and syndiotactic propagation to catalytic species of type **C3** (with two surface vacancies, and both active sites too open for site control, so that chain-end control can prevail). Isotactoid chain propagation was traced to C_1-symmetric catalytic species of type **C2**, with one surface vacancy and therefore intermediate between **C1** and **C3**, for a logical continuity and also for the impressive similarity in the microstructure of the isotactoid PP sequences obtained with HY-ZNCs and that of isotactoid PP chains produced with a number of C_1-symmetric *ansa*-metallocene catalysts mimicking, at least to some extent, the steric environment of Ti in **C2**.[15,57,59] Indirect experimental confirmation to the model came from propene polymerization results with molecular bis(phenoxyamine)Zr/Hf catalysts with local transition metal environments simulating those of model species **C1** and **C3**, yielding indeed isotactic and syndiotactic PP, respectively.[60]

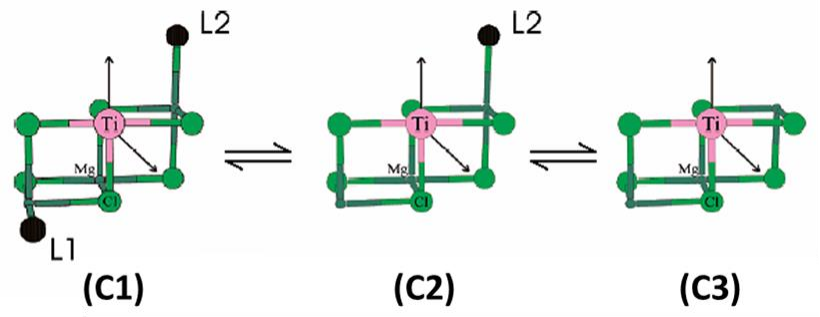

Figure 1.15. Dynamic 3-site model of catalytic species for HY-ZNCs.[57] Species **C1**, **C2**, **C3** would be responsible for (highly) isotactic, isotactoid, and syndiotactic chain propagation, respectively. **L1** and **L2** are surface Cl atoms or chemisorbed LB molecules.

Importantly, species of type **C1** can form on $MgCl_2$(110)-like edges with proper combinations of metal (Mg or Ti), **L1** and **L2** (Cl or LB)[57,59]; this resolves the contradiction between the QM conclusion of the latter edges as the only possible docking site for $TiCl_4$[9] and Corradini's model

claiming stereoselective sites on $MgCl_2$(100)-like edges only (Figure 1.9).[34] Another notable point of the model is that the observed formation of stereoblock chains (e.g. isotactic/syndiotactic)[57,58] can be easily traced to a dynamic/fluxional character of the surface, with vacancies forming and disappearing, e.g. as a result of LB adsorption/desorption or 'spill-over' processes.[57]

1.3.6. Catalyst regioselectivity and H_2 response

For a long time, the regioselectivity of HY-ZNCs for iPP has been a largely overlooked issue. As a matter of fact, routine ^{13}C NMR spectra of the polymers produced with these catalysts seemingly do not provide evidence for the presence of regiodefects, and the notion that the favored regiochemistry of propene insertion is 1,2 (primary; Figure 1.18-a) came from the observation of the chain ends by means of ^{1}H NMR (vinylidene groups formed via β-H elimination), or ^{13}C NMR in the special case of trans-alkylation with ^{13}C-enriched main group metal alkyls.[15,31] This has been taken as an indication of an exceedingly high regioselectivity (>99.9%), until more sophisticated methods of quantification based on propene hydro-oligomerization[61] or copolymerization with [1-^{13}C]-ethene or [3-^{13}C]-propene[62-64] unveiled a different and to a certain extent more complicated reality.

As a matter of fact, it was found out that, in the absence of LBs, HY-ZNCs are not more regioselective than e.g. typical *ansa*-zirconocene catalysts, the average fraction of 2,1 propene insertions in the form of isolated head-to-head/tail-to-tail enchainments (Figure 1.18-c) being around 1.0%.[63] These, however, mainly concentrate in the isotactoid and syndiotactic polymer sequences, and the multiplicity of stereochemical environments in which the regiodefective units are embedded results into an extensive splitting and broadening of the corresponding signals in the ^{13}C NMR spectra, which therefore are hardly detectable. Catalysts modified with LBs, on the other hand, are much more regioselective, and can yield PP samples with less than 0.1% 2,1 units; for these catalysts too, the regiodefects are not distributed at random, and tend to occur in isotactoid and syndiotactic chains/blocks.[64] All this strongly indicates that the vicinity of LB molecules to the active sites impacts not only on the enantioselectivity of 1,2 propene insertion, but also on the ability of the monomer to insert 'upside-down' (Figure 1.16). DFT calculations on models of catalytic species support this conclusion.[64]

Figure 1.16. Space-filling model of 2,1 propene insertion at a catalytic species of type **C1** in Figure 1.15, highlighting the steric interactions hindering this insertion already when **L2** = Cl.[64]

The occasional occurrence of a 2,1 insertion is believed to create steric congestion at the active site, due to the formation of a methyl branch α to the Ti center. This hypothesis was formulated to explain the observation of a strong catalyst activation effect produced by the addition of H_2 as a chain transfer agent[61,65] (all industrial processes for iPP make use of H_2 to regulate polymer average molar mass[2,3]); the proposed explanation was that the small H_2 molecule can approach a Ti-CH(CH_3)-CH_2-P moiety (P = Polymeryl) much faster than the larger molecule of propene, thus generating a saturated CH_3-CH_2-CH_2-P chain end and a Ti-H bond where chain growth can re-start (Figure 1.17-b).[61,65,66] Said chain ends are in fact detected by ^{13}C NMR in H_2-terminated PP samples in comparable amounts with the CH_3-CH(CH_3)-P ones expected from hydrogenolysis of chains with a last-inserted 1,2 propylene unit (Figure 1.17-a).[61,66]

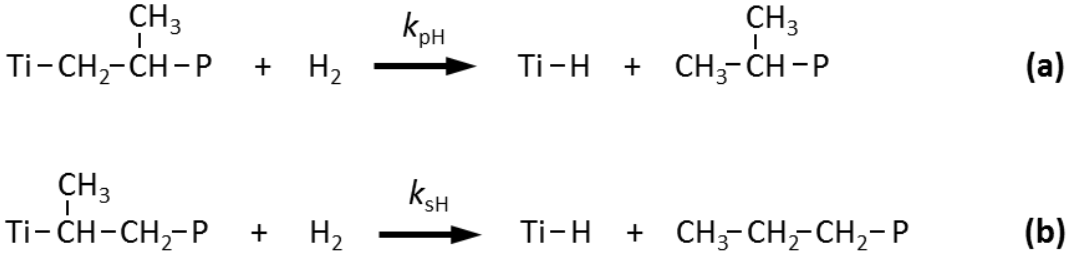

Figure 1.17. Hydrogenolysis of PP chains with a last-inserted 1,2 (a) and 2,1 (b) propylene unit (P = Polymeryl).

It may be worthy to add at this stage that propene insertion into a Ti-H is poorly regioselective, and entails the formation of both propyl and isopropyl; the latter, which are also poorly reactive,

are partly hydrogenated to propane, whereas in part undergo 1,2 propene insertion to a Ti-(2,3-dimethylbutyl) moiety.[67]

The combination of the above observations strongly suggests that growing chains with a last-inserted 2,1 propylene unit (Figure 1.17-b and 1.18) are poorly reactive toward propene, and therefore have been named 'dormant sites'.[61,66] Quantitative studies of propene 'hydro-oligomerization' concluded that, if one assumes $k_{pH} \sim k_{sH}$ (Figure 1.17), then $k_{sp} \sim 10^{-2}$-10^{-3} k_{pp} (Figure 1.18), and the fraction of 'dormant' sites $C^*_d \sim (1 + k_{sp}/k_{ps})^{-1}$ can be very high (50-90%, indicatively).[61,64,66] More recently, Landis noted that the hypothesis would be flawed if $k_{pH} < k_{sH}$[68]; however, studies on molecular model catalysts did not give evidence for that.[69] Moreover, questioning the 'dormant site' concept would require to find another plausible explanation for the said activating effect by H_2, and for that by ethene as well (another small molecule seemingly able to react much faster than propene with 'dormant sites'; Figure 1.19).[62]

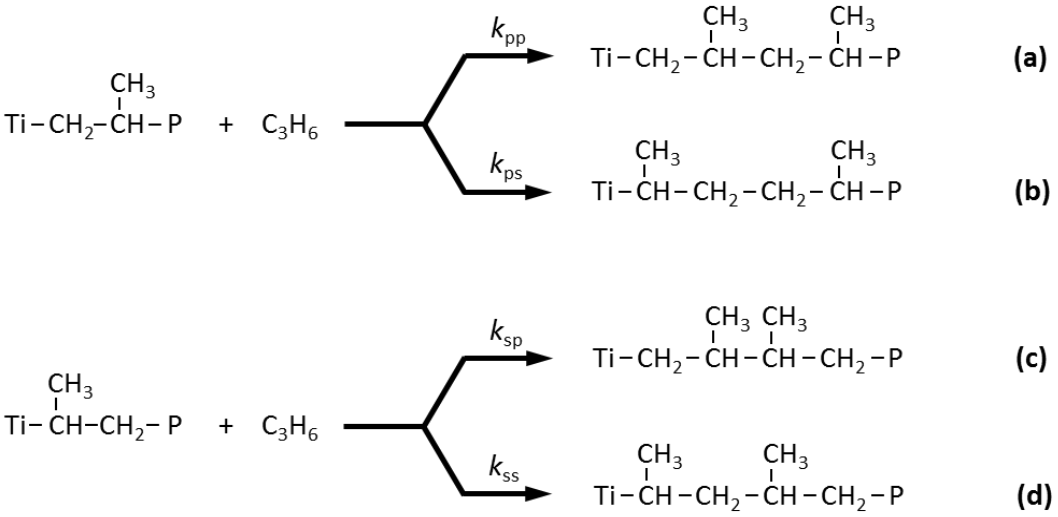

Figure 1.18. The four possible regiochemical modes of propene into a Ti-P bond (P= Polymeryl).[15]

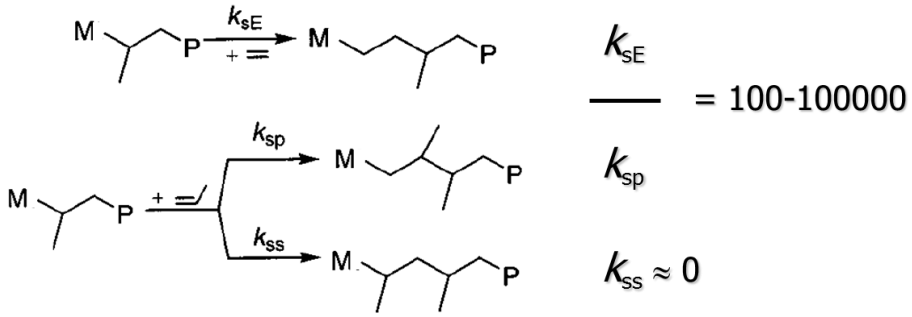

Figure 1.19. Relative insertion rates of ethene and propene at a 'dormant site' (P = Polymeryl).[62]

An important factual observation is that PP samples prepared with most HY-ZNCs in the presence of H_2 are (much) more stereoregular than those made without H_2.[61,66,70] It has been suggested that the reactivity toward propene insertion of a last-inserted stereoirregular propylene unit is also lower than that of a 'normal' one[66,70], but this seems not enough to account for the overall effect. In our opinion, one possible explanation is that the most stereoselective catalytic species in a given catalyst system are also the most dormant, and that therefore re-activation by H_2 of such species is comparatively larger.

A central aspect of the question is that, if it is true that H_2 reacts in preference to propene at 'dormant sites', growing PP chains with a last-inserted 2,1 propylene unit represent elective targets for hydrogenolysis, and the so-called 'hydrogen response' of a HY-ZNC (that is the amount of H_2 needed to lower PP average molar mass to a desired value) will be crucially dependent on catalyst regioselectivity, which in turn is modulated by the LBs.[64,71] On the other hand, to the best of our knowledge, no systematic QSAR studies on this point have been reported in the literature.

1.4. Thesis Layout

This dissertation is structured in five chapters. Following the present General Introduction (Chapter 1), Chapter 2 is dedicated to a detailed presentation of the HTE tools and methods implemented and used throughout the experimental work. In Chapter 3 we will report and discuss the thorough mechanistic information on HY-ZNCs provided by the combined use of the Freeslate Core Module and PPR48 platforms (with the integrated analytical tools downstream); in particular, the chapter highlights the dynamic composition of the active surfaces, their modulation by means of the ID, ED, and –to a certain extent– AlR_3 activator, and the relationships with all important aspects of catalyst behavior (i.e. activity, productivity, stereoselectivity, regioselectivity, polymer molar mass capability) in propene polymerization under industrially relevant conditions. Chapter 4, on the other hand, will demonstrate how, waiting for a full 'white-box' model, a predictive 'black-box' QSAR model of catalyst modification by means of proper AlR_3/ED combinations can be implemented for the most widely used industrial HY-ZNC system, namely $MgCl_2$/$TiCl_4$/diisobutyl-*ortho*-phthalate – AlR_3/dialkyldialkoxysilane (to the best of our knowledge, an unprecedented achievement). Chapter 5 will briefly summarize the conclusions of the work, and provide an outlook for its continuation.

References

(1) Jansz, J. *Presentation at Fifth Annual India Chemical Industry Outlook Conference in Mumbai*, **2012** (www.chemweek.com/Assets/Session3_EBB_Jansz.pdf)

(2) Cecchin, G.; Morini G; Piemontesi, F. In *Encyclopedia of Chemical Technology*; John Wiley and Sons: New York (NY), 2006; Vol. 26, pp. 502-554.

A thorough monography on ZNCs, covering both $TiCl_3$-based and $MgCl_2$-supported systems, and chemical as well technological aspects, with a rich bibliography with scientific articles and patents.

(3) *Polypropylene Handbook: Polymerization, Characterization, Properties, Applications*; Moore, E.P. Jr., Ed.; Hanser Publishers: Munich, 1996.

Competent and complete book on all aspects of PP catalysis (including heterogeneous and molecular systems), physical structure, mechanical and rheological properties, industrial production technology, and end-use applications. The main, obvious limitation is its publication date, which makes it obsolete with respect to the latest developments.

(4) Resconi, L.; Cavallo, L.; Fait, A.; Piemontesi, F. *Chem. Rev.* **2000,** *100(4)*, 1253−1345.

(5) *Tailor-Made Polymers via Immobilization of Alpha-Olefin Polymerization Catalysts*; Severn, J. R.; Chadwick, J. C., Eds.; Wiley-VCH: Weinheim, 2008.

(6) Tullo, A. H, *C&EN* **2010**, *88(42)*, 10-16.

(7) *High Throughput Screening in Catalysis*; Hagemeyer, A.; Strasser, P.; Volpe, A. F., Jr., Eds.; Wiley-VCH: Weinheim, 2004.

(8) See, e.g.: Scordamaglia, R.; Barino, L. *Macromol. Theory Simul.* **1998**, *7,* 399-405.

(9) D'Amore, M.; Credendino, R.; Budzelaar, P. H. M.; Causá, M.; Busico, V. *J. Catal.* **2012***, 286,* 103-110.

(10) Busico, V.; Pellecchia, R.; Cutillo, F.; Cipullo, R. *Macromol. Rapid Commun.* **2009**, *30*, 1697-1708.

(11) Boor, J., Jr. *Ziegler-Natta Catalysts and Polymerizations*; Academic Press: New York (NY), 1979.

(12) Kissin, Y. V. *Isospecific polymerization of olefins*; Springer-Verlag: New York (NY), 1985.

(13) Kissin, Y. V. *Alkene Polymerization Reactions with Transition Metal Catalysts*; Elsevier: Amsterdam, 2008.

(14) *Chem. Rev.* **2000,** *100(4)*, 1167-1682.

This special issue of *Chem. Rev.* was dedicated to the developments of molecular olefin polymerization catalysis from the metallocene boom until the discovery of late-transition-metal-based catalysts.

(15) Busico, V.; Cipullo, R. *Progr. Polym. Sci.* **2001**, *26*, 443-533.

This review is entirely dedicated to the high-field ^{13}C NMR elucidation of PP microstructure, with special emphasis on its mechanistic applications to active-site 'fingerprinting'.

(16) Magni, E.; Somorjai, G. A. *Surf. Sci.* **1997**, *377-379*, 824-827.

(17) Mori, H.; Sawada, M.; Higuchi, T.; Hasebe, K.; Otsuka, N.; Terano, M. *Macromol. Rapid Commun.* **1999**, *20*, 245-250.

(18) (a) Brambilla, L.; Zerbi, G.; Piemontesi, F.; Nascetti, S.; Morini, G. *J. Mol. Catal. A: Chem.* **2007**, *263*, 103-111. (b) Brambilla, L.; Zerbi, G.; Piemontesi, F.; Nascetti, S.; Morini, F. *J. Phys. Chem. C* **2010**, *114*, 11475-11484.

(19) Crozier, P. A.; Oleshko, V. P.; Westwood, A. D.; Cantrell, R. D. *J. Electron Microscopy* **2002**, *51 (Supplement)*, S27-S39.

(20) Cheruvathur, A. V.; Langner, E. H. G.; Niemantsverdriet, J. W. H.; Thüne, P. C. *Langmuir* **2012**, *28*, 2643-2651.

(21) See, e.g.: Sozzani, P.; Bracco, S.; Comotti, A.; Simonutti, R.; Camurati, I. *J. Am. Chem. Soc.* **2003**, *125,* 12881-12893.

(22) Natta, G.; Allegra, G.; Corradini, P. *J. Polym. Sci.* **1961**, ***156***, 399-410.

(23) Corradini, P.; Barone, V.; Fusco, R.; Guerra, G. *Eur. Polym. J.* **1979**, *15*, 1133-1141.

(24) (a) Cossee, P. *J. Catal.* **1964**, *3*, 80-88. (b) Arlman, E. *J. Catal.* **1964**, *3*, 89-98. (c) Arlman, E. J.; Cossee, P. *J. Catal.* **1964**, *3***,** 99-104.

(25) Cossee, P. The Mechanism of Ziegler-Natta Polymerization. II. Quantum Chemical and Crystal-Chemical Aspects. In *The Stereochemistry of Macromolecules*; Ketley, A. D., Ed.; Marcel Dekker: New York (NY), 1967; Vol. 1, Chapter 3, pp. 145-175.

(26) Sementa, L.; D'Amore, M.; Barone, V.; Busico, V.; Causa', M. *PCCP* **2009**, *11*, 11264-11275.

(27) Ewen, J. A.; Jones, R. L.; Razavi, A.; Ferrara, J. D. *J. Am. Chem. Soc.* **1988**, *110*, 6255-6256.

(28) (a) Zambelli, A.; Locatelli, P.; Bajo, G.; Bovey, F. A. *Macromolecules* **1975**, *8*, 687-689. (b) Zambelli, A.; Locatelli, P.; Zannoni, G.; Bovey, F. A. *Macromolecules* **1978**, *11*, 923-924. (c) Zambelli, A.; Locatelli, P.; Bajo, G. *Macromolecules* **1979**, *12*, 154-156.

(29) Corradini, P.; Guerra, G.; Fusco R.; Barone, V. *Eur. Polym. J.* **1980**, *16*, 835-842.

(30) Corradini, P.; Busico, V.; Cavallo, L.; Guerra, G.; Vacatello, M.; Venditto, V. *J. Mol. Catal.* **1992**, *74*, 433-442.

(31) Zambelli, A.; Sacchi, M. C.; Locatelli, P.; Zannoni, G. *Macromolecules* **1982**, *15*, 211-212.

(32) Corradini, P.; Guerra, G.; Cavallo, L. *Acc. Chem. Res.* **2004**, *37***,** 231-241.

(33) Giannini, U. *Makromol. Chem.* **1981**, *Suppl. 5*, 216-229.

(34) Corradini, P.; Barone, V.; Fusco, R.; Guerra, G. *Gazz. Chim. Ital.* **1983**, *113*, 601-607.

(35) Albizzati, E.; Giannini, U.; Morini, G.; Galimberti, M.; Barino, L.; Scordamaglia, R. *Macromol. Symp.* **1995**, *89*, 73-89.

(36) (a) Kashiwa, N.; Yoshitake, J. *Makromol. Chem.* **1984**, *195*, 1133-1138. (b) Chien, J. C. W.; Wu, J. C. *J. Polym. Sci., A: Polym. Chem.* **1982**, *20*, 2461-2476.

(37) Chien, J. C. W.; Hu, Y. *J. Polym. Sci., A: Polym. Chem.* **1989**, 27, 897-913.

(38) Busico, V.; Corradini, P.; Ferraro, A.; Proto, A. *Makromol. Chem.* **1986**, *187*, 1125-1130.

(39) Albizzati, E.; Giannini, U.; Balbontin, G.; Camurati, I.; Chadwick, J. C.; Dall'Occo, T.; Dubitsky, Y.; Galimberti, M.; Morini, G.; Maldotti, A. *J. Polym. Sci. A: Polym. Chem.* **1997**, *35*, 2645-2652.

(40) Busico, V.; Corradini, P.; De Martino, L.; Proto, A.; Savino, V.; Albizzati, E. *Makromol. Chem.* **1985**, *186*, 1279-1288.

(41) Noristi, L; Barbè, P. C.; Baruzzi, G. *Makromol. Chem.* **1991**, *192*, 1115-1127.

(42) Martinsky, C.; Minot, C.; Ricart, J. M. *Surf. Sci.* **2001**, *490*, 237-250.

(43) Seth, M.; Margl, P. M.; Ziegler, T. *Macromolecules* **2002**, *35*, 7815-7829.

(44) (a) Boero, M.; Parrinello, M.; Terakura, K. *J. Am. Chem. Soc.* **1998**, *120*, 2746-2752. (b) Boero, M.; Parrinello, M.; Hüffer, S.; Weiss, H. *J. Am. Chem. Soc*. **2000**, *122*, 501-509. (c) Boero, M.; Parrinello, M.; Weiss, H.; Hüffer, S. *J. Phys. Chem. A* **2001**, *105*, 5096-5105.

(45) (a) Monaco, G.; Toto, M.; Guerra, G.; Corradini, P.; Cavallo, L. *Macromolecules* **2000**, *33*, 8953-8962. (b) Correa, A.; Credendino, R.; Pater, J. T. M.; Morini, G.; Cavallo, L. *Macromolecules* **2012**, *45*, 3695-3701.

(46) (a) Stukalov, D. V.; Zilberberg, I. L.; Zakharov, V. A. *Macromolecules* **2009**, *42*, 8165-8171. (b) Stukalov, D. V.; Zakharov, V. A.; Zilberberg, I. L. *J. Phys. Chem. C* **2010**, *114*, 429-435.

(47) (a) Taniike, T.; Terano, M. *Macromol. Rapid Commun.* **2007**, *28*, 1918-1922. (b) Taniike, T.; Terano, M. *Macromol. Chem. Phys.* **2009**, *210*, 2188-2193. (c) Taniike, T.; Terano, M. *J. Catal.* **2012**, *293*, 39-50.

(48) (a) Toto, M.; Morini, G.; Guerra, G.; Corradini, P.; Cavallo, L. *Macromolecules* **2000,** *33,* 1134-1140. (b) Correa, A.; Piemontesi, F.; Morini, G.; Cavallo, L. *Macromolecules* **2007,** *40,* 9181-9189. (c) Credendino, R.; Pater, J. T. M.; Liguori, D.; Morini, G.; Cavallo, L. *J. Phys. Chem. C* **2012**, *116*, 22980−22986.

(49) Busico, V.; Causà, M.; Cipullo, R.; Credendino, R.; Cutillo, F.; Friederichs, N.; Lamanna, R.; Segre, A.; Van Axel Castelli, V. *J. Phys. Chem. C*, **2008**, *112*, 1081-1089.

(50) Credendino, R.; Busico, V.; Causà, M.; Barone, V.; Budzelaar, P.H.M.; Zicovich-Wilson, C. *PCCP* **2009**, *11*, 6525-6532.

(51) Credendino, R.; Pater, J. T. M.; Correa, A.; Morini, G.; Cavallo, L. *J. Phys. Chem. C* **2011**, *115*, 13322-13328.

(52) D'Amore, M.; Capone, F.; Budzelaar, P. H. M.; Busico, V., manuscript in preparation.

(53) Bahri-Laleh, N.; Correa, A.; Mehdipour-Ataei, S.; Arabi, H.; Haghighi, M.N.; Zohuri, G.; Cavallo, L. *Macromolecules*, **2011**, *44*, 778-783.

(54) Mori, H; Terano, M. *Trends Polym. Sci.* **1997**, *5*, 314-321, and refs. therein.

(55) Mejzlik, J; Lesna, M; Kratochvila, J. *Adv. Polym. Sci.* **1986**, *81*, 83-120, and refs. therein.

(56) Morini, G.; Albizzati, E.; Balbontin, G.; Mingozzi, I.; Sacchi, M. C.; Forlini, F.; Tritto, I. *Macromolecules* **1996**, *29*, 5770-5776.

(57) Busico, V.; Cipullo, R.; Monaco, G.; Talarico, G.; Vacatello, M.; Chadwick, J. C.; Segre, A. L.; Sudmeijer, O. *Macromolecules* **1999**, *32*, 4173-4182.

(58) Macko, T.; Cutillo, F.; Busico, V.; Brüll, R. *Macromol. Symp.* **2010**, *298*, 182-190.

(59) Busico, V.; Cipullo, R.; Talarico, G. Active species in heterogeneous Ziegler-Natta catalysts: "the father of all models". In *Micro-Kinetics and Dynamics of Individual Active Sites in Catalytic Reactions*; Terano, M.; Otsuka, N., Eds.; Technology and Education Publishers: Tokyo, 2001; pp. 41-52.

(60) Busico, V.; Cipullo, R.; Ronca, S.; Budzelaar, P. H. M. *Macromol. Rapid Commun.* **2001**, *22*, 1405-1412.

(61) (a) Busico, V.; Cipullo, R.; Corradini, P. *Makromol. Chem., Rapid Commun.* **1992**, *13*, 15-20. (b) Busico, V.; Cipullo, R.; Corradini, P. *Makromol. Chem.* **1993**, *194*, 1079-1093.

(62) Busico, V.; Cipullo, R.; Ronca, S. *Macromolecules* **2002**, *35*, 1537-1542.

(63) Busico, V.; Cipullo, R.; Polzone, C.; Talarico, G.; Chadwick, J. C. *Macromolecules* **2003**, *36*, 2616-2622.

(64) Busico, V.; Chadwick, J. C.; Cipullo, R.; Ronca, S.; Talarico, G. *Macromolecules* **2004**, *37*, 7437-7443.

(65) Tsutsui, T; Kashiwa, N; Mizuno, A. *Makromol. Chem.-Rapid Commun.* **1990**, *11*, 565-570.

(66) Busico, V.; Cipullo, R.; Chadwick, J. C.; Modder, J. F.; Sudmeijer, O. *Macromolecules* **1994**, *27*, 7538-7543.

(67) Chadwick, J. C.; Heere, J. J. R.; Sudmeijer, O. *Macromol. Chem. Phys.* **2000**, *201*, 1846-1852.

(68) Landis, C. R.; Sillars, D. R.; Batterton, J. M. *J. Am. Chem. Soc.* **2004**, *126*, 8890-8891.

(69) Busico, V.; Cipullo, R.; Romanelli, V.; Ronca, S.; Togrou, M. *J. Am. Chem. Soc.* **2005**, *127*, 1608-1609.

(70) Chadwick, J. C. ; Van Kessel, G. M. M. ; Sudmeijer, O. *Macromol. Chem. Phys.* **1995**, *196*, 1431-1437.

(71) Chadwick, J. C.; van der Burgt, F. P. T. J.; Rastogi, S.; Busico, V.; Cipullo, R.; Talarico, G.; Heere, J. J. R. *Macromolecules* **2004**, *37*, 9722-9727.

Chapter 2. The High Throughput Experimentation Approach: Tools and Methods

2.1. Introduction

'High-Throughput Experimentation' (HTE) is a general/generic designation for any technique which can generate a 'high(er)' flow of data, and therefore information, compared with 'conventional' operation.[1] As a matter of fact, pieces of equipment conceived for combinatorial or parallel use are often claimed to be high-throughput, irrespective of the acceleration factor they can actually provide. A typical case is the parallel heating carousel manufactured by Radleys (Figure 2.1)[2], which in reality is little more than a compact array of 6 conventional heating mantles still requiring standard manual operation.

Figure 2.1. Radleys Carousel 6 Plus: not all that is parallel is HTE!

In the context of the present thesis, we only refer to an equipment or operation as 'high-throughput' when the achievable flow of information is 'much' higher with respect to a 'conventional' counterpart, where 'much' means something between 1 and 3 orders of magnitude; inevitably, this requires extensive miniaturization and automation at the stage of data generation, and sophisticated software tools for data logging and analysis.[1] Similarly, we will

consider 'high-throughput' a research approach with the same acceleration factor; considering that no approach in the field of our interest, namely ZN catalysis, can consist of one single unit operation, and no sequence of operations can be faster than its slowest component, we will adopt the term exclusively for a 'workflow' of tools each of which operates high-throughput-wise. A fully de-bottlenecked HTE workflow for investigating ZN olefin polymerization is very sophisticated and demanding in terms of installation, operation and maintenance, and deserves the additional qualification of 'state-of-the-art'.

At the Laboratory for Stereoselective Polymerizations (LSP), one such workflow has been assembled throughout the last 6 years[3], for the reasons explained in the previous chapter, and was used extensively to carry out the present thesis. In the following sections, we will illustrate in detail its features, as a whole and with reference to the individual platforms and analytical tools composing it. The presentation includes an introduction to the philosophy of the approach, an analysis of the operation protocols, and an extensive demonstration of data reliability and reproducibility.

One last preliminary remark concerns computational chemistry. The combination of experiments with modeling or simulation studies has become the norm in modern chemical investigations, to the point that the term 'in-silico experiments' has been introduced to designate chemical experiments run in computer chips, in particular by means of Quantum Mechanics (most typically based on the DFT approximation).[4] We are strong believers in the effectiveness of this approach; however, the complexity of ZN catalysis is still beyond the possibility of an entirely computational study, and in-silico ZN catalytic processes are not yet realistic in all respects.[5] Therefore, in the present study 'High Throughput Computation' (HTC) was not used upstream to the HTE exploration, as is instead the norm at LSP when investigating molecular catalysts.

2.2. Choosing the HTE strategy

Originally implemented in the pharmaceutical industry for the identification of novel drugs with a combinatorial approach, HTE (or, according to a slightly different definition, High-Throughput Screening, HTS) methodologies have widely spread into organometallic catalysis research, where they are used for parallel ligand/precatalyst synthesis and catalyst screening operations.[1] More specifically in polyolefin catalysis, a HTE approach is justified in view of the large number of chemical (precatalyst, activator(s), selective modifier(s), scavenger(s), (co)monomer(s), etc.) and

physical variables that must be explored, and the comparatively narrow window for optimum operation featured by many catalysts of industrial interest.

State-of-the-art HTE platforms are undeniably expensive with respect to both acquisition and maintenance. Moreover, the extensive miniaturization of typical HTE reactors, with working volumes between 1 and 10 mL, have been looked at with skepticism with respect to the ability to operate under industrially relevant conditions; their large surface-to-volume ratio has also been pointed to as a likely cause of easy contamination (always to be considered when dealing with organometallic catalysts, and in particular olefin polymerization ones based on highly oxophilic early transition metals). On the other hand, in recent years it has been demonstrated, with an important contribution by LSP, that these platforms can be extremely reproducible, at least when they are fully contained in a glove-box environment and feature extensive robotic operation (which adds the non-negligible side benefit of liberating operators from repetitive tasks).[3] A number of technical, economic and environmental aspects, in turn, are rather in favor of reactor miniaturization; for highly exothermic reactions like olefin polymerization, a larger surface-to-volume ratio can only be beneficial, and the amounts of chemicals to be fed into mini-reactors are correspondingly small, which means lower costs and lower wastes, not to mention the possibility that a (new) catalyst be only available in minute quantity.

Once the decision to adopt HTE is taken, the next important step is to define its use strategy. In the vast majority of cases, HTE is aimed to support and speed-up trial-and-error approaches, i.e. enhance the probability of fortuitous discovery. This moves from the known fact that roughly half of all scientific discoveries are serendipitous in origin[6], and one may plausibly speculate that such a fraction is even higher in a very complex empirical field like organometallic catalysis.[7] The layout of a typical HTE polyolefin catalysis workflow for trial-and-error applications is shown in Figure 2.2.[1,8] The protocol is strictly hierarchical, and usually consists of three stages. In the first one, a *primary screening* is applied in which a very large number of experiments (of the order of 10^3 per day) in very small scale (<1 mL) are aimed to the rapid discovery of catalyst structures that are promising in at least some respects ('hits'); in this, accuracy can be traded for throughput, and qualitative trends are more important than precise data. Hits identified at this stage are then verified and improved in a subsequent *secondary screening* stage, in which the catalyst performance properties for the targeted application are assessed using a 'larger' scale (1–10 mL), and fewer experiments (10^2 per day 'only') run under more-commercially relevant conditions. Catalysts that meet most or all pre-determined performance criteria ('leads') are then passed to a tertiary stage,

where they are optimized through structural elaboration, followed by conventional scale-up in bench reactors or pilot plants, with a view to industrial implementation. The first successful case histories reported in the open literature[9-11] seem to demonstrate a substantial shortening of the time elapsed from the initial hits to commercial exploitation.

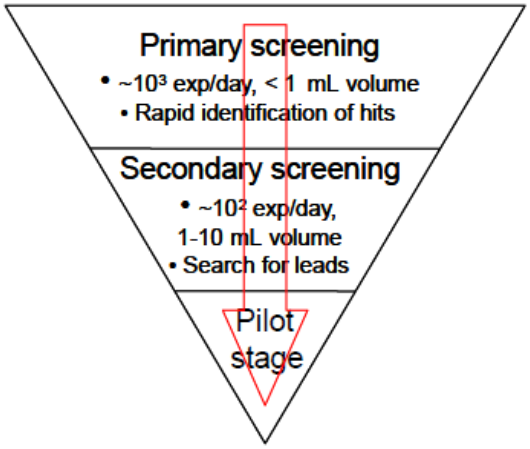

Figure 2.2. A typical open-sequence trial-and-error organometallic catalysis HTE workflow.[8]

In our opinion, the main drawback of this approach is a *low cost/effectiveness balance*. On the cost side, for a meaningful primary screening thousands of candidates need to be tested, which requires the availability of a suitably larger number of building blocks for ligand and precatalyst synthesis. Such huge chemical libraries are extremely demanding even for large companies, and definitely out of reach in academia. Concerning the effectiveness, while suited for the search of 'small molecule solutions' in fields like pharma chemistry[1] (where such solutions exist by definition, based on the principles of substrate-receptor interactions), it looks not obvious to us that the search should be productive in organometallic catalysis, particularly with molecular catalysts, where the assumption that a small molecule in the role of ancillary ligand to a metal can do the job is not necessarily correct.

For the above reasons, at LSP a different approach was implemented, in which the 'funnel-like' open-sequence trial-and-error HTE configuration of Figure 2.2 was changed into a HTC&HTE feed-back loop one (Figure 2.3). The main feature of this workflow is the early introduction of HTC, meant to represent an *in silico* equivalent of the primary screening of Figure 2.2. State-of-the-art DFT tools are used here to identify in-silico –among hundreds or thousands of model candidates– possible 'hits'; these are then experimentally prepared and screened in HTE platforms generating suitably large experimental databases of quantitative structure/activity relationships (QSAR), used

to benchmark and tune the HTC part, thus sustaining the HTC&HTE loop throughout catalyst structural amplification. This operation mode should ultimately produce a predictive QSAR model (hopefully but not necessarily of 'white-box' character), thus changing a blind into an oriented search. In this case too, the effectiveness of the approach has been demonstrated, e.g. in the structural amplification of bis(phenoxyamine)Zr and Hf catalysts[12], and more studies are currently in the pipeline.

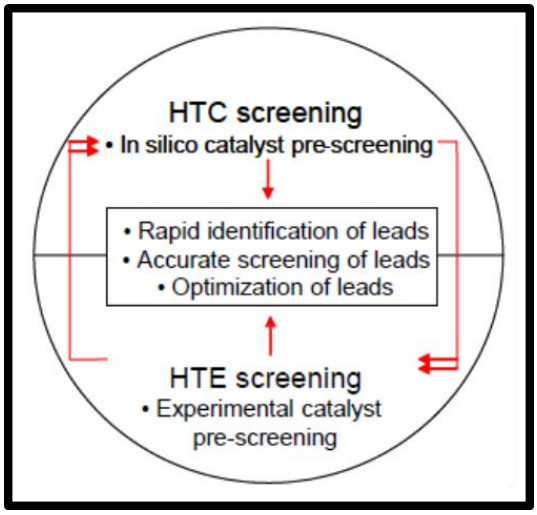

Figure 2.3. The feed-back loop configuration of the molecular catalysis HTC&HTE workflow at LSP.

The choice of HTE strategy best-suited to a given problem is not always univocal. For the one of interest to the present thesis, that is the exploration and rational improvement of HY-ZNCs for iPP, the extensive modulation of catalyst performance by means of electron donors introduced and discussed in Chapter 1 is a clear indication that the question does admit a 'small-molecule solution'. Moreover, as also noted before, the DFT tools to model ZN catalytic surfaces are not yet at the level of robustness and reliability that would be necessary for a meaningful HTC primary screening. Therefore, a trial-and-error approach starting with an experimental primary screening (Figure 2.2) looked like the most plausible option. On the other hand, after building up a QSAR database of adequate size, we wanted to use it for the implementation of white-box and/or black-box models able to interpret and predict the effects of electron donors on catalyst performance. Thus, our conclusion was that the best practice with these complicated heterogeneous catalyst systems is a proper combination of the approaches in Figures 2.2 and 2.3. A suitable workflow, as implemented at LSP, is shown in Figure 2.4.

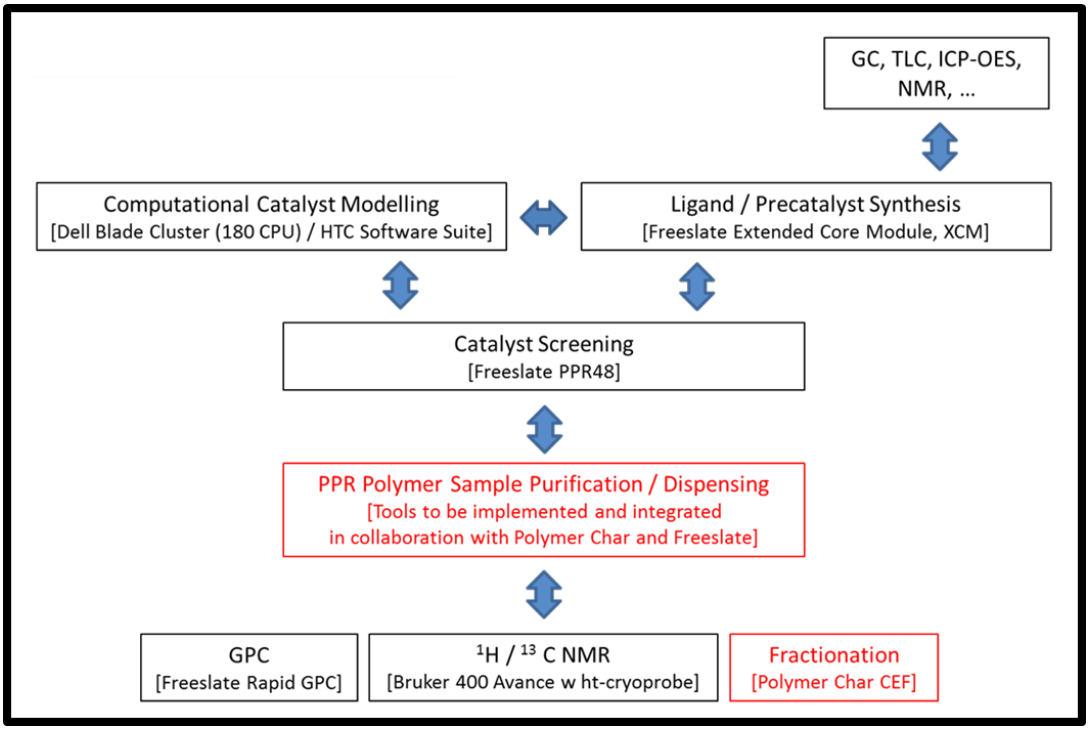

Figure 2.4. Layout of the HY-ZNC HTE workflow at LSP (in red, parts still under implementation).

At the heart of the workflow are two large state-of-the-art HTE platforms (described in detail in following sections), in which precatalyst activation and catalyst screening studies can be performed in an open sequence (Figure 2.2) or a closed sequence (Figure 2.3). Downstream to each platform and fully integrated with it are fast analytical tools which accommodate without bottlenecks the throughput of catalysts and polymers for the necessary characterizations; specially notable are a Freeslate Rapid-GPC setup[13], and a Bruker Avance III 400 NMR spectrometer[14] equipped with a high-temperature cryoprobe[15], both ensuring an individual PP sample analysis time (including ^{13}C NMR!) below 30 min, hence adequate to the throughput of the PPR48. As a result, in principle, every day some 50 catalyst systems can be prepared and tested, and the polymers thereof fully characterized at state-of-the-art level; to the best of our knowledge, this is the most powerful polyolefin catalysis workflow to operate in academic environment worldwide.

In absolute terms, the said throughput is not high to the point that the integration of the analytical tools with the HTE platforms must be on-line. As a matter of fact, sample transfer and preparation for the various analyses is presently manual, which does not create bottlenecks, but certainly represents a waste of human resources that could be more usefully employed otherwise. The implementation of robotic tools for the rapid dissolution, filtration, and dosing of polymer samples in view of GPC, DSC, NMR and CEF analysis is already in progress (in collaboration with Freeslate

and Polymer Char, in the framework of a project in the program of the Dutch Polymer Institute). A HTE tool, namely the Polymer Char Crystallization Elution Fractionation (CEF) setup[16], that was satisfactorily benchmarked and selected for the workflow to measure the Index of Isotacticity (I.I.) and crystallinity distribution curve of PP samples in small scale (down to 30 mg) and short time (less than 30 min), was not yet available for this thesis; PP fractionations were carried out by means of parallel Kumagawa solvent extractors, which was admittedly a pitfall in terms of data acquisition time and reliability.

2.3. Platforms and analytical tools

In this section, we describe the platforms and main analytical tools included in the workflow of Figure 2.4 and used in the present work. A compact overview is given in Table 2.1. More detailed specifications of the two HTE platforms and their use protocols are provided in the remaining part of this section and the following one, whereas the workflow analytics is covered in § 2.5. A final section (§ 2.6) is dedicated to workflow validation.

Table 2.1. List of platforms and integrated main analytical tools in the HY-ZNC HTE workflow of Figure 2.4.

Part/Function	***Unit Operation***	***Platform/Analytical Tool***
Computational Modeling	Parallel Computation	Cluster of DELL PowerEdge M610 Blade Servers (180 cpu's)
Precatalyst Activation	HTE Precatalyst Treatment	Freeslate Extended Core Module
	Metal Analysis	Agilent 700 series ICP- OES
	NMR Analysis	Bruker Avance 400
Catalyst Screening	Taring/Weighing	Mettler-Toledo Bodhan Balance Automator
	HTE Propene Polymerization	Freeslate PPR48
	Product Drying	Genevac EZ-2 Plus Drying Station
Polymer Characterization	GPC Analysis	Freeslate Rapid GPC
	$^{1}H/^{13}C$ NMR Analysis	Bruker Avance III 400 with high-temperature cryoprobe and robotic pre-heated sample changer

2.3.1. Freeslate Extended Core Module (XCM™) platform[17]

This platform (Figure 2.5) is a state-of-the-art HTE setup for parallel organic and organometallic synthesis. Housed in a triple high-performance MBraun LabMaster glove-box, it enables the robotic handling, weighing and dispensing of solid, liquid and slurry air-/moisture-sensitive compounds according to fully automated protocols.

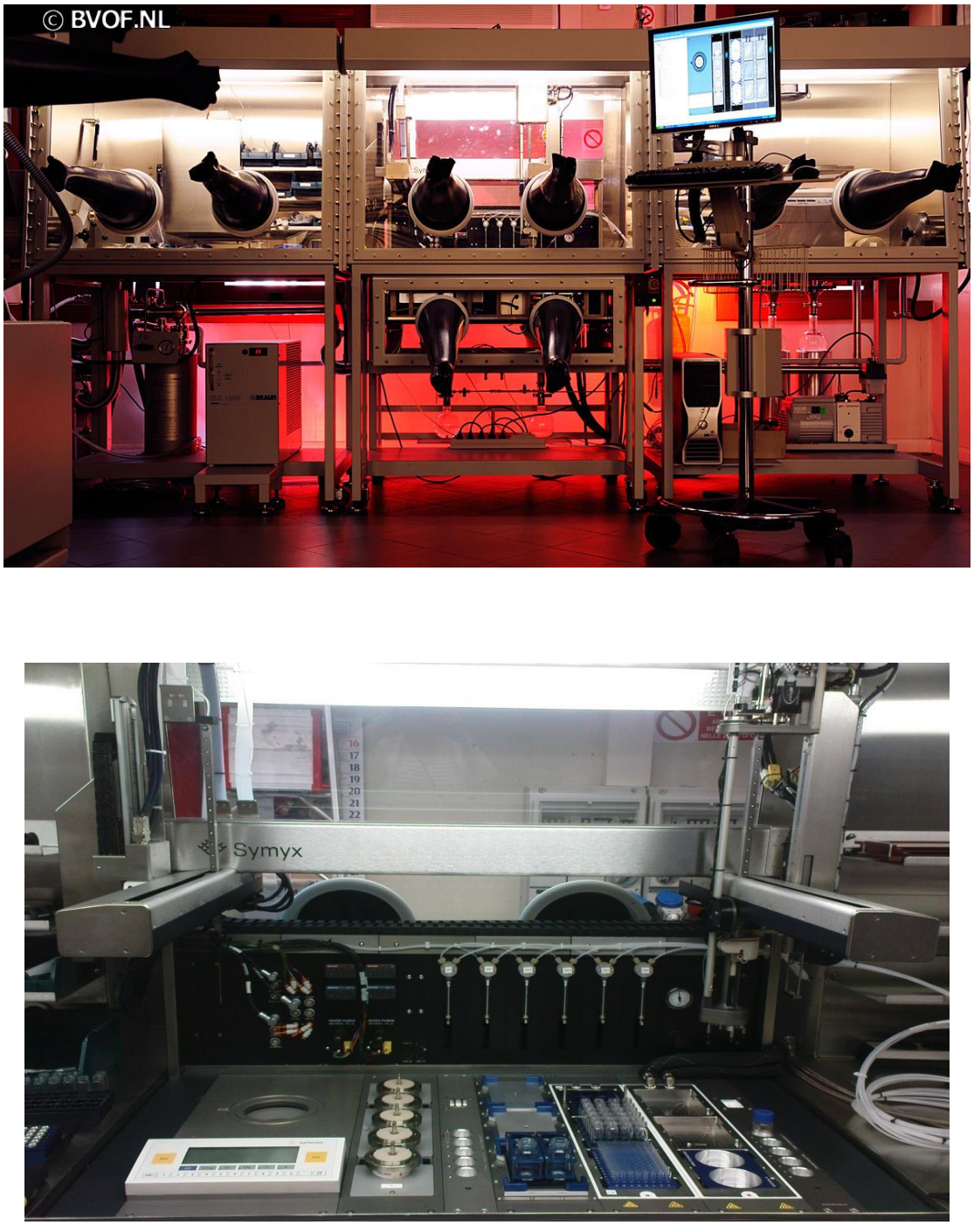

Figure 2.5. Overall view of the Freeslate Extended Core Module™ setup (top), and close-up of the experimentation deck (bottom).

The main features are:

- Two independent robotic arms bearing a vial gripper (right arm), and dedicated needles for handling solutions (right arm) and slurries (left arm)
- Heated/cooled reaction decks (arrays of 96x1 mL, 24x4 mL, 24x8 mL, 8x20 mL vials with individual magnetic stirring)
- Internal deck-integrated analytical balance (Sartorius WZ614-CW), with ion-suppressor system
- Powdernium™ Automated Powder Dosing System
- Solvent purification system (MBraun SPS-5, integrated off-line)
- Internal centrifugal drying station (Savant SPD121P)
- Two high pressure reactors (arrays of 96x1.0-1.2 mL, 25 bar max operation pressure at 200°C, with individual magnetic stirring), for primary screenings of organometallic catalysts
- Freeslate LEA software package (PPR Client®, Library Studio®, PolyView®, Epoch®, Impressionist®)
- Renaissance Application Server
- Oracle Database Server

2.3.2. Freeslate Parallel Pressure Reactor (PPR48) [18]

This platform (Figure 2.6) is a state-of-the-art HTE setup for the parallel secondary screening of organometallic catalysts under pressure. Equipped with 48 high-pressure mini-reactors, it is fully contained in a triple high-performance MBraun LabMaster glove- box.

Some of its main features are:

- 48 parallel, individually controlled mini-reactors (5 mL working volume, 35 bar maximum operating pressure, 200°C maximum operating temperature) specially designed for catalytic olefin polymerizations, equipped with disposable glass inserts and mechanical stirring with magnetically coupled heads and disposable paddles (800 rpm maximum stirring speed)
- Dual-arm, integrated liquid- and slurry-handling Cavro robot (with solution and slurry-injection needles)
- Dual injector ports for liquids and slurries
- MBraun SPS-5 solvent purification system, with solvent-line termini inside the glove-box

- Mixed-bed Grubbs-type catalyst columns for the purification of gaseous monomer (ethene and propene), with distribution lines plumbed into the mini-reactors
- Freeslate LEA software package (PPR Client®, Library Studio®, PolyView®, Epoch®, Impressionist®)
- Freeslate Renaissance Application Server
- Oracle Database Server

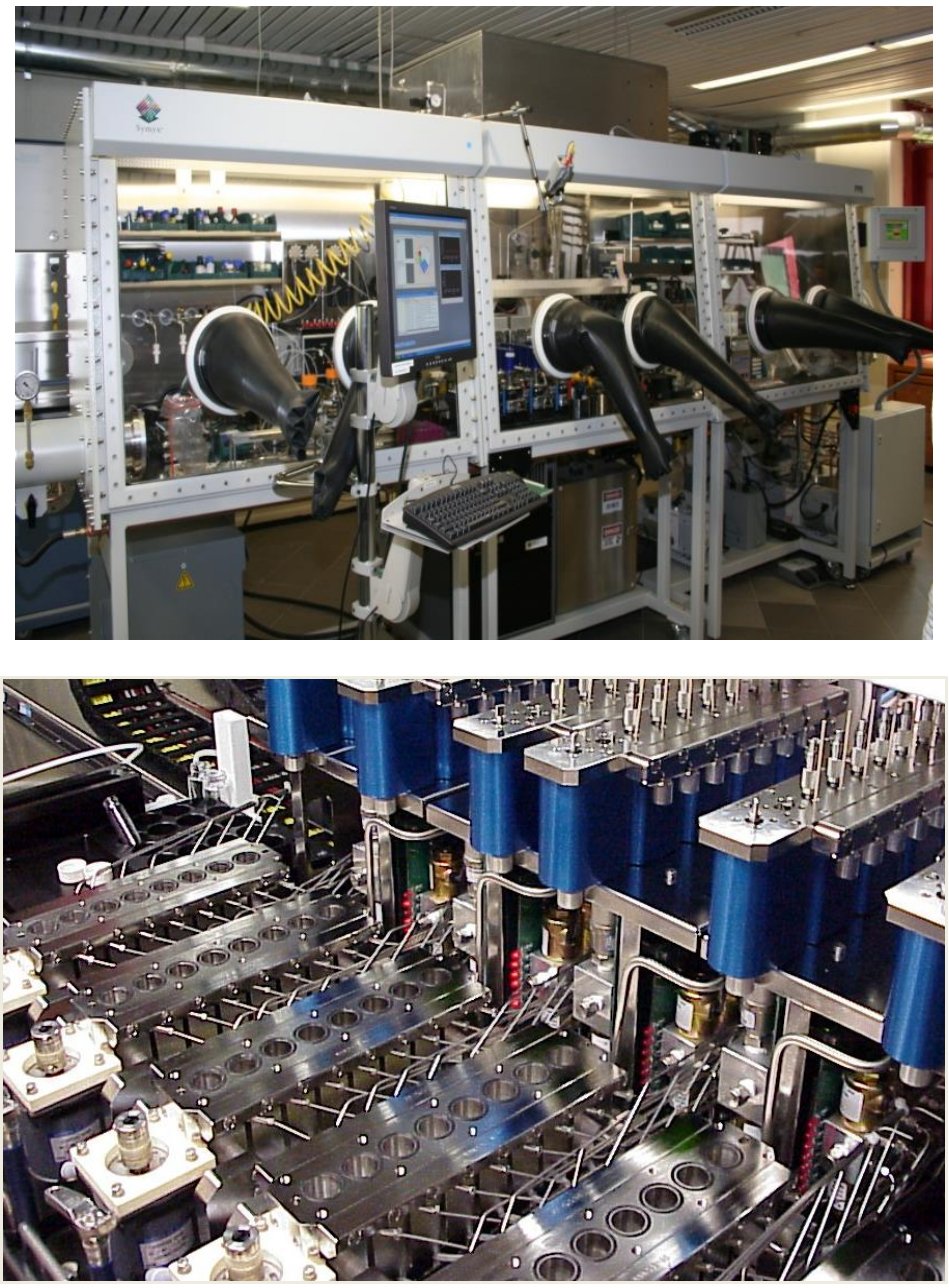

Figure 2.6. Overall view of the Freeslate PPR48 setup (top), and close-up of the 6 reaction modules with the 48 mini-reactors (bottom).

2.4. ‘Design of Experiment’ (DoE) and execution protocols

2.4.1. Preparing the DoE

The XCM™ and PPR48 platforms were used for HTE experiments of precatalyst activation (§ 2.4.2) and catalyst screening in propene polymerization (§ 2.4.3), respectively. In spite of the very different scope, the software suite for the ‘Design of Experiment’ (DoE) and the preparation of the related execution protocols was the same (namely, the Freeslate Library Studio® package). What follows is a schematic description of how a typical array of experiments (so-called ‘library’) was designed.

1. An empty 6x8 plate (in case of a PPR library) or a 6x4 plate (in case of an XCM™ library) is generated

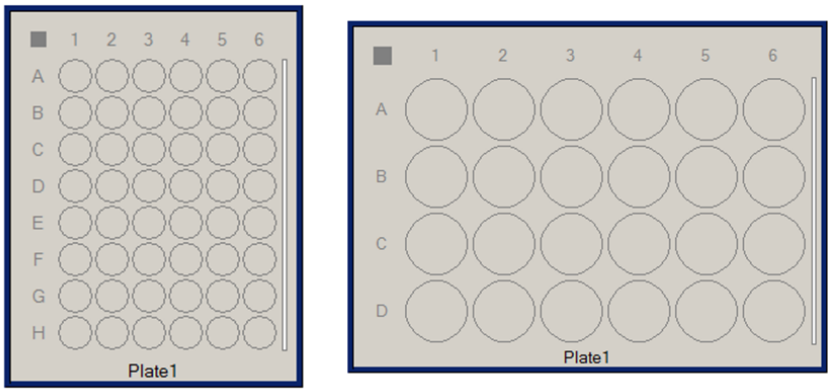

2. Chemicals are uploaded into the database, defined (in terms of name, molecular weight and density), and properly combined so as to obtain the starting solutions/mixtures

	Mixture				Component			
	Color	Name	Density	Inventory	Name	Role	Concentration	Unit
1		Diisobutyldimethoxysilane_50mM in Heptane	0,6859 Ideal Mixing		Diisobutyldimethoxysilar		50,0000	mmol/l
					Heptane			remainder
2		SABIC ZNiPP Catalyst 2.2wt% Ti_3mg/ml in hep	0,6849 Ideal Mixing		SABIC ZNiPP Catalyst :		3,0000	mg/ml
					Heptane			remainder
3		TEAL PreAlk_20mM in Heptane	0,6844 Ideal Mixing		TEAL Alkyl Premix		20,0000	mmol/l
					Heptane			remainder
4		TEAL scavenger_20mM in Heptane	0,6844 Ideal Mixing		TEAL scavenger		20,0000	mmol/l
					Heptane			remainder
5		Heptane_Chaser	0,6840 Ideal Mixing		Heptane		100,0000	vol%
6		Diisobutyldimethoxysilane_0.2mM	0,6859 Ideal Mixing		Diisobutyldimethoxysilar		50,0000	mmol/l
					Heptane			remainder
7		TEAL Activator_s	0,6844 Ideal Mixing		TEAL Alkyl		20,0000	mmol/l
					Heptane			remainder
8		TEAL Alkyl Premix_300mM	0,6902 Ideal Mixing		TEAL Alkyl Premix		300,0000	mmol/l
					Heptane			remainder

3. The thus-created solutions/mixtures are then added (following a specific order) to the plate cells, and given a tag (e.g. ‘solvent’, ‘scavenger’, ‘catalyst’, etc). The amount of each solution/mixture is automatically calculated based on an user-defined combination formula, which sets the chemical parameters (e.g. ‘total volume’, ‘molar ratio’, ‘catalyst amount’, etc). An example of chemicals additions to the 48 PPR cells is shown below

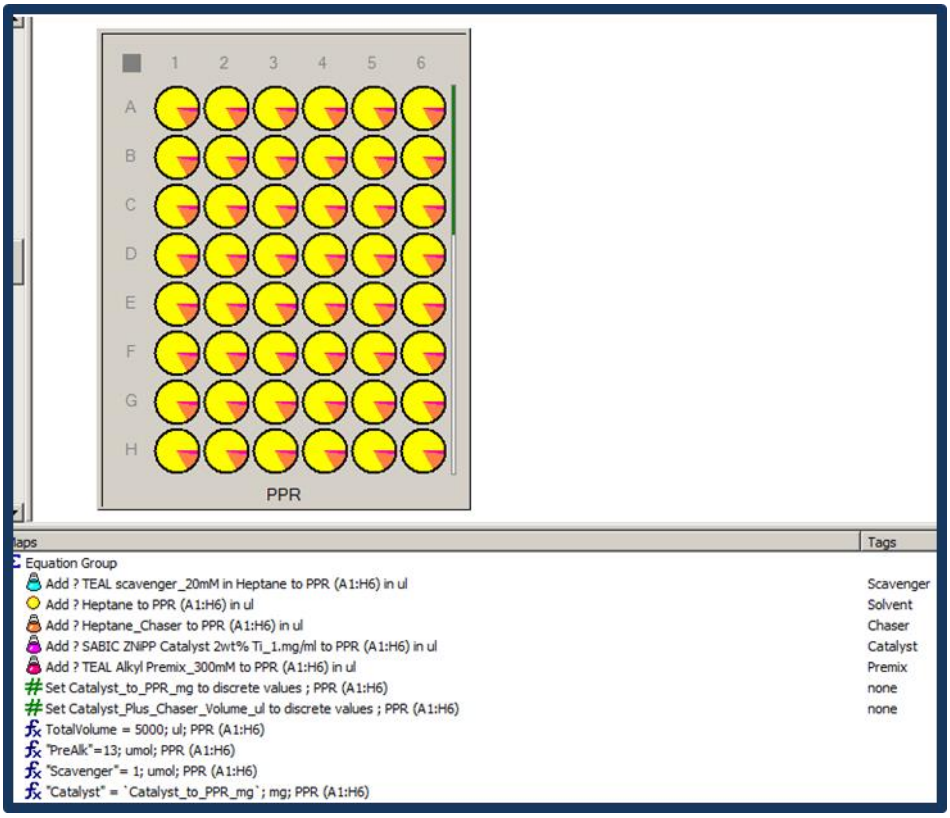

4. The operating reactor parameters are defined and individually set for each plate position

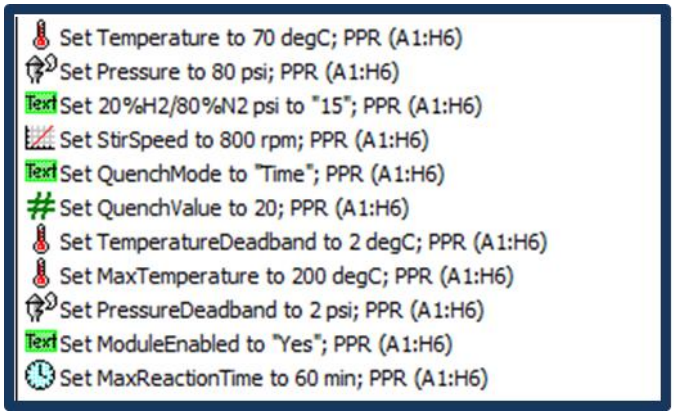

5. Finally, a worksheet is obtained, listing the amount requested for each solution/mixture, including the amounts of the individual starting chemicals.

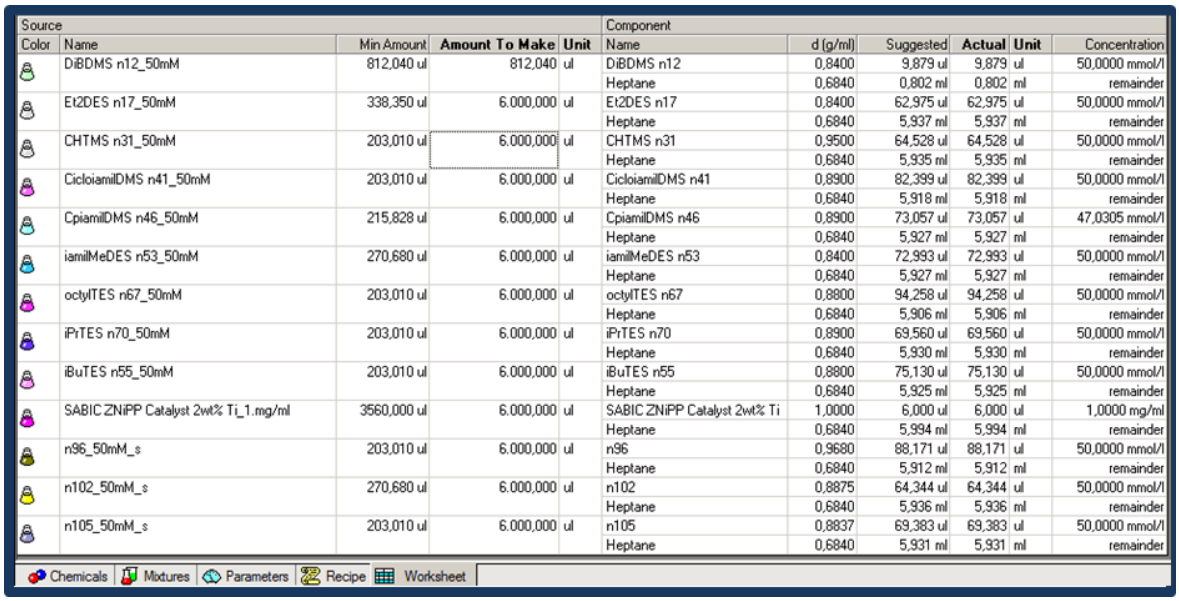

Source					Component					
Color	Name	Min Amount	**Amount To Make**	**Unit**	Name	d (g/ml)	Suggested	**Actual**	**Unit**	Concentration
	DiBDMS n12_50mM	812,040 ul	812,040	ul	DiBDMS n12	0,8400	9,879 ul	9,879	ul	50,0000 mmol/l
					Heptane	0,6840	0,802 ml	0,802	ml	remainder
	Et2DES n17_50mM	338,350 ul	6.000,000	ul	Et2DES n17	0,8400	62,975 ul	62,975	ul	50,0000 mmol/l
					Heptane	0,6840	5,937 ml	5,937	ml	remainder
	CHTMS n31_50mM	203,010 ul	6.000,000	ul	CHTMS n31	0,9500	64,528 ul	64,528	ul	50,0000 mmol/l
					Heptane	0,6840	5,935 ml	5,935	ml	remainder
	CicloiamilDMS n41_50mM	203,010 ul	6.000,000	ul	CicloiamilDMS n41	0,8900	82,399 ul	82,399	ul	50,0000 mmol/l
					Heptane	0,6840	5,918 ml	5,918	ml	remainder
	CpiamilDMS n46_50mM	215,828 ul	6.000,000	ul	CpiamilDMS n46	0,8900	73,057 ul	73,057	ul	47,0305 mmol/l
					Heptane	0,6840	5,927 ml	5,927	ml	remainder
	iamilMeDES n53_50mM	270,680 ul	6.000,000	ul	iamilMeDES n53	0,8400	72,993 ul	72,993	ul	50,0000 mmol/l
					Heptane	0,6840	5,927 ml	5,927	ml	remainder
	octylTES n67_50mM	203,010 ul	6.000,000	ul	octylTES n67	0,8800	94,258 ul	94,258	ul	50,0000 mmol/l
					Heptane	0,6840	5,906 ml	5,906	ml	remainder
	iPrTES n70_50mM	203,010 ul	6.000,000	ul	iPrTES n70	0,8900	69,560 ul	69,560	ul	50,0000 mmol/l
					Heptane	0,6840	5,930 ml	5,930	ml	remainder
	iBuTES n55_50mM	203,010 ul	6.000,000	ul	iBuTES n55	0,8800	75,130 ul	75,130	ul	50,0000 mmol/l
					Heptane	0,6840	5,925 ml	5,925	ml	remainder
	SABIC ZNiPP Catalyst 2wt% Ti_1.mg/ml	3560,000 ul	6.000,000	ul	SABIC ZNiPP Catalyst 2wt% Ti	1,0000	6,000 ul	6,000	ul	1,0000 mg/ml
					Heptane	0,6840	5,994 ml	5,994	ml	remainder
	n96_50mM_s	203,010 ul	6.000,000	ul	n96	0,9680	88,171 ul	88,171	ul	50,0000 mmol/l
					Heptane	0,6840	5,912 ml	5,912	ml	remainder
	n102_50mM_s	270,680 ul	6.000,000	ul	n102	0,8875	64,344 ul	64,344	ul	50,0000 mmol/l
					Heptane	0,6840	5,936 ml	5,936	ml	remainder
	n105_50mM_s	203,010 ul	6.000,000	ul	n105	0,8837	69,383 ul	69,383	ul	50,0000 mmol/l
					Heptane	0,6840	5,931 ml	5,931	ml	remainder

Chemicals | Mixtures | Parameters | Recipe | Worksheet

The library is then saved in the Oracle Database, and given an Identification Number (Library ID) through which the design is retrieved by the software controlling the platform (Freeslate Automation Studio® for the XCM™; Freeslate Impressionist® for the PPR).

2.4.2. Precatalyst activation experiments

The activation studies of HY-ZNCs were executed using the XCM™, under full control by the Freeslate Automation Studio® software, which provides a very user-friendly U/I panel ('Instrumentation Resource') enabling the control of all platform's resources (Figure 2.7). In a typical experiment, an aliquot of $MgCl_2$/$TiCl_4$/diisobutyl-*ortho*-phthalate (DBP) solid precatalyst is suspended in a hydrocarbon diluent (e.g. heptane), and added with aliquots of Al-Alkyl and External Donor (ED) solutions in the same hydrocarbon; the catalyst system is left to react for a desired time at a given temperature under magnetic stirring, after which the solid and liquid phases are separated, individually recovered, and sent to the analysis for the inorganic and organic part. Prior to the automated computer-controlled execution of the experiment, the following preliminary operations are performed:

- A proper number (24 for a typical experiment) of 8 mL vials (treated for at least 12 h at 200°C under vacuum) is labeled and placed into a 6x4 rack, which is then positioned onto an available slot of the deck
- Parylene™ coated magnetic mini-stir bars are added to all vials
- Solvent(s), heptane solutions of Al-Alkyl and ED are prepared, and placed on pre-defined deck positions
- The proper powder dispensing head of the Powdernium^{TM} is loaded with the precatalyst (whose amount is calculated based on the DoE)

The preparation of the mixtures, as well as the execution of the experiment, are controlled by a specific Automation Studio® procedure (Figure 2.8), after automatically retrieving from the Oracle Database the reaction conditions as set in the DoE for the library with the given ID.

Figure 2.7. Freeslate Automation Studio® U/I panel controlling the XCM^{TM} platform resources.

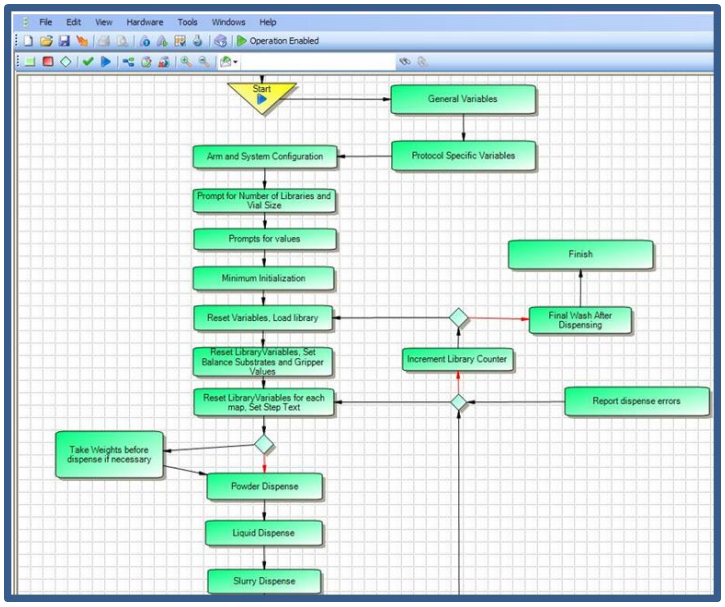

Figure 2.8. Freeslate Automation Studio® mixture preparation procedure.

The sequence of operations performed by the robot is as follows:

1. The powder dispensing head is taken out from the deck by coupling it with the left arm hopper
2. The following solid dispense loop is performed for each of the 24 vials:
    a. The vial is engaged by the right arm gripper and brought to the balance
    b. The powder dispensing hopper approaches the vial and doses the catalyst by weight
    c. The vial is then brought back by the right arm gripper to the original plate position
3. The right arm solution needle adds to all 24 vials the proper amounts of solvent (heptane), ED and Al-alkyl solutions (in chemical-loop mode)
4. Vials are capped and heated up to the reaction temperature. Once the temperature reaches the set point, the stirring is activated (800 rpm), and the reaction time counting starts
5. After reaching the desired reaction time, stirring is stopped and a cold quench is performed by manually transferring the vials into a cold metal plate
6. The solid phases are then separated from the liquid ones and washed as follows:
    i. The reaction vial rack is transferred to the Savant SPD121P centrifugal drying station, and centrifuged at 1400 rpm for 20 min
    ii. The rack is carefully placed back onto the Deck, so as to let the robot aspirate the supernatants (2.7 mL per vial, constituting the liquid phases of the mixtures)

which are transferred to labeled 4 mL vials and stored. Equivalent amounts of heptane are added to the reaction vials to wash the solid phases

7. Step #6 is repeated a second time identically, and a third time with pentane in the place of heptane
8. The rack is re-positioned into the Savant drying station, where it is kept at 45°C for 3 hours at 1400 rpm under vacuum for final drying
9. The thus-collected liquid and solid phases of the reacted catalyst mixtures are sent to the proper characterizations (see § 2.5).

2.4.3. Propene polymerization experiments

Propene polymerization experiments were executed in the PPR48 platform, under on-line monitoring and control of a dedicated Freeslate software (Impressionist®), through an interactive user-friendly window ('Active Experiment', Figure 2.9), which automatically retrieves from the Oracle Database the reaction conditions as set in the DoE associated with the given library ID.

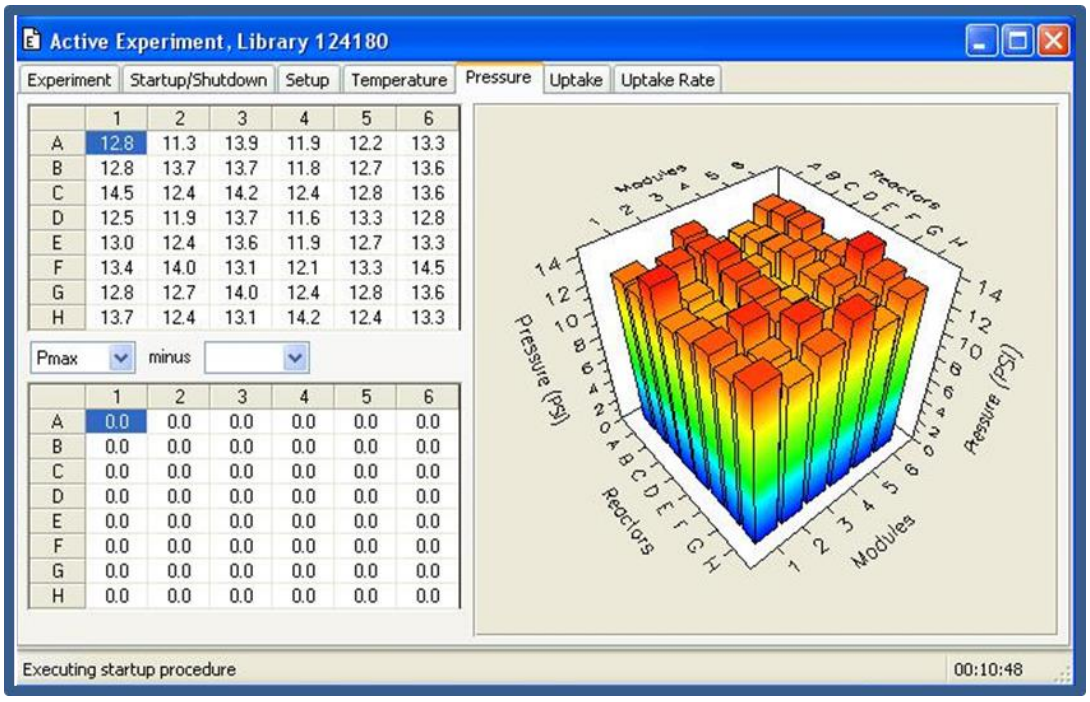

Figure 2.9. Impressionist® Active Experiment window monitoring the 48 PPR cells.

The preparation of the PPR48 platform in view of the polymerization library is performed as follows, under the guidance and control of the 'Start-up' Impressionist® procedure:

1. The upper parts of the reaction modules ('stir-tops') are taken off, and disposable pre-weighed glass vials (pre-treated for at least 12 h at 200°C under vacuum) and PEEK stirring paddles (pre-treated for at least 36 h at 250°C under vacuum) are placed into their dedicated housings
2. The stir-tops are then re-positioned, secured by tightening ten ¾" screws, and a leak test is performed to check the sealing of all modules (if detected, leaks are fixed)
3. Monomer Tescom® regulators, gas (monomer and quench) lines, and reactors are conditioned by 5 pressurization/depressurization cycles, followed by a continuous flow of propene for 1 min
4. 1.0 μmol of scavenger ($AlEt_3$) in 4.2 mL of heptane is dosed into each cell with a robotically operated syringe through the solution injection port
5. The modules are then pre-pressurized with 20 psi of propene, and a second pressure test is performed to make sure that the solvent injection did not compromise any cell's sealing
6. Next, 15 psi of a H_2/N_2 mixture (20/80 v/v) are added
7. The modules are then heated up to 70°C, and reactor stirring is activated (800 rpm)
8. A final pressure of 80 psi is reached by over-pressurizing the modules with further propene

Typical temperature and pressure trends throughout points 5-8 are shown in Figure 2.10.

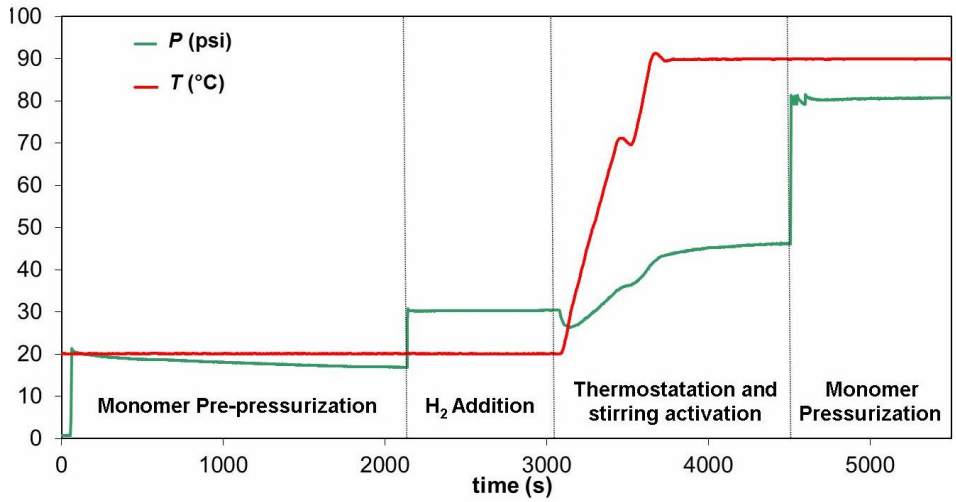

Figure 2.10. Typical temperature and pressure profiles throughout the PPR start-up phase for a representative reaction cell.

Once the reactor start-up is completed, and the reactors have been equilibrated for at least 10 min, the catalyst system is robotically prepared (according to the DoE), and injected sequentially

into the 48 cells based on a dedicated Impressionist® procedure ('Catalyst Injection'). The sequence of operations performed by a specially-designed robotic slurry needle is as follows:

- In a 1.2 mL glass vial, 3.4 μmol of ED and 68 μmol of $AlEt_3$ are pre-contacted at 23°C (glove-box internal temperature, maintained by a dedicated cooling unit) for 1.5 min in 1.1 mL of heptane ([ED]/[Al] = 0.05)
- Proper volumes of precatalyst slurry (1.0 mg mL^{-1} in isododecane, kept under vortexing in a 8 mL stainless steel vial) and of ED/$AlEt_3$ solution are sampled out of the respective vials with a robotically operated syringe (in which they are separated by a 50 μL nitrogen gap), and injected into each cell. Additional 'buffer' and 'chaser' heptane volumes, 'sandwiching' the chemically active aliquots in the syringe, are aspirated so as to achieve a clean injection, and reach a final working volume in each cell of 5.0 mL with an [Al]/[Ti] ratio of ~ 300.
- As the catalyst is injected into a given cell, a specific command ('Fire Event') is given by the injection procedure, starting the on-line monitoring of the polymerization. The cell pressure is continuously monitored, and any pressure drop resulting from the conversion of propene is compensated by adding more monomer, so as to keep the pressure at a constant value within a pre-set dead band (typically ±2 psi relative to the set point). Figure 2.11 illustrates a representative cell pressure profile throughout a propene polymerization experiment. The final increase is caused by the reaction quench with dry air (see below).

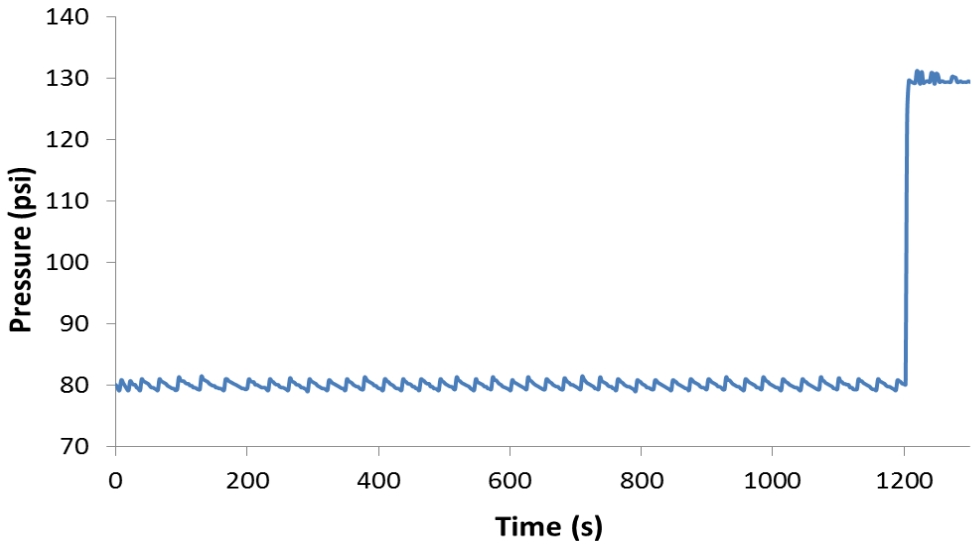

Figure 2.11. Typical pressure profile for a PPR48 cell during a propene polymerization experiment.

The integration of the pressure drop data over time gives, in pressure units, the overall conversion of propene (labeled as 'Uptake', and expressed in psi). The first derivative of the uptake with respect to reaction time corresponds to propene conversion rate ('Uptake Rate', expressed in psi/min). Both parameters are calculated, and plotted on-line on the PPR computer screen as the polymerization proceeds. Figure 2.12 shows typical plots of uptake and uptake rate versus time for the experiment whose cell pressure trace is reported in Figure 2.11.

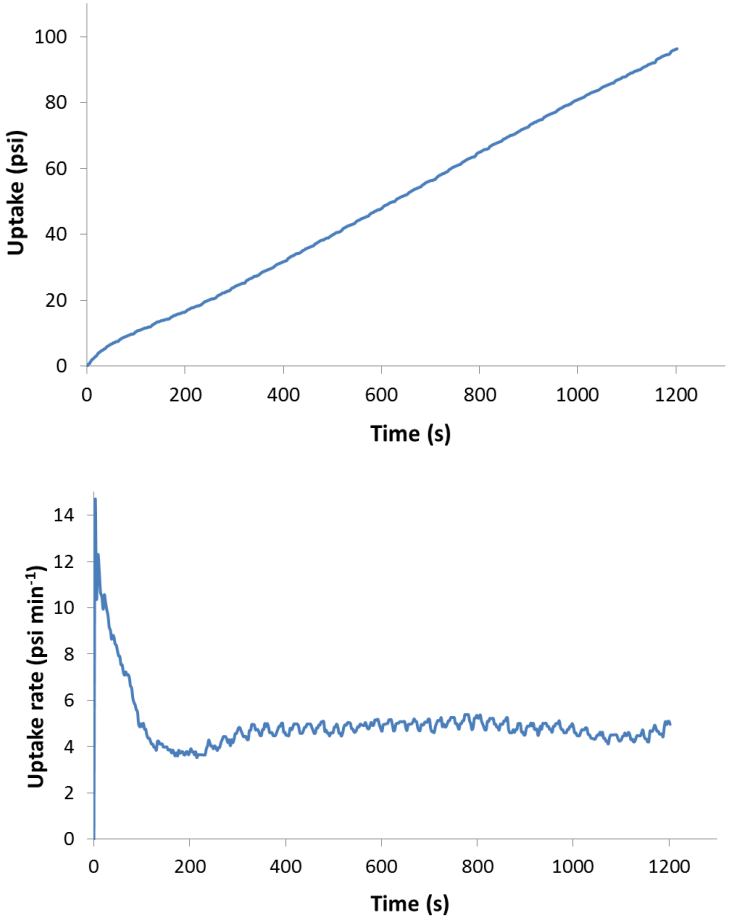

Figure 2.12. Typical profiles of propene uptake (top) and uptake rate (bottom) vs reaction time for a polymerization experiment in the PPR48 (for the pressure profile in the same experiment, see Figure 2.11).

- In order not to over-fill the mini-reactors, the polymerization is quenched once a desired reaction time or uptake value has been attained in each given cell, by over-pressurizing the cell with ~50 psi of dry air (oxygen is an effective poison for the active sites). This is clearly seen in Figure 2.11, showing the sudden increase in cell pressure at about 1200 s reaction time, which was the quench time set in the DoE for that specific cell.

Once all cells are quenched, the reactor cool-down procedure is started. The heating is switched off, and as soon as the temperature drops below 60 °C, the following operations are performed:

- The modules are de-pressurized, purged with nitrogen, and opened by unscrewing and taking off the stir-tops
- The disposable glass inserts containing the polymer samples in the hydrocarbon diluent are taken out
- The PEEK stirring paddles are removed and disposed
- The cells are gently cleaned up with heptane-soaked napkins
- The stir-tops are placed back and tightened
- The reaction modules are thoroughly decontaminated for at least 6 hours (most typically overnight), by means of a dedicated Impressionist® procedure ('Bake and Purge'), which heats them up to 90°C (or higher when deemed necessary), and performs nitrogen pressurization/depressurization cycles through the reactors and all gas lines.

The vials containing the polymerization products are then brought out of the glove-box, and transferred to a Genevac EZ2-Plus centrifugal evaporator (Figure 2.13), where they are dried to constant weight for 12 h at 60°C; this is checked by means of a Mettler-Toledo Bohdan Balance Automator (Figure 2.14). The weighing robot, used also at the experiment preparation stage to pre-weigh the disposable glass vials prior to their loading into the PPR48 cells, is controlled by a specific Freeslate integration software package, which uploads the readings directly into the Oracle Database. The polymer samples are then recovered and sent to the characterizations (§ 2.5).

Figure 2.13. Genevac EZ-2 Plus Drying Station.

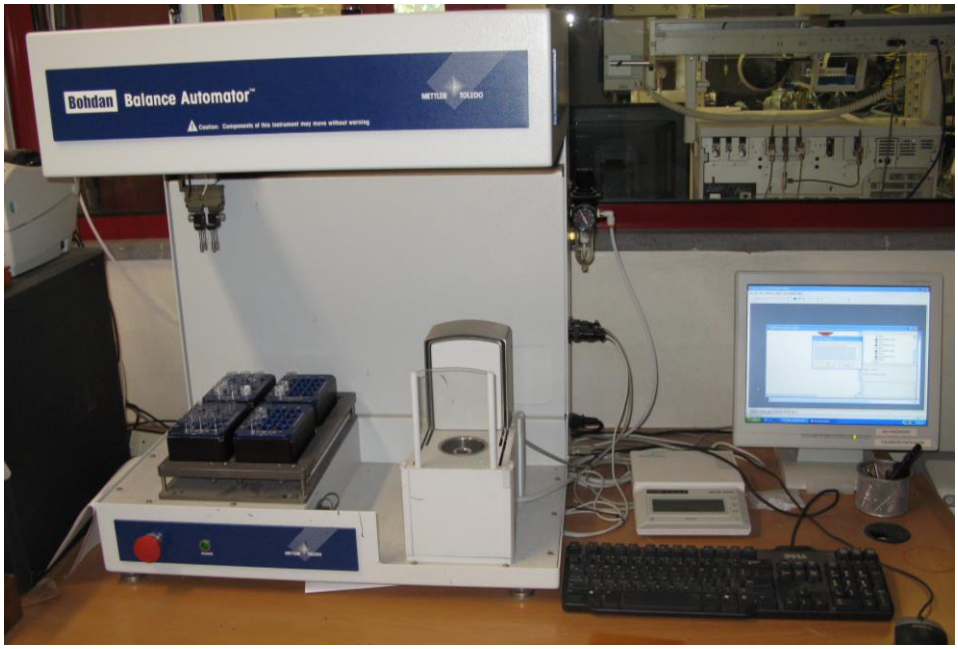

Figure 2.14. Mettler-Toledo Bodhan Balance Automator.

2.5. Analytical characterizations

2.5.1. Precatalyst activation experiments

The main objective of the precatalyst activation study of which under § 2.4.2 was to follow quantitatively the chemical processes that occur at the surface of a HY-ZNC for iPP following the reaction of the solid precatalyst with the liquid phase containing the Al-alkyl cocatalyst and the ED. As will be thoroughly discussed in Chapter 3, for the specific precatalyst of composition $MgCl_2/TiCl_4$/DBP it is known that under polymerization conditions the phthalate ID reacts with the Al-alkyl, which causes its desorption from the catalyst surface[19], and an extensive reduction of the ester groups ending up with the formation of a complex mixture of products (e.g. tertiary alcohols).[20] At the same time, ED and Al-alkyl molecules chemisorb in the place of the ID or at additional surface locations, and the Ti(IV) adducts are alkylated and reduced by the Al-Alkyl to active (Ti(III)?) and inactive (Ti(II?) species (a complex and still poorly understood process that may also lead to the removal of part of the Ti from the catalyst surface).[19]

As explained before, HTE experiments in the XCM^{TM} platforms were carried out to monitor the above chemistry under realistic conditions (albeit in the absence of monomer and H_2). In particular, after exposing the precatalyst to a variety of Al-alkyl/ED solutions at different reaction

times, the solid and liquid phases were separated, recovered, and analyzed to quantify their compositions.

Donor and metal quantifications for the solid phases were carried out by means of Nuclear Magnetic Resonance (NMR) and Inductively Coupled Plasma Optical Emission Spectrometry (ICP-OES), respectively. Quantitative ^{1}H NMR analyses were performed with a Bruker Avance DRX 400 spectrometer operating at 400 MHz, on methanol-d_4 solutions of ~20 mg aliquots of each solid. Acquisition conditions were: 5 mm probe; acquisition time, 3.0 s; relaxation delay, 5.0 s; pulse angle, 90°; spectral width, 10 ppm; 100 transients. Peak assignment was based on the literature, and preliminary ^{1}H NMR characterizations of the investigated donor molecules. A typical ^{1}H NMR spectrum of an activated solid phase after recovering and dissolution in the NMR solvent is shown in Figure 2.15. Quantitative determinations were based on peak integrations against that of an aliquot of acetonitrile added as an internal standard (methyl peak at δ = 2.05 ppm downfield of TMS).

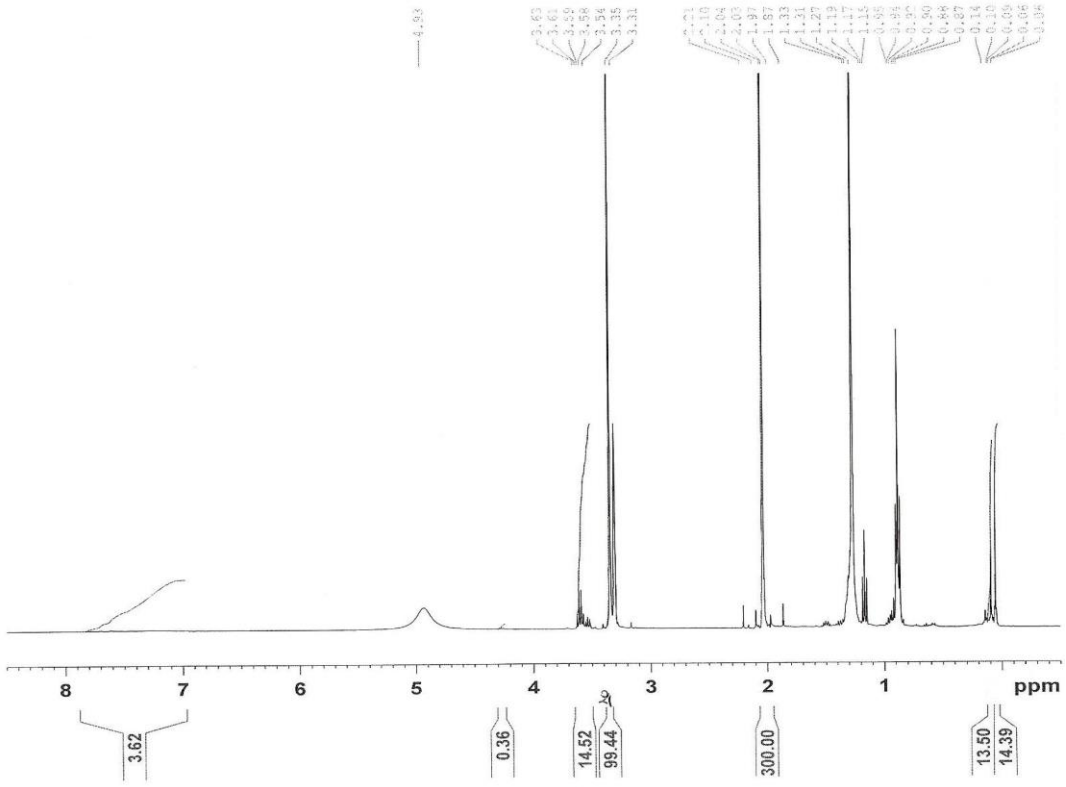

Figure 2.15. Typical ^{1}H NMR spectrum of a methanol-d_4 solution of the solid phase recovered after the exposure of a $MgCl_2/TiCl_4$/DBP phase to an AlR_3/Alkoxysilane combination.

ICP-OES analyses were carried out using an Agilent 700 series setup (Figure 2.16), on water solutions of the solid phases (~25 mg) treated in sequence with 2.0 mL of concentrated H_2SO_4,

2.0 mL of concentrated HNO_3, and (if needed) 2.0 mL of H_2O_2 (total time 16 hrs). The spectrometer was calibrated using commercial metal standard solutions (metal concentrations in the 1-100 ppm range).

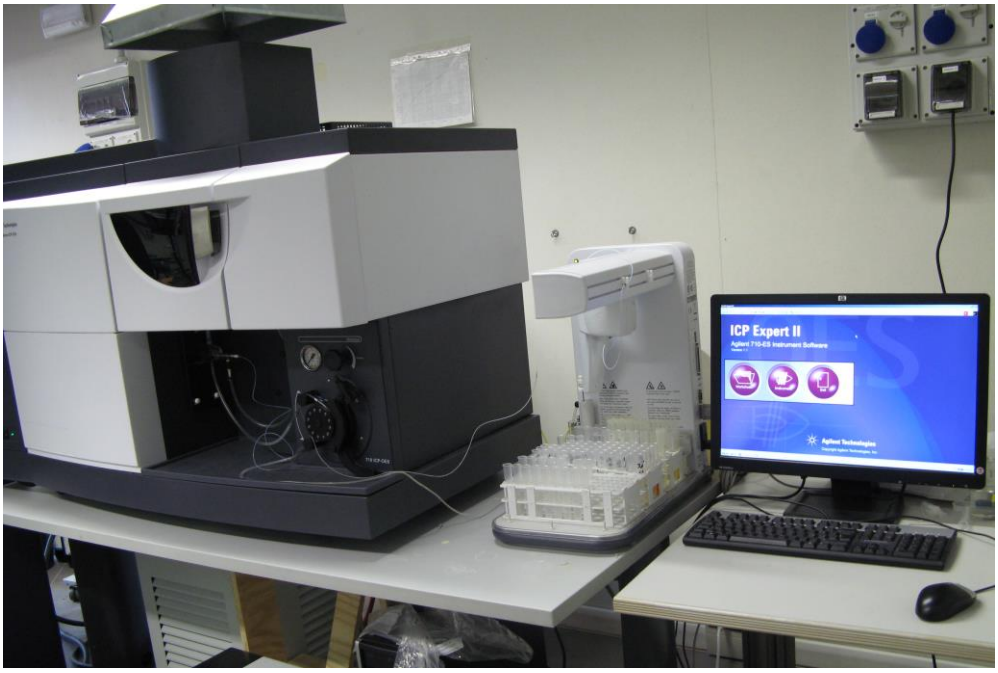

Figure 2.16. ICP-OES Agilent 700 series setup.

2.5.2. Propene polymerization experiments

All polymer samples produced in the PPR48 were characterized by means of high-temperature Gel Permeation Chromatography (GPC), to measure the molecular mass distribution; ^{1}H and ^{13}C NMR, to assess chain microstructure; solvent fractionation, to estimate the I.I. (Chapter 1).

GPC analyses were performed using a Freeslate Rapid GPC setup (Figure 2.17), equipped with a Polymer Char IR4 infrared detector, and a set of 2 mixed-bed Agilent PLgel 10 µm columns. The platform is controlled by the Freeslate Automation Studio® software, which directly uploads the results into the Oracle Database. Working on the preparation deck of the setup, polymer solutions in 1,2-dichlorobenzene (DCB), added with 0.25 mg/mL of 4-methyl-2,6-di-*tert*-butylphenol (BHT) as a stabilizer, were robotically prepared by dissolving a pre-weighed polymer amount in a volume of DCB/BHT so as to achieve a concentration of ~1.0 mg/mL; after 2 h at 160°C under gentle stirring to ensure complete dissolution, the samples were robotically injected into the system at 145°C. Due to the high DCB flow and the possibility to inject a sample solution in partial overlap to

the previous one, the individual analysis time was below 20 min. Universal calibration was carried out with 10 monodisperse polystyrene samples (M_n between 1.3 and 3700 KDa). In each 48-sample library, 2 samples were of a known iPP reference produced with an *ansa*-zirconocene catalyst, to check for consistency.

Figure 2.17. Overall view of the Freeslate Rapid GPC setup (top), and close-up of the robotic sample preparation deck (bottom).

Quantitative ^{1}H and ^{13}C NMR spectra of the polymers were recorded with a Bruker Avance III 400 spectrometer (Figure 2.18-top), equipped with a high-temperature cryoprobe (for 5 mm tubes)

and a robotic pre-heated sample changer (Figure 2.18-bottom). The unique S/N ratio of this setup, almost 10-fold higher than for a conventional spectrometer, results into an almost 100-fold reduction in acquisition time to achieve a given S/N value.

Figure 2.18. Overall view of the Bruker Avance III 400 NMR spectrometer (top), and close-up of the pre-heated robotic sample-changer (bottom).

Polymer solutions (30 mg/mL in tetrachloroethane-1,2-d_2 added with 0.25 mg/mL BHT) were prepared and analyzed at 125°C under the following conditions:

- *^{1}H NMR:* 10.0 ms pulse width (90° pulse); 32K time domain data points; 10 ppm spectral width; 2.0 s acquisition time; 10 s relaxation delay; 1 transient
- *^{13}C NMR*: 4.5 ms pulse width (45° pulse); 64K time domain data points; 240 ppm spectral width; 2.3 s acquisition time; 5.0 s relaxation delay; 1.5K transients

Waiting for the implementation of a Polymer Char CEF setup (Figure 1.4), I.I. measurements were carried out by means of solvent fractionation in a custom-made setup for parallel Kumagawa extractions (6 at a time), downscaled with respect to conventional ones so as to accommodate the low amounts of polymer (100-150 mg) produced in the PPR48 mini-reactors. In order to obtain I.I. values close to those resulting from the hot-xylene method (Chapter 1), we found out that extraction with boiling pentane is the best option (the I.I. value corresponding to the weight fraction of insoluble polymer). Exhaustive Kumagawa extraction required a reflux time of 8 hrs; running the setup twice a day represents a moderate bottleneck to the workflow, considering that the number of different PP samples obtained in one 48-cell library ranges between 15 and 20, because the polymerization experiments for secondary screening purposes are carried out in duplicate/triplicate and include up to 6 internal reference cells (Chapter 4).

2.6. Validation of the HTE platforms

2.6.1. XCM^{TM} platform

To validate the protocol implemented for the investigation of HY-ZNC activation (§ 2.4.2), and the XCM^{TM} platform used for its execution, several aliquots of the same $MgCl_2/TiCl_4$/DBP precatalyst were reacted with $(Me)_2Si(OEt)_2$ and/or $AlEt_3/(Me)_2Si(OEt)_2$ solutions, and the ID, ED, Ti and Al contents of the solid phases recovered after the reaction measured by means of ^{1}H NMR and ICP-OES (Table 2.2). In spite of the miniaturization of the equipment, and the extreme reactivity of the systems, the absolute error on the results is fairly small (of course, the relative error is comparatively large on low measured amounts).

Table 2.2. ID, ED, Ti and Al contents, as determined by ^{1}H NMR and ICP-OES, of the solid phases recovered after reacting aliquots of a $MgCl_2/TiCl_4$/DBP precatalyst with $(Me)_2Si(OEt)_2$ (**Catalyst System 1**) and $AlEt_3/(Me)_2Si(OEt)_2$ (**Catalyst System 2**) in heptane slurry at 70°C.

Catalyst System 1			**Catalyst System 2**				
Cell #	ID [a,b,c]	ED [a,b]	Cell #	ID [a,b,c]	ED [a,b]	Ti [a,d]	Al [a,d]
1	5.2	0.54	9	2.4	4.9	5.44	9.48
2	7.0	0.24	10	2.5	4.5	5.93	10.59
3	6.9	0.23	11	2.2	4.1	5.69	10.29
4	6.0	0.24	12	2.0	4.1	5.78	9.84
5	6.4	0.25	13	1.8	5.9	5.68	10.53
6	5.9	0.18	14	1.8	6.2	5.78	10.04
7	6.8	0.22	15	1.3	6.4	5.65	10.25
8	6.0	0.33	16	1.4	5.3	5.67	10.04
Averages:	6.3 ± 0.6	0.28 ± 0.11	*Averages:*	1.9 ± 0.4	5.2 ± 0.9	5.70 ± 0.14	10.1 ± 0.4

Reaction conditions: *T* = 70°C; heptane diluent, 3.8 mL; precatalyst amount, 25 mg; [Al]/[Ti] = 25; [Si]/[Al] = 0.10; contact time = 30 min.
[a] mol% wrt Mg. [b] ^{1}H NMR. [c] Initial content, 7.9 mol% wrt Mg. [d] ICP-OES.

2.6.2. PPR48 platform

Running propene polymerization experiments in hydrocarbon slurry with a HY-ZNC under industrially relevant conditions using mini-reactors contained in a glove-box is not a trivial exercise. A first delicate and critical issue is how to sample and dispense reproducibly a solid catalyst in minute amounts (≤0.10 mg; larger quantities would lead to excessive polymerization rates and poor reactor control) out of a catalyst slurry without problems of sedimentation or separation, the latter possibly favored by the known accumulation of static charges in the glove-box environment.

In the first place, one should realize that 0.10 mg of a typical HY-ZNC correspond to a number of secondary particles in the 10^3-10^4 range; per se, this is adequate to a reproducible sampling in a slurry volume of 0.1-1.0 mL. The slurry injection system of the Freeslate PPR48 has been engineered to effectively overcome the problems related with the possible decantation of the slurry or sedimentation of the catalyst in the syringe and along the transfer lines down to the injector port. In particular, a smart design of the needle, featuring a sealed round tip and a side opening, ensures that (a) piercing the rubber septum which seals the injection port occurs

smoothly with minimal rupture risk, and (b) the slurry is injected from inside the mini-reactor gas cap parallel to its long axis, hence straight into the liquid phase (Figure 2.19).

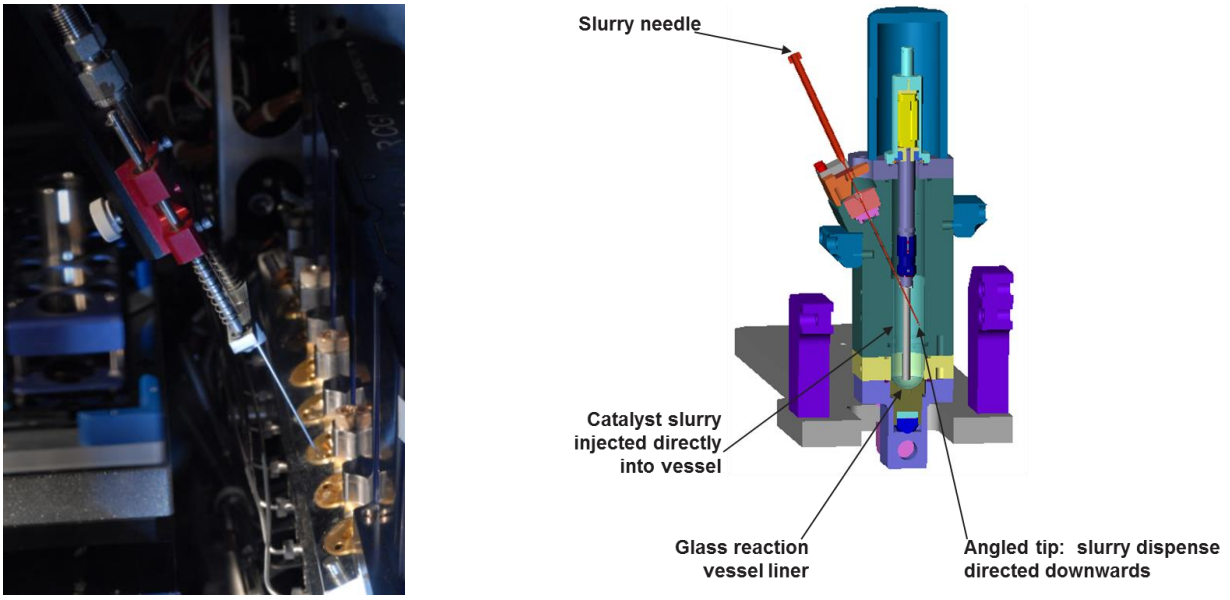

Figure 2.19. Close-up of the slurry needle of the Freeslate PPR48 approaching an injector port (left), and schematics of needle, injector port and reaction cell design (right).

Equally important, albeit less sophisticated, precautions entail the use of a stainless steel vial (Figure 2.20) for the precatalyst slurry, to prevent the accumulation of static charges on the walls and disperse those on the catalyst particles, and of a hydrocarbon diluent featuring low volatility and moderate viscosity (e.g. isododecane). Last but not least, keeping the vial constantly under intensive vortexing (800 rpm) is an obvious recommendation (Figure 2.20).

Figure 2.20. Stainless-steel vial containing the precatalyst slurry, housed in a high-speed vortexer.

The catalyst dispensing system and protocol were validated by simulating the process with open 8 mL glass vials as destination, instead of the PPR48 reaction cells. Several slurry aliquots were collected throughout a period of time similar to that needed for the execution of a library of polymerization experiments (4 h), and sent to OES-ICP analysis (for details see § 2.5.1). Based on the measured Ti contents, the overall solid amounts dispensed to the individual vials were calculated, and compared to the designed ones. Typical results are reported in Table 2.3 and shown graphically in Figure 2.21; the agreement is impressive, with a standard deviation as low as 2%.

Table 2.3. Results of a representative HY-ZNC slurry dispensation test.

Aliquot #	Aliquot Volume (µL) [a]	Ti, expected (µg) [b]	Ti, measured (µg)	Agreement (%)
1	75	480	466	97
2	100	640	637	100
3	120	768	789	97
4	80	512	526	97
5	80	512	514	100
6	100	640	605	95
7	150	960	961	100
8	150	960	913	95
9	80	512	473	92
10	75	480	463	96
11	100	640	611	95

[a] Slurry concentration, 2.0 mg/mL. [b] Ti content of the precatalyst, 3.2 wt%.

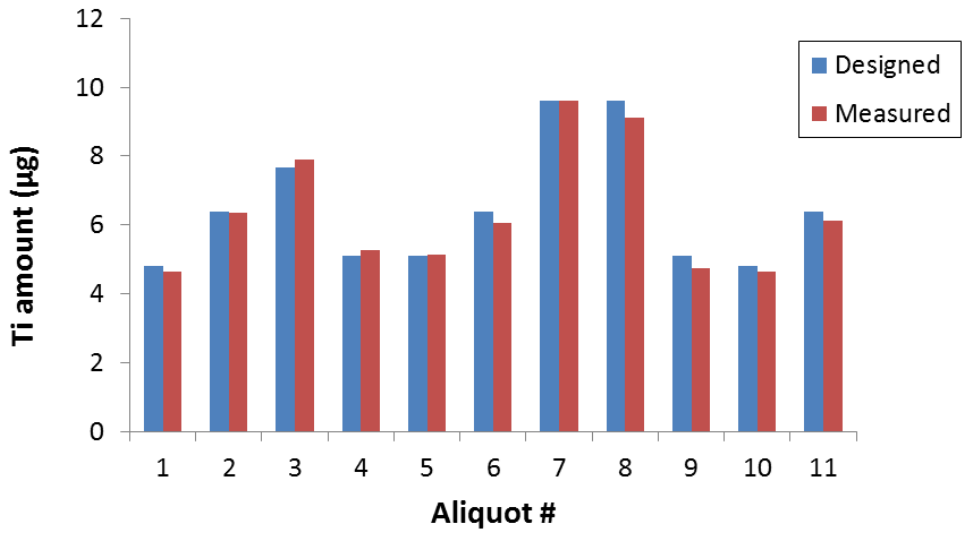

Figure 2.21. Results of a representative HY-ZNC slurry dispensation test (data from Table 2.3).

Other possible causes of poor reproducibility are mini-reactor contamination (e.g. resulting from solvents, monomers, glassware etc), poor reaction control (e.g. temperature and pressure fluctuations, reactor leaks, etc), and mass transfer limitations (e.g. due to inadequate stirring). To evaluate this part, we carried out sets of propene polymerization experiments with an industrial HY-ZNC system of composition $MgCl_2/TiCl_4$/DBP – $AlEt_3/(^iBu)_2Si(OMe)_2$, chosen as a validation standard.

A representative case is shown in Figure 2.22, where we plot the observed polymer yields as a function of the injected catalyst amounts in a library of experiments in heptane slurry at 70°C. The linear relationship demonstrates that all hypothesized sources of irreproducibility are negligible; in particular, the amount of catalyst lost due to system contamination, estimated by extrapolation to zero yield, was as low as 0.008 ± 0.005 mg, that is less than 10% of a typical catalyst loading in a PPR48 cell. Moreover, Figure 2.22 rules out the hypothesis of mass-transfer limitations in the explored range of catalyst loading.

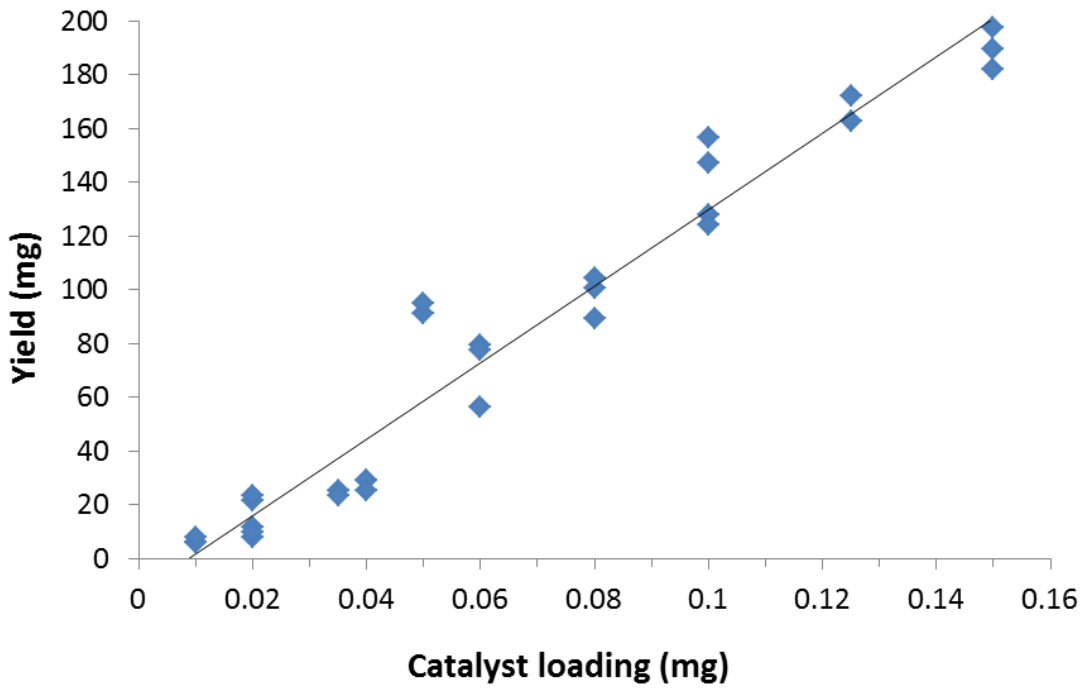

Figure 2.22. Polymer yield as a function of catalyst loading for a PPR48 library of propene polymerization experiments in the presence of catalyst system $MgCl_2/TiCl_4$/DBP – $AlEt_3/(^iBu)_2Si(OMe)_2$. Reaction conditions: T =70°C; $p(C_3H_6)$ = 4.4 bar; $p(H_2)$ = 0.20 bar; heptane diluent, 5.0 mL; [Al]/[Ti] ~ 550; [Si]/[Al] = 0.10; reaction time, 20 min.

Another typical validation test is provided in Table 2.4, reporting data of propene polymerization and PP sample characterizations for an identical set of 8 PPR48 experiments (1 reaction module)

with the same catalyst system and reaction conditions of Figure 2.22. All values of standard deviation are at 'physiological' levels; in particular, that on catalyst productivity is what would be accepted for a '*good*' conventional bench reactor, and those on average polymer molar masses are as expected for high-quality GPC measurements.[21] The only partial exception is the I.I. measurement, suffering somehow from the low sample amounts (as already explained in § 2.5.2); this confirms the need to implement a different evaluation method (i.e. CEF analysis, Figure 2.4).

Table 2.4. Results of 8 identical PPR48 propene polymerization experiments in the presence of catalyst system $MgCl_2/TiCl_4$/DBP – $AlEt_3/(^iBu)_2Si(OMe)_2$ in heptane slurry at 70°C.

Library ID #	Cell	R_p [a]	I.I. (%)	M_n (KDa)	M_w (KDa)	M_w/M_n	[*mmrrmm*] [b]
118680	1A	49.9	96.2	44	185	4.2	.40
	3A	62.4	96.2	41	169	4.1	.34
	1B	51.3	95.8	55	210	3.8	.36
	2B	58.4	95.4	51	222	4.4	.38
	3B	48.6	94.5	44	190	4.3	.40
	1C	56.1	96.7	53	225	4.2	.39
	3C	57.8	94.4	43	210	4.9	.34
	2D	56.8	94.3	53	278	5.2	.39
averages:		55 ± 5	95.4 ± .9	48 ± 5	210 ± 30	4.4 ± .4	.37 ± .02

Reaction conditions: T = 70°C; $p(C_3H_6)$ = 4.4 bar; $p(H_2)$ = 0.20 bar; heptane diluent, 5.0 mL; [Al]/[Ti] ~ 200; [Si]/[Al] = 0.10; reaction time, 20 min.
[a] Catalyst productivity, in $g_{PP}\, mg_{Ti}^{-1}\, h^{-1}\, bar^{-1}$. [b] ^{13}C NMR fraction of isolated stereodefects in the 'isotactic' (boiling-pentane-insoluble) PP fraction.

One last demonstration of reliability of the PPR48 platform is given in Table 2.5, reporting results of average productivity in propene polymerization measured for the aforementioned catalyst system, under the experimental conditions of Table 2.4, in identical experiments carried out in independent libraries throughout a period of several weeks. The observed value of standard deviation (10%) is practically identical to that obtained for identical experiments carried out in one given library (Table 2.4), which is a remarkable demonstration of reproducibility not only for the PPR48 setup, but also for the overall platform and integrated tools.

Table 2.5. Results of identical propene polymerization experiments belonging to different PPR48 libraries in the presence of catalyst system $MgCl_2/TiCl_4$/DBP – $AlEt_3/(i\text{Bu})_2Si(OMe)_2$.

Library ID	Library date	No. of replicas	$R_{p,av}$ [a]
106380	26/05/2008	3	61
106440	28/05/2008	2	65
106500	30/05/2008	2	65
106880	12/06/2008	2	50
106700	6/06/2008	2	55
107960	31/10/2008	11	70
106800	10/06/2008	2	56
106600	4/06/2008	3	60
106940	13/06/2008	2	56
106980	17/06/2008	4	61
106740	9/06/2008	2	59
			60 ± 6

Reaction conditions: T = 70°C; $p(C_3H_6)$ = 4.4 bar; $p(H_2)$ = 0.20 bar; heptane diluent, 5.0 mL; [Al]/[Ti] ~ 200; [Si]/[Al] = 0.10; reaction time, 20 min.
[a] $g_{PP}\, mg_{Ti}^{-1}\, h^{-1}\, bar^{-1}$

2.7. Upscaling of PPR data

2.7.1. Introduction

In § 2.6.2 we demonstrated that the polymerization data obtained with the PPR48 platform are very reliable and consistent. The next question is to what extent such data are representative of the behavior of larger reaction units, such as the bench and pre-pilot slurry and gas-phase ones typically used in industry.

In the framework of this thesis, a translatability study was performed in collaboration with Sabic (Competence Center of Geleen, The Netherlands), as a part of the program of an ongoing bilateral Research Collaboration Agreement with LSP. In particular, the propene polymerization performance of 5 different HY-ZNCs in the PPR48 at LSP with that in a gas phase installation ('TORR') at Sabic were compared. Figure 2.23 shows a picture of the latter unit.

Figure 2.23. The 'TORR' gas-phase reactor at the Sabic Competence Center of Geleen (The Netherlands).

2.7.2. Platform and protocol comparisons

The main features of the PPR48 HTE platform were described in § 2.3.2. A comparison with those of its industrial counterpart can be found in Table 2.6.

Table 2.6. Propene polymerization conditions for comparative experiments in the PPR48 platform at LSP and the 'TORR' installation at Sabic.

	PPR	TORR
Reactor phase	Slurry	Gas
Reactor operative volume (L)	0.05	1.8
Polymerization total pressure (barg)	5.5	20
Polymerization temperature (°C)	70	70
Polymerization time (min)	20	60
p_{H2}/p_{C3H6}	0.045	0.042
Catalyst loading (mg)	0.10	15
Al/Ti (mol/mol)	200	200
Al/Si (mol/mol)	20	10
Typical yield (g *per* experiment)	~ 0.2	~ 300

The propene polymerization protocol for the TORR installation was structured so as to mimic as close as possible PPR operation (§ 2.4.3); an objective limitation in this respect is that the PPR cells work on slurries, whereas the 'TORR' operates in gas-phase. In detail, the protocol was as follows:

- At ambient conditions, AlR_3, ED and precatalyst are sequentially added to the reactor under a light nitrogen outflow (15 mg of catalyst, [Al]/[Ti] = 200, [Al]/[Si] = 10)
- Heptane is added so as to reach a total volume of 8 mL
- The reactor is heated up to 70°C and pressurized at 20 barg with propene and hydrogen
- When the chosen experimental conditions are reached, the reaction time count starts.
- As the reaction proceeds, the total pressure is kept constant by adding propene and hydrogen, and the hydrogen level is kept at 4 % (constantly measured via on-line GC)
- After 1 hour reaction time, the reactor is depressurized, cooled down to RT and the polymer is taken out.

2.7.3. Results and Discussion

Five HY-ZNC systems, that is combinations of the same $MgCl_2/TiCl_4$/DBP precatalyst with $AlEt_3$ and 5 different alkoxysilane EDs, were tested in the PPR48 and TORR platforms under comparable conditions. The polymerization results are reported comparatively in Table 2.7. The correlations between catalyst productivities and PP average molecular masses are shown in Figures 2.24 and 2.25, respectively.

Table 2.7. Comparison of the main results of propene polymerization in the presence of $MgCl_2/TiCl_4$ /DBP – $AlEt_3$/ED catalyst systems in the PPR48 and the 'TORR' gas-phase reactor.

	R_p (% STD)		M_w (KDa)		M_w/M_n		I.I. (%)		[*mmrrmm*]	
ED	PPR	TORR	PPR	TORR	PPR	TORR	PPR	TORR	PPR	TORR
1	89	100	172	165	4.4	4.5	97	97	0.42	0.4
2	72	48	170	145	5.0	3.9	97	98	0.31	0.2
3	66	73	245	178	4.9	4.7	98	97	0.51	0.5
4	88	73	341	295	8.7	5.6	98	98	0.30	0.2
5	116	91	175	208	5.6	4.1	97	98	0.43	0.3

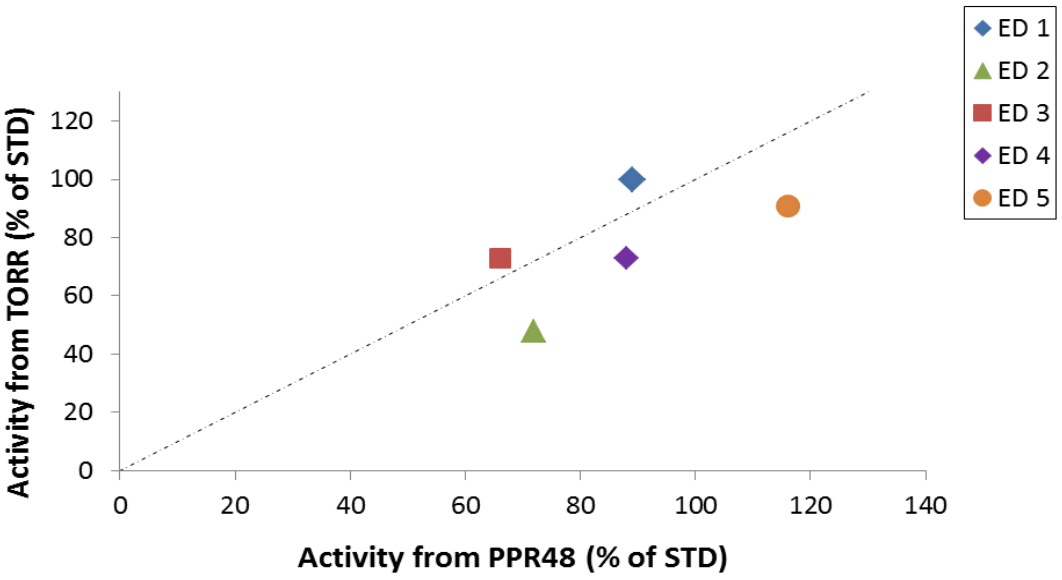

Figure 2.24. Correlation between observed catalyst productivities in the PPR48 and the 'TORR' installation for the five tested HY-ZNCs (data from Table 2.7).

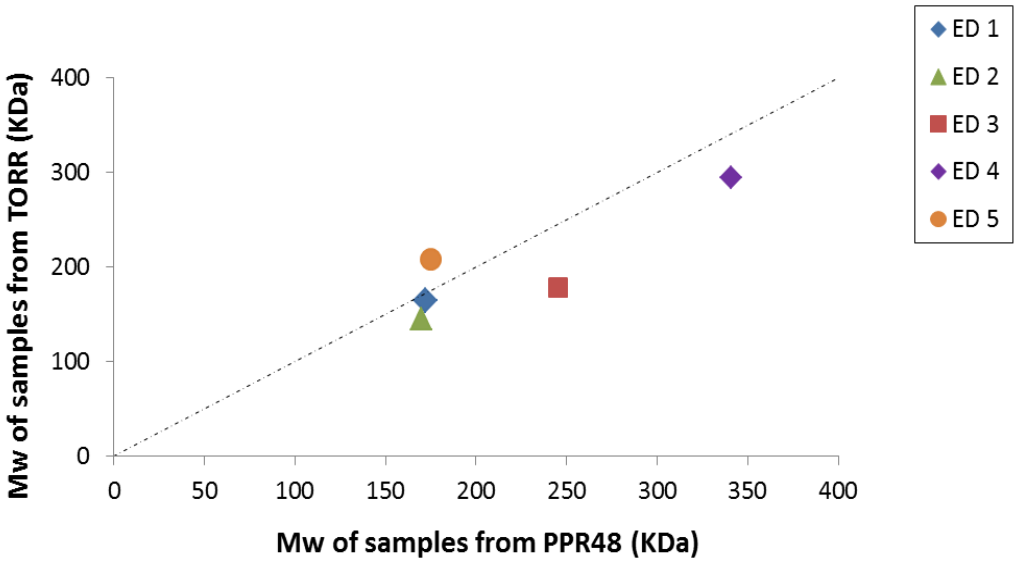

Figure 2.25. Correlation between observed PP M_w values in the PPR48 and the 'TORR' installation for the five tested HY-ZNCs (data from Table 2.7).

In our opinion, the agreement between the two sets of data is more than satisfactory –surprising, even, if one considers that the comparison is between experiments in heptane slurry (PPR48) vs gas-phase ('TORR'). We believe that this is not the place to discuss the reasons why this turned out to be the case; for the purpose of this work, the main conclusion is that the PPR48 clearly represents a valid HTE screening tool for HY-ZNCs, and generates results that can be confidently translated to industrial use conditions. This is specially important for the significance of the following Chapters 3 and 4.

References

(1) *High Throughput Screening in Catalysis*; Hagemeyer, A.; Strasser, P.; Volpe, A. F., Jr., Eds.; Wiley-VCH: Weinheim, 2004.

(2) http://www.radleys.com/pages/products/carousel-6-plus.shtml

(3) Busico, V.; Pellecchia, R.; Cutillo, F.; Cipullo, R. *Macromol. Rapid Commun.* **2009**, *30*, 1697-1708.

(4) See, e.g.: (a) Torrent, M.; Solá, M.; Frenking, G. *Chem. Rev.* **2000**, *100*, 439-494, and refs. therein. (b) Miteva, M. A.; Lee, W. H.; Montes, M. O.; Villoutreix, B. O. *J. Med. Chem.* **2005**, *48*, 6012-6022, and refs. therein.

(5) D'Amore, M.; Credendino, R.; Budzelaar, P. H. M.; Causá, M.; Busico, V. *J. Catal.* **2012***, 286,* 103-110, and refs. therein.

(6) See, e.g.; Dunbar, K.; Fugelsang, J. Causal thinking in science: How scientists and students interpret the unexpected. In *Scientific and Technical Thinking*; Gorman, M. E.; Tweney, R. D.*;* Gooding, D.; Kincannon, A., Eds.; Lawrence Erlbaum Associates: Mahwah (NJ), 2005; pp. 57-79.

(7) See, e.g.: Busico, V. *Dalton Trans.* **2009**, *41*, 8794-8802.

(8) Boussie, T. R.; Volpe, T. R.; Diamond, G. M.; Goh, C.; Hall, K. A.; LaPointe, A. M.; Leclerc, M.; Lund, C.; Murphy, V.; Shoemaker, J. A. W.; Tracht, U.; Turner, H.; Zhang, J.; Uno, T.; Rosen, R. K.; Stevens, J. C. *J. Am. Chem. Soc*. **2003**, *125*, 4306-4317.

(9) Frazier, K. A.; Boone, H. W.; Vosejpka, P. C.; Stevens, J. C. US 6,953,764 (2005), Dow Global Technologies Inc.

(10) Boussie, T. R. ; Diamond, G. M.; Goh, C. ; Hall, K. A.; LaPointe, A. M.; Leclerc, M.; Murphy, V.; Shoemaker, J. A. W.; Turner, H.; Rosen, R. K.; Stevens, J. C.; Alfano, F.; Busico, V.; Cipullo, R.; Talarico, G. *Angew. Chem. Int. Ed.* **2006**, *45*, 3278-3283.

(11) Arriola, D. J.; Carnahan, E. M.; Hustad, P. D.; Kuhlman, R. L.; Wenzel, T. T. *Science* **2006**, *312*, 714-719.

(12) Ciancaleoni, G.; Fraldi, N.; Cipullo, R.; Busico, V.; Macchioni, A.; Budzelaar, P. H. M. *Macromolecules*, **2012**, *45(10)*, 4046-4053.

(13) http://www.freeslate.com/applications/chemicals-energy/polyolefins-polymers/rapid-gpc

(14) http://www.bruker.com/products/mr/nmr/avance-iii-hd/overview.html

(15) http://www.bruker.com/products/mr/nmr/probes/cryoprobes.html

(16) http://www.polymerchar.com/cef

(17) http://www.freeslate.com/products-services/cm3-workflows

(18) http://www.freeslate.com/products-services/reactors/ppr

(19) Noristi, L; Barbè, P. C.; Baruzzi, G. *Makromol. Chem.* **1991**, *192*, 1115-1127.

(20) See, e.g.: Barbè, P.C.; Cecchin, G.; Noristi, L. *Adv. Polym. Sci.* **1986**, *81*, 1-81, and refs. therein.

(21) See, e.g. Author(s): D'Agnillo, L.; Soares, J. B. P.; Penlidis, A. *J. Polym. Sci. B: Polym. Phys.* **2002**, *40*, 905-921.

Chapter 3. Toward a 'White-Box' Model of HY-ZNCs

3.1. Introduction

In Chapter 1, we revised and critically discussed the experimental and computational modeling information on HY-ZNCs based on the literature. In the present chapter, we will report and organize our own original data, coming in part from precatalyst activation studies in the XCM^{TM} setup, meant to quantify the changes in catalyst composition and local structure resulting from catalyst-cocatalyst interactions; in part from polymerization experiments in the PPR platform, where the goal was to correlate catalyst behavior with the aforementioned surface information. Tools, methods and experimental protocols were described in detail in Chapter 2.

Our ultimate aim, as explained in the General Introduction to the thesis, was to assemble –if not yet a working 'white-box' model of HY-ZNC behavior– a large database of structural and molecular kinetic information in preparation of rational surface design. We focused mainly on two classes of HY-ZNCs, namely $MgCl_2/TiCl_4$ – AlR_3, as the simplest combination able to polymerize propene with high productivity to a partly stereoregular polymer, and $MgCl_2/TiCl_4$/diisobutyl-*ortho*-phthalate (DBP) – $AlEt_3$/ED (typically, ED = $R'_xSi(OR'')_{4-x}$), the most widespread system for the industrial production of iPP. More than the importance for application, the main reason to choose the latter system was that DBP is known to react with AlR_3 and desorb from the catalytic surfaces, where it is largely replaced by the ED in the early stages of the polymerization; this feature is stimulating from the mechanist standpoint, and offers the possibility to modulate the local environment of the active species (evidently much more limited in systems where the ID is not reactive and therefore pre-defined). When deemed necessary, on the other hand, the study was extended to other $MgCl_2/TiCl_4$/ID – $AlEt_3$/ED systems.

In Chapter 2, when discussing our HTE strategy, we admitted that HTC is not yet ripe as a primary screening tool for HY-ZNCs. On the other hand, an extensive DFT-D investigation of these systems is presently ongoing at LSP, also in the framework of the Dutch Polymer Institute program. Part of the results, dealing with the structure and morphology of $MgCl_2$ crystallites and the chemisorption of $TiCl_4$

on their lateral terminations, have already been published, and as such were covered in Chapter 1. Others, on the other hand, concerning the chemisorption of model and industrially relevant LBs, have only been presented at conferences and are not yet easily available, but are highly relevant to interpret the HTE results of this chapter; in the following section, therefore, we summarize these latest advances.

3.2. Recent periodic DFT-D modeling results at LSP for $MgCl_2$/LB adducts

According to state-of-the-art DFT-D studies, well-formed crystals of neat α-$MgCl_2$ feature, in addition to basal 001 planes, primarily 104 lateral terminations exposing 5-coordinated Mg atoms (Figure 3.1). These are lower in energy by ~0.5 J/m^2 than 110 terminations, exposing 4-coordinated Mg atoms.[1,2]

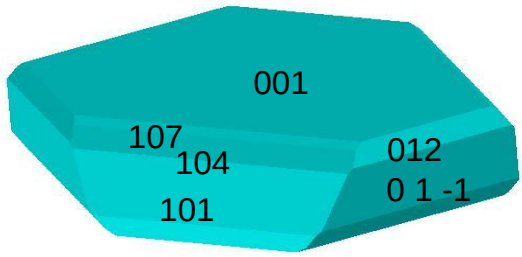

Figure 3.1. Computational model of a well-formed 'neat' α-$MgCl_2$ crystal, based on periodic DFT-D results of surface energy. Only basal planes and 104 (or equivalent) lateral terminations are present.[1,2]

On the other hand, in the presence of LBs the relative stability of $MgCl_2$(104) and $MgCl_2$(110) can be reversed by chemisorption processes, which tend to favor the latter as being more Lewis-acidic. As an example, for the chemisorption of H_2O D'Amore et al. calculated, under standard conditions, Δ*E* = -87 kJ/mol, Δ*G* = -20 kJ/mol on $MgCl_2$(104); the corresponding values for $MgCl_2$(110) are Δ*E* = -127 kJ/mol, Δ*G* = -74 kJ/mol for the binding of the first water molecule, and Δ*E* = -111 kJ/mol, Δ*G* = -60 kJ/mol for that of a second one (thus fully saturating the surface). Similar results were obtained for other small LBs such as ammonia or ethanol.[3]

With larger LBs, on the other hand, like are all HY-ZNC modifiers of industrial interest, the picture is more complicated, because as soon as the degree of surface coverage reaches values in excess to θ ~ 1/3, indicatively, steric interference starts to become important, at least on well-formed crystals, with major consequences. An interesting case is that of $Me_2Si(OMe)_2$, which represents a small model of alkoxysilane ED; according to the literature[4], these EDs chelate the 4-coordinated Mg on $MgCl_2$(110), which indeed turned out to be the case according to our own periodic DFT-D calculations up to θ = 1/2 (Figure 3.2; Δ*E* = -156 kJ/mol, Δ*G* = -79 kJ/mol).[3] Upon further increasing θ, on the other hand, the molecule was forced to adopt a monodentate adsorption, with a far less effective binding (Δ*E* = -109 kJ/mol, Δ*G* = -29 kJ/mol).[5] Considering that industrially relevant alkoxysilane ED are much bulkier than $Me_2Si(OMe)_2$, as being substituted with sterically demanding alkyl groups (e.g. isopropyl, isobutyl, etc), one can speculate that the situation of Figure 3.2 for such EDs is already at the upper limit of θ on a well-formed crystal surface.

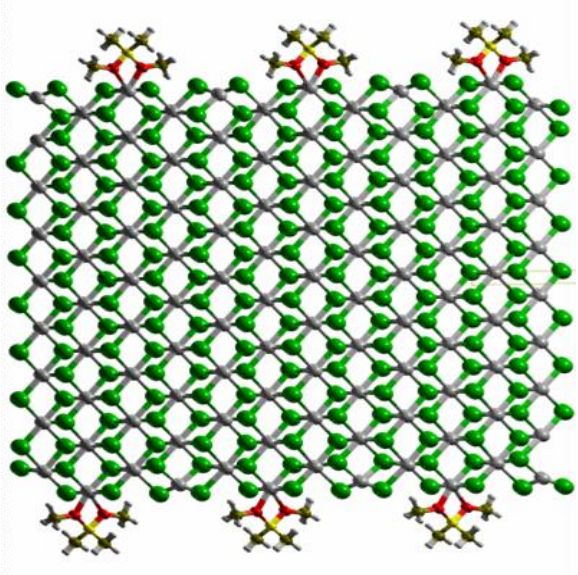

Figure 3.2. Periodic DFT-D model of chemisorption of $Me_2Si(OMe)_2$ on $MgCl_2$(110) in the 'chelate' mode at θ = 1/2.[3]

ID molecules like dialkyl-*ortho*-phthalates can be even bulkier than typical alkoxysilanes. They were claimed to bind in the so-called 'bridge' mode on $MgCl_2$(104)[4], and indeed our periodic DFT-D results agreed with the classical literature model (Figure 3.3-left for the comparatively small dimethyl-*ortho*-phthalate (DMP; Δ*E* = -119 kJ/mol, Δ*G* = -36 kJ/mol at θ = 2/3).[5] On the other hand, for the same molecule the commonly assumed 'chelate' mode on $MgCl_2$(110)[4], with both carbonyl groups bound to

a single 4-coordinated Mg, turned out to be unfeasible due to severe steric repulsion between DMP molecules bound to neighboring structural layers, and a monodentate, much weaker binding was found the only option (Figure 3.3-right).[5] This conclusion substantially agrees with a recent Molecular Dynamics periodic simulation by Parrinello.[6]

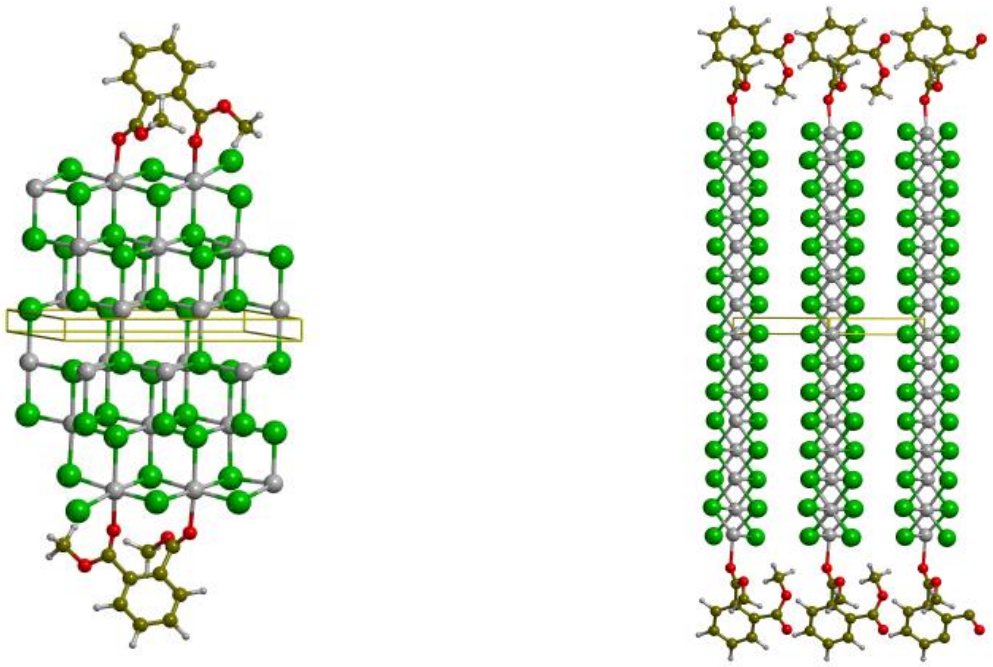

Figure 3.3. Periodic DFT-D models of chemisorption of dimethyl-*ortho*-phthalate (DMP) on $MgCl_2$(104) in 'bridge' mode at θ = 2/3 (left), and on $MgCl_2$(110) in monodentate mode at θ = 1 (right).5

The experimental evidence, on the other hands, points to primary $MgCl_2$ particles of very small average dimensions and extensive rotational and stacking disorder of the structural layers (Chapter 1). More realistic models of such particles can be built like in Figure 3.4-left, making it possible to carry out mono-dimensional periodic DFT-D calculations for exposed edges.[3] The result is important, because it clearly points out to what extent the binding modes of LBs of industrial use depend on $MgCl_2$ *crystallite size*, along with the *type of lateral terminations*. An outstanding example is in Figure 3.4-right, showing DMP very well-bound in the 'chelate' mode onto a $MgCl_2$(110)/$MgCl_2$(001) edge at θ = 1/2.[5]

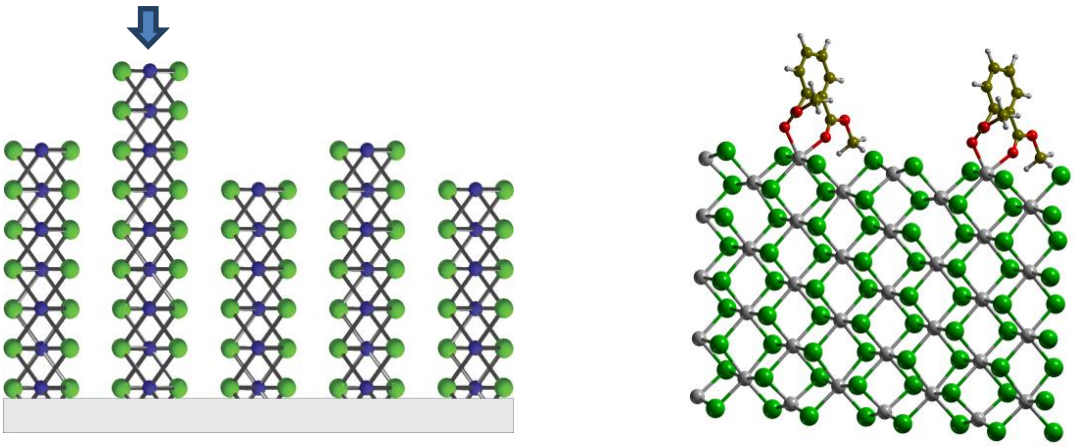

Figure 3.4. Model of a 'rough' $MgCl_2(110)$ surface (left)[3], and periodic DFT-D model of 'chelate' chemisorption ($\theta = 1/2$) for dimethyl-*ortho*-phthalate (DMP) on a 'protruding' $MgCl_2(110)/MgCl_2(001)$ edge (right; the arrow to the left points to the said edge on the 'rough' surface).[5]

An important comment at this stage is that achieving a full coverage of lateral $MgCl_2$ crystallite terminations with ID and/or ED molecules does not seem trivial. The inevitable mismatch between these rather large and often conformationally flexible organic moieties is likely to leave behind local surface vacancies, which seems in line with the 3-site model of catalytic species for HY-ZNCs discussed in the final part of Chapter 1, with its static and dynamic implications.[7] It is also worthy to note that, in situations like those hypothesized in Figures 3.2 and 3.4-right, it is not difficult to imagine that an alkoxysilane ED can replace a dialkyl-*ortho*-phthalate ID, fitting well in the surface area liberated by the latter after reacting with the AlR_3 cocatalyst (vide infra), and also why bulky alkoxysilanes are necessary to effectively cover the catalytic surfaces.

On the other hand, it is interesting to recall the full and compact surface coverage that, according to periodic DFT-D calculations, can be achieved by means of the epitaxial chemisorption of $TiCl_4$ on $MgCl_2(110)$ terminations (Figure 3.5).[8] The $TiCl_4$ units are octahedral, hence coordinatively saturated; therefore, they are expected not to interact with LBs, whereas the stripping of one or both terminal Cl atoms by a strong Lewis acid such as AlR_3 should be feasible. How the surface looks like in small and highly disordered primary particles, of course, remains to be seen. We will come back to all this in the following sections.

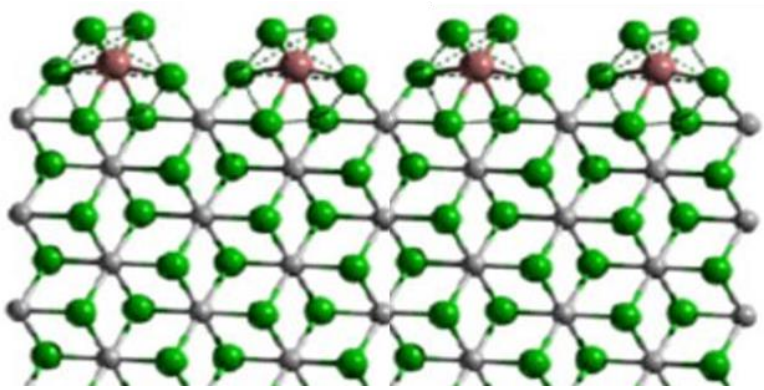

Figure 3.5. DFT-D model of $TiCl_4$ adsorption on $MgCl_2$(110).[8]

3.3. Experimental investigation of the catalytic surfaces via chemical reactivity studies

To better face the complexity of HY-ZNCs systems, we adopted a factorized approach, meaning that we investigated possible binary and ternary combinations of system components before looking at the full 'cocktail'.

Apart from $MgCl_2$/LB, covered widely in the previous section, pairs of interest for experiments are $MgCl_2/TiCl_4$, $MgCl_2/AlR_3$, $MgCl_2$/ID, $MgCl_2$/ED, and AlR_3/ED.

3.3.1. $MgCl_2/TiCl_4$ and $MgCl_2/AlR_{3-x}Cl_x$

A most practical method to prepare binary $MgCl_2/TiCl_4$ adducts (as long as controlling the morphology is not an issue) is to co-mill extensively the two components (e.g. in a ball mill or planetary mill with air-tight jars). According to the literature, the maximum amount of $TiCl_4$ that binds to the $MgCl_2$ matrix strong enough not be removed by hot washing with heptane (at 80-100°C) is ~1-2 wt.-% of Ti metal (corresponding to a Mg/Ti mole ratio ~20-50).[9-11] Samples prepared according to this method feature primary particles with average lateral dimensions of ~10 nm, and some residual stacking of structural layers along the *c* axis.[2] We prepared one such sample for subsequent polymerization studies; the powder X-ray diffraction spectrum is shown in Figure 3.6-a. When the sample was reacted with $AlMe_3$, a certain amount of CH_4 was liberated, which may be attributed to hydrolysis by chemisorbed water (quantified as ~0.2 wt.-%); this may look surprising, in view of the extreme

reactivity of water with $TiCl_4$. On the other hand, if it is true that $TiCl_4$ only binds to $MgCl_2(110)$[8], and $MgCl_2(104)$ is the lowest-energy lateral termination of neat $MgCl_2$[1,2], one may speculate that $TiCl_4$ and adventitious water are chemisorbed on different lateral $MgCl_2$ terminations.

Milling $MgCl_2$ alone ended up with rather similar samples (Figure 3.6-b), which was somehow unexpected considering the lack of stabilization by adsorbates. On the other hand, in spite of all precautions, such samples always turned out to contain non-negligible amounts of water (as measured, e.g., by reacting them with $AlMe_3$ and quantifying by GC analysis the methane evolved); this suggests that the lateral crystallite terminations are decorated with chemisorbed H_2O molecules. In § 3.2 we reported DFT(-D)-calculated values of water-on-$MgCl_2$ chemisorption energy; based on these values, one can estimate that an extremely low water pressure (~10^{-5} bar) is enough to saturate the exposed Mg on lateral $MgCl_2$ crystal terminations at room temperature. As an example, a sample with the X-ray powder diffraction spectrum of Figure 3.6-b, obtained with a planetary mill after 6 h of dry milling at 600 rpm, and estimated to feature primary particles with average dimensions of ~8 nm along *a* and *c*[12], turned out to contain ~0.6 wt.-% of water, corresponding to a Mg/H_2O mole ratio ~30, i.e. similar to the Mg/Ti ratio in saturated $MgCl_2/TiCl_4$ adducts.

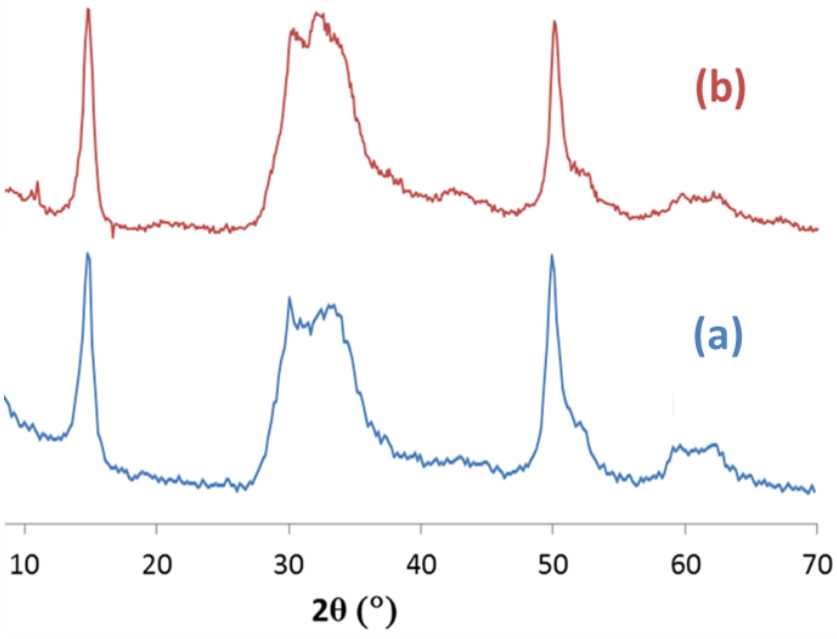

Figure 3.6. Powder X-ray diffraction spectra of an $MgCl_2/TiCl_4$ adduct (a), and a physically activated $MgCl_2(/H_2O)$ sample (b); see text for details.

Intriguingly, treating said (or similar) $MgCl_2(/H_2O)$ sample(s) with neat $TiCl_4$ ([Mg]/[Ti] = 0.5) in the 25-70°C temperature range resulted into a very modest Ti adsorption; ICP-OES analyses indicated Ti amounts as low as ~0.3 wt.-% in the solid recovered after 1 h of contact time, hot-washing and drying.[13] Our educated guess is that, in order to develop comparatively large amounts of $MgCl_2(110)$ terminations where $TiCl_4$ can adsorb, more intensive physical or chemical activation treatments in the presence of $TiCl_4$ are necessary for the latter to effectively steer surface formation. This may follow from a relatively mild chemisorption energy of $TiCl_4$ on $MgCl_2(110)$, according to the most recent DFT-D estimates ($\Delta E \geq$ -120 kJ/mol, $\Delta G \geq$ -25 kJ/mol under standard conditions).[8]

The same $MgCl_2(/H_2O)$ sample of Figure 3.6-b was treated for 30 min in the XCM™ at 70°C in heptane slurry with $AlEt_3$ (TEA), $AlEt_2Cl$ (DEAC), and mixtures thereof. After washing with heptane twice and a last aliquot of pentane (Chapter 2), the solid phases were dried, and analyzed by ICP-OES for Al, with the results of Table 3.1.

Table 3.1. Al contents of the solid phases recovered after treatment of physically activated $MgCl_2$ (sample of Figure 3.6-b) with TEA, DEAC, and mixtures thereof at 70°C in heptane slurry.

Entry	Al-Alkyl	Al (mol% wrt Mg)
1	TEA	4.7
2	TEA/DEAC (95/5)	4.1
3	TEA/DEAC (5/95)	3.4
4	DEAC	3.1

Reaction conditions: $MgCl_2$, 25 mg; heptane, 3.8 mL; $[Al_{total}]/[Mg] = 25$, T = 70°C; t = 30 min.

Unfortunately, the data are not informative on the nature of the chemisorbed Al species (a high-resolution solid-state NMR investigation, hopefully able to address this question and others similar, is about to start in the framework of the Dutch Polymer Institute program). On the other hand, it is interesting to note that their amount is close to that of chemisorbed H_2O; this may indicate that the adsorbates are hydrolysis products of TEA or DEAC. High-level QM calculations (courtesy of Dr. Christian Ehm) concluded that the $Me_2Al\text{-}O\text{-}AlMe_2$ moiety shown in Figure 3.7-a and 3.7-b, which can

be looked at as a first building block of more complex aluminoxane structures, binds to a small model of $MgCl_2$ surface (Figure 3.7-c) by at least 40 kJ/mol stronger than $AlMe_3$; based on that, we consider aluminoxane moieties as most plausible adsorbates.

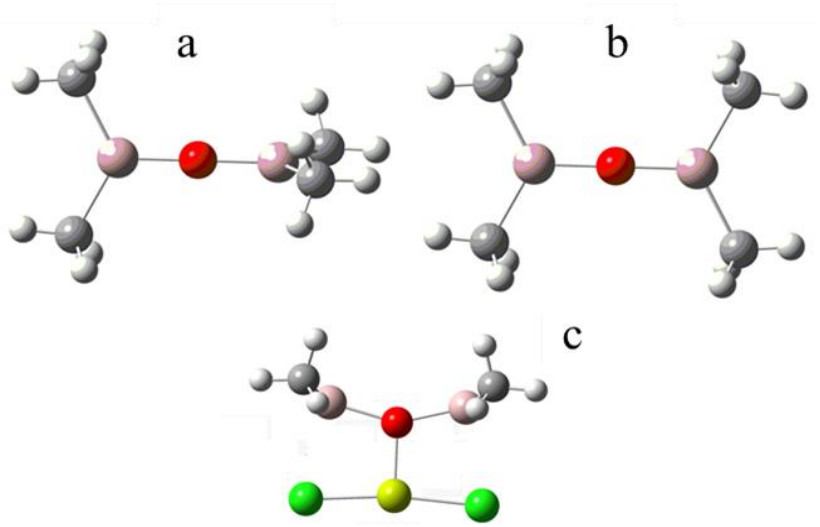

Figure 3.7. Ball-and-stick representations of Me_2Al-O-$AlMe_2$ in the Ground State (a), in a conformation suited for Lewis interactions (b, ΔE = +12.5 KJ/mol), and forming an adduct with a $MgCl_2$ fragment (c, ΔE = -133 kJ/mol; only one Me per Al shown in view of symmetry).[14]

3.3.2. AlR_3/ED

$MgCl_2/TiCl_4$(/ID) precatalysts are activated by reacting them with AlR_3(/ED) mixtures.[9,10] Most typically, the Al-trialkyl is $AlEt_3$, and when the ID is a diester (like DMP) or a 1,3-diether, the preferred ED is an alkoxysilane of formula $R'_xSi(OR'')_{4-x}$, where R'' = Me or Et, x = 2 or 3, and the R' groups can be equal or different. Other Al-trialkyls (e.g. $AlMe_3$, $Al(^iBu)_3$) can also be used, although catalyst productivity tends to be lower compared with $AlEt_3$; at odds with 'violet'-$TiCl_3$-based catalysts, activation with AlR_2Cl yields very low catalyst productivity and is not beneficial with respect to the stereoselectivity.

It has been reported that, in hydrocarbon solution at moderate temperature, AlR_3/alkoxysilane mixtures react, giving rise to R/OR" metathesis (Eq3.1).[15]

$$AlR_3 + R'_2Si(OR'')_2 \rightarrow AlR_2(OR'') + RR'_2Si(OR'') \qquad 3.1$$

In our hands, this turned out not to be the case. As an example, in Figure 3.8 we show an overlay of the ^{1}H NMR spectra in cyclohexane-d_{12} solution of neat (^{i}Bu)$_2$Si(OMe)$_2$, and its mixtures with AlEt$_3$ ([Al]/[Si] ~ 10) after a contact time of 30 min at 25°C and 70°C.

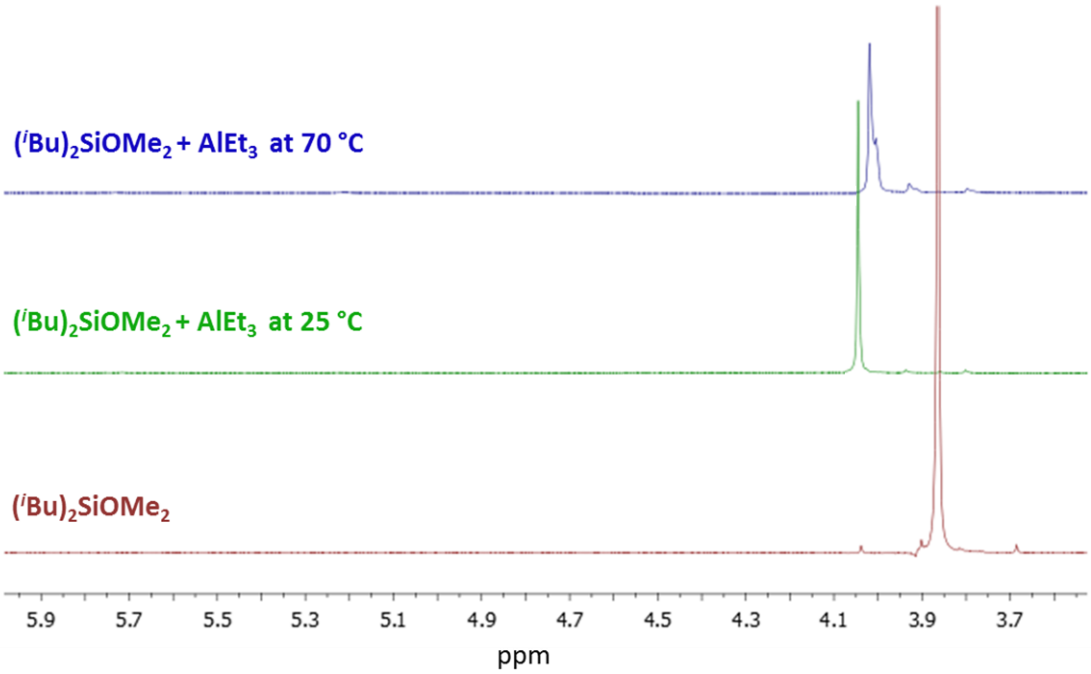

Figure 3.8. Overlay of the ^{1}H NMR spectra (detail of the δ = 3.6-6.0 ppm region downfield of TMS) in cyclohexane-d_{12} solution of neat (^{i}Bu)$_2$Si(OMe)$_2$, and its mixtures with AlEt$_3$ ([Al]/[Si] ~ 10) at 25°C and 70°C (contact time = 30 min).

The spectra demonstrate that Lewis acid-base adducts with clear Et$_3$Al←OMe interactions are formed, as indicated by the shift of the CH_3-(O-Si) signal to lower field (4.04 ppm compared with 3.89 ppm for the pure compound at 25°C). On the other hand, no evidence was found of OMe/Et exchange (Eq3.1) in the investigated conditions and temperature range; in particular, the diagnostic signal of the CH_3-(O-Al) moiety at around 5.7 ppm did not show up.

3.3.3. More complex systems

From ternary systems onward, categorization based on the number of components is not practical. A more logical classification is as follows:

- $MgCl_2/TiCl_4$ + AlR_3

- $MgCl_2/TiCl_4$/DBP + AlR_3 (including a study of the reactivity between DBP and $AlEt_3$ in solution)
- $MgCl_2/TiCl_4$(/ID) + $R'_2Si(OMe)_2$
- $MgCl_2/TiCl_4$(/ID) + (AlR_3/)ED

The corresponding results are reported and commented below.

3.3.3.1. *$MgCl_2/TiCl_4$ + AlR_3*

Aliquots of a $MgCl_2/TiCl_4$ precatalyst (Figure 3.6-a) were contacted in the XCM™ at 70°C for 30 min under magnetic stirring with heptane solutions of $AlMe_3$ (TMA), $AlEt_3$ (TEA) and Al^iBu_3 (TIBA), after which the solid phases were recovered, washed, dried, and characterized by means of ICP-OES for metal quantifications. The results are reported in Table 3.2 and Figure 3.9.

Table 3.2. Metal contents of the solid phases recovered after reacting $MgCl_2/TiCl_4$ with different AlR_3 in heptane.

Entry	AlR_3	Ti [a]	Al [a]
0	-	3.8	-
1	TMA	3.5	3.3
2	TEA	3.5	3.4
3	TIBA	3.6	4.0

Reaction conditions: *T* = 70°C; heptane, 3.8 mL; precatalyst, 25 mg; [Al]/[Ti] = 25; *t* = 30 min.
[a] mol% wrt Mg

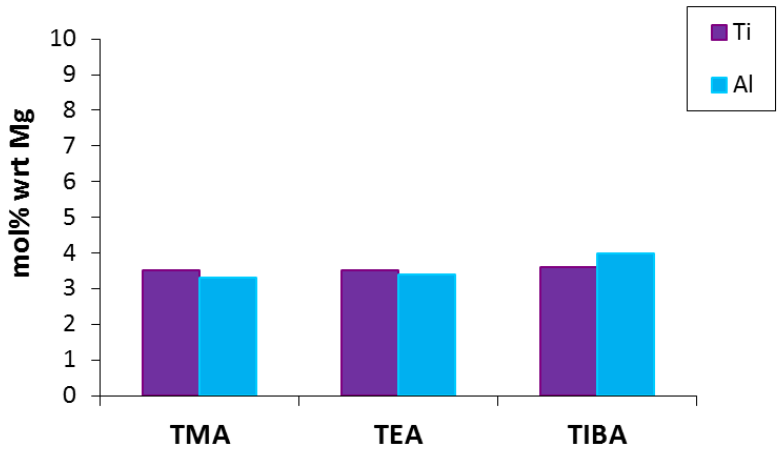

Figure 3.9. Al and Ti contents of the solid phases recovered after reacting $MgCl_2/TiCl_4$ with different AlR_3 in heptane at 70°C (data from Table 3.2).

For all three screened AlR_3, the Al content of the reacted solid phase turned out to be equimolar to its Ti content within the experimental error. In our opinion, this very simple finding strongly suggests that (a) the AlR_3 molecules bind quantitatively to the surface $TiCl_x$ species, likely forming Cl-bridged hetero-dinuclear adducts, and (b) all surface Ti adducts in the precatalyst are readily accessible, which rules out the hypotheses that part of the Ti is buried in the $MgCl_2$ lattice, and/or only the outer 'skin' of the secondary aggregates would be accessible prior to polymerization and particle expansion. We interpret the result with the cartoon model of Figure 3.10.

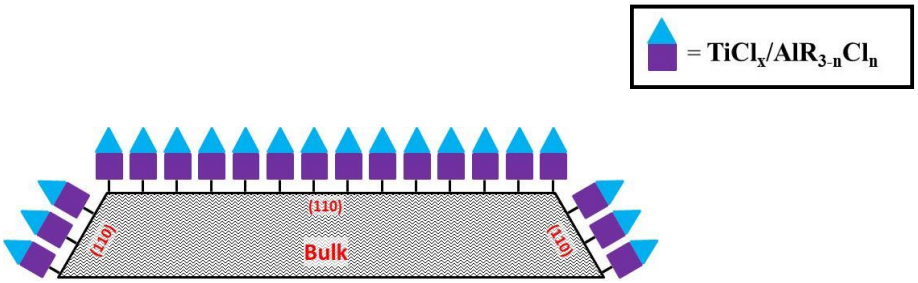

Figure 3.10. Cartoon representation of the solid phase obtained from the reaction of $MgCl_2/TiCl_4$ with AlR_3 (Table 3.2 and Figure 3.9; see also Figure 3.5).

3.3.3.2. *$MgCl_2/TiCl_4$/DBP + AlR_3*

The reaction of this precatalyst with AlR_3 in heptane solution is known to imply extensive surface modifications, because in addition to the alkylation/reduction of the $TiCl_4$ species, DBP is also attacked by the Al-alkyl.[9,10,16] According to the literature[17], the reaction of DBP with excess $AlEt_3$ proceeds through two distinct stages, that is (i) the rapid formation of Lewis acid-base adducts, and (ii) slower chemical reactions between the ester groups and 'free' $AlEt_3$. Complexes between organic esters and organo-aluminum compounds are well-described, and form rapidly already at room temperature, with the lone pairs on the carbonyls being donated to electron-deficient Al centers. In the presence of excess $AlEt_3$, this reduces the carbonyl groups yielding a number of Al-alkoxy species (Eq3.2):

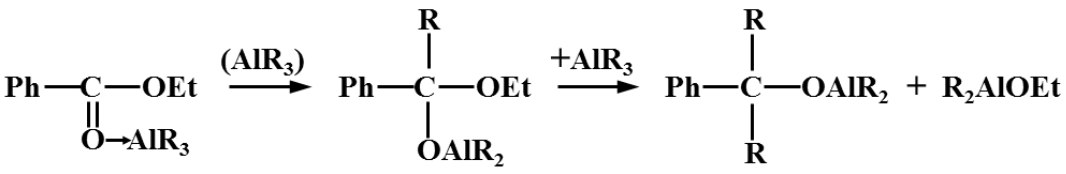

3.2

We could investigate this chemistry by means of ^{13}C NMR. Figure 3.11 shows an overlay of the ^{13}C NMR spectra in benzene-d_6 solutions of DBP alone, and after 30 min of contact time at 25°C with an excess of $AlEt_3$ ([Al]/[Ti] = 22). It can be seen that in the latter case the carbonyl signal at 167 ppm disappeared, whereas peaks diagnostic for several reduction products at 113 ppm and in the region between 60 and 75 ppm showed up. The aromatic pattern at around 140 ppm, in turn, was more complex than for DBP, confirming the loss of the original molecular symmetry.

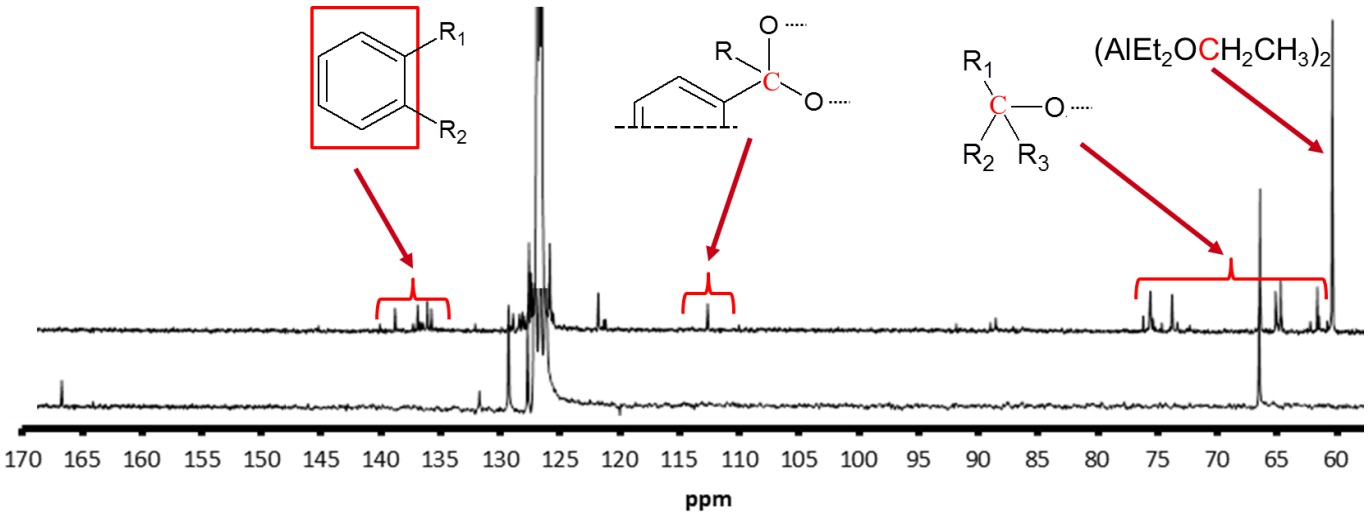

Figure 3.11. Detail of the ^{13}C NMR spectra in benzene-d_6 of DBP (bottom), and an $AlEt_3$/DBP mixture ([Al]/[DBP] = 22) left to react at 25°C for 30 min (top).

Following the reaction by monitoring, with a suitable technique (e.g. NMR or GC), the build-up of DBP reduction products is not practical, due the complexity of their pattern (Scheme 3.1, including the hydrolysis of the O-AlR_2 bonds after methanol *work-up*). Therefore, for studies of DBP reactivity in $MgCl_2$/$TiCl_4$/DBP (pre)catalysts, we opted for analyzing the solid phases for the unreacted DBP fraction (vide infra).

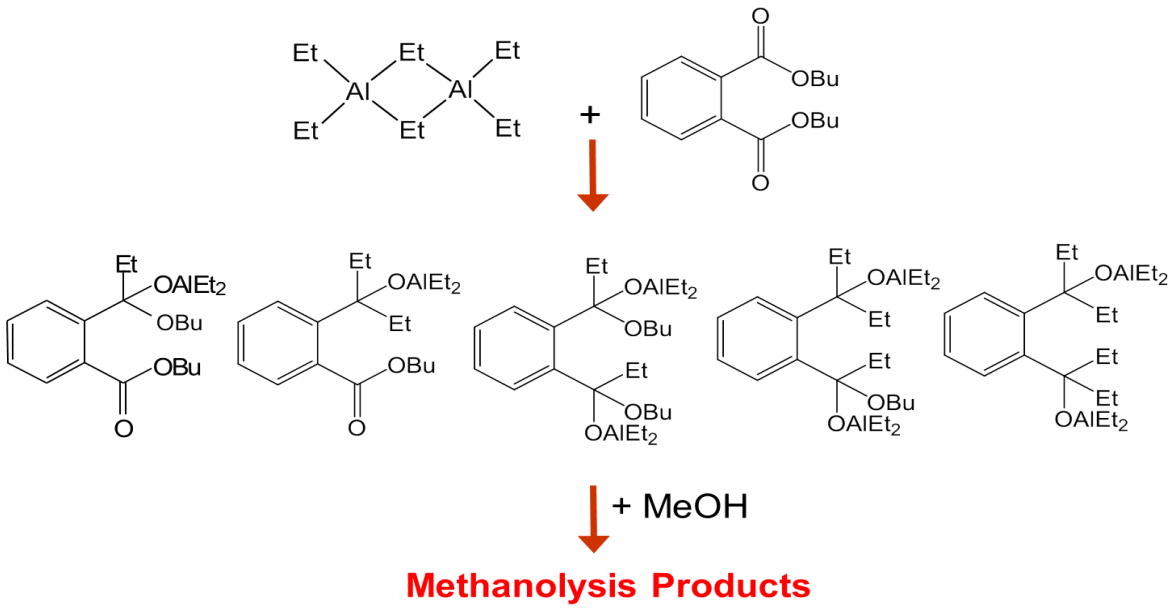

Scheme 3.1.

The same chemistry is to be expected under polymerization conditions, which typically entail higher values of *T* and [Al]/[DBP] ratio. This was confirmed by our studies, which quantified the change in composition of the solid catalyst when aliquots of $MgCl_2/TiCl_4$/DBP precatalyst were treated in the XCM^{TM} at 70°C for 30 min under magnetic stirring with heptane solutions of $AlMe_3$ (TMA), $AlEt_3$ (TEA) and Al^iBu_3 (TIBA). Downstream to the reaction, the solid phases were recovered, washed with heptane and pentane, dried, and characterized by means of ICP-OES and NMR analyses of metals and organic residues, respectively. For the latter, in particular, we found that the most accurate quantification protocol was based on ^{1}H NMR, and entailed re-dissolving the samples in methanol-d_4, and integrating the aromatic protons of DBP, as such or in any possible reduction product, against the signal of acetonitrile added as an internal standard.

The results are reported in Table 3.3 and Figure 3.12. ^{1}H NMR analysis confirmed that DBP was largely removed from the solid catalyst under the investigated conditions; as a matter of fact, the cumulative aromatic proton integral measured in the solid phases recovered after reaction with AlR_3 (irrespective of the nature of R) was only 15% of the original one; this translates into a mole amount of residual aromatic moieties of 1.2 mol% wrt Mg, compared with an initial value of 7.9 mol%. ICP-OES analysis,

on the other hand, showed massive Al incorporations for all screened Al-Alkyls, ranging from 13.3 mol% wrt Mg for TIBA to 18.8 mol% wrt Mg for TEA; this corresponds to Al/Ti mole ratios well above unity, and points to additional adsorption sites other than the surface Ti species. One can speculate that, along with hetero-dinuclear Cl-bridged Al-Ti species (homologous to the case of the binary $MgCl_2/TiCl_4$ precatalyst (§ 3.3.3.1), Al-alkoxides deriving from the reaction with DBP (Eq3.2) can replace DBP on the $MgCl_2$ surface. As a matter of fact, the total mol amount of Al is not far from the summed mol amounts of Ti and DBP in the original precatalyst. A cartoon model might look like in Figure 3.13; the representation is even more over-simplified than it may appear, considering that the different size of the R groups on Al and its consequences on the dimerization equilibria of the Al-species and on surface coverage upon chemisorption were disregarded.

Table 3.3. Metal and aromatics contents of the solid phases recovered after reacting $MgCl_2/TiCl_4$/DBP with different AlR_3 in heptane at 70°C.

Entry	Al-Alkyl	Ti [a]	Al [a]	DBP [a,b]
0	-	7.5	-	7.9
1	TMA	7.4	14.8	1.1
2	TEA	5.6	18.8	1.3
3	TIBA	5.1	13.3	1.2

Reaction conditions: *T* = 70°C; heptane, 3.8 mL; precatalyst, 25 mg; [Al]/[Ti] = 25; *t* = 30 min.
[a] mol% wrt Mg. [b] Total of DBP and its reduction products.

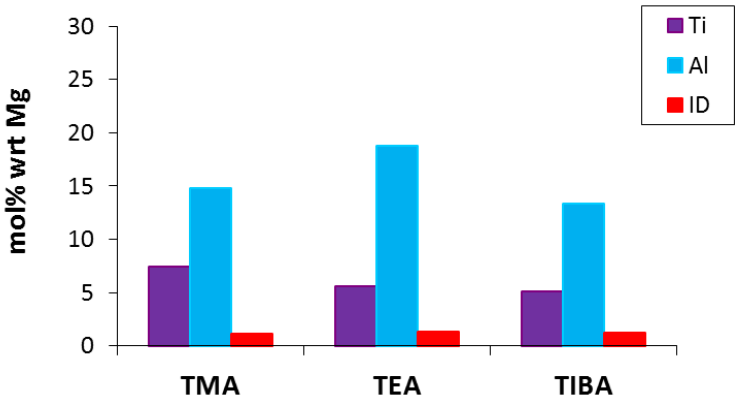

Figure 3.12. Contents of Al, Ti, and DBP and/or its reduction products (cumulatively indicated as ID), in the solid phases recovered after reacting $MgCl_2/TiCl_4$/DBP with different AlR_3 in heptane at 70°C (data from Table 3.3).

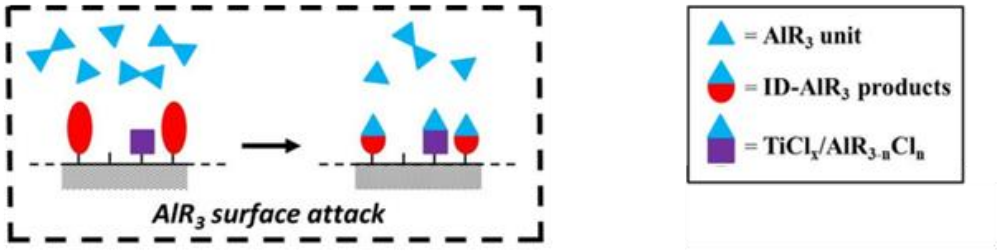

Figure 3.13. Cartoon representation of the solid phases obtained from the reaction of $MgCl_2/TiCl_4$/DBP with AlR_3 (Table 3.3 and Figure 3.12).

3.3.3.3. *$MgCl_2/TiCl_4$(/ID) + $R'_2Si(OR'')_2$*

Based on the data and tentative interpretations of the previous sections, it seems plausible to predict that treating both $MgCl_2/TiCl_4$ and $MgCl_2/TiCl_4$/DBP precatalysts with an ED (without adding an AlR_3) will sort very limited effects. As a matter of fact, according to the latest DFT-D models[8], the surface $TiCl_4$ species would be octahedral and coordinatively saturated (Figure 3.5), and the $MgCl_2$ surface would be shielded by said species or – when present – by DBP molecules (unless the latter can be displaced by the ED). To verify this educated guess, we treated both systems in the XCM™ with a heptane solution of $Me_2Si(OEt)_2$ (a prototypical alkoxysilane ED) at 70°C, [Si]/[Ti] = 2.5 for 30 min. Following the protocols described before, we then analyzed the solid phases by ICP-OES and ^{1}H NMR, in the latter case after re-dissolution in methanol-d_4. The ^{1}H NMR spectra gave evidence for some ED incorporation, but – quite surprisingly – quantitative integration against an internal standard clearly pointed out values of CH_3Si-/-OCH_2CH_3 proton ratios not in line with the original alkoxysilane structure. As an example, Figure 3.14 shows the ^{1}H NMR spectrum in methanol-d_4 of the re-dissolved solid phase recovered after treating $MgCl_2/TiCl_4$/DBP with $(Me)_2Si(OEt)_2$ as explained before; the -CH_3/-OCH_2CH_3 proton ratio turned out to be 4.1/40, instead of the expected 60/40. The most likely interpretation for this finding is that a metathetical exchange occurred between ethoxy groups on Si and Cl atoms on the surface, likely as shown in Scheme 3.2. Considering that the alkoxysilane is not a Lewis acid (like e.g. AlR_3), the scheme assumes an associative mechanism with the formation of a Ti(μ-Cl)(μ-OEt)Si fragment, requiring in turn the presence of (at least) one terminal Cl and one coordination vacancy (□) in *cis* geometry on the involved Ti center. Notably, the latter requirement is *not* satisfied by the model of surface $TiCl_4$ species on $MgCl_2$(110) proposed in Figure 3.5.[8]

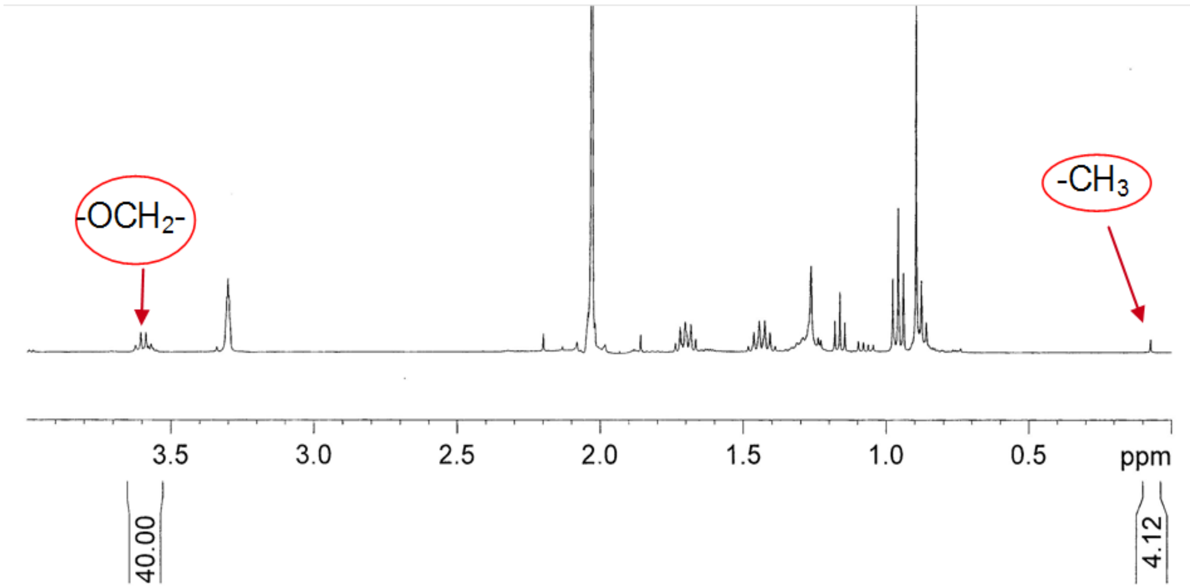

Figure 3.14. ^{1}H NMR spectrum in methanol-d_4 of the solid phase recovered after treating $MgCl_2$/DBP/$TiCl_4$ with $(Me)_2Si(OEt)_2$ in heptane solution. Reaction conditions: T = 70°C; t = 30 min; heptane, 3.8 mL; precatalyst, 25 mg; [Si]/[Ti] = 2.5.

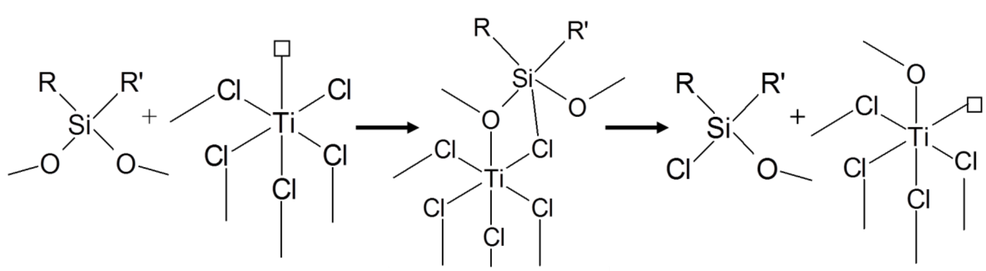

Scheme 3.2.

The reaction occurred with $MgCl_2/TiCl_4$, $MgCl_2/TiCl_4$/DBP, and also –for comparison– $MgCl_2/TiCl_4$/2,2-diisobutyl-1,3-dimethoxypropane (DMP), that is a precatalyst featuring an ID known to be poorly reactive with AlR_3/alkoxysilane solutions. Quantitative results for all three precatalysts, treated under the same conditions with a more industrially relevant alkoxysilane ED, namely $^i Bu_2Si(OMe)_2$ used at variable [Si]/[Ti] ratio, are provided in Table 3.4, and in graphical form in Figure 3.15.

Table 3.4. ^{1}H NMR quantification of methoxy groups in the solid phases recovered after the reaction of $MgCl_2/TiCl_4$, $MgCl_2/TiCl_4$/DBP, and $MgCl_2/TiCl_4$/DMP (DMP = diisobutyl-1,3-dimethoxypropane) with $^{i}Bu_2Si(OMe)_2$ in heptane at 70°C.

Entry	Precatalyst	[Si]/[Ti]	Ti (µmol)	Methoxy	
				µmol	mol % wrt Ti
1	$MgCl_2/TiCl_4$	5	5.3	3.2	61
2		6	5.3	3.0	57
3		10	5.3	2.8	53
4		15	5.3	2.8	53
5	$MgCl_2/TiCl_4$/DBP	1.25	8.8	4.8	55
6		3.75	7.5	6.0	80
7		6.25	8.8	9.6	109
8		13	7.5	9.7	129
9		20	8.8	11.8	134
10	$MgCl_2/TiCl_4$/DMP	1.25	7.0	4.4	63
11		2.5	7.0	7.6	108
12		6	8.6	11.4	133
13		15	8.7	13.8	158
14		20	8.7	13.8	159

Reaction conditions: *T* = 70°C; heptane, 3.8 mL; precatalyst, ~ 30 mg ; *t* = 30 min.

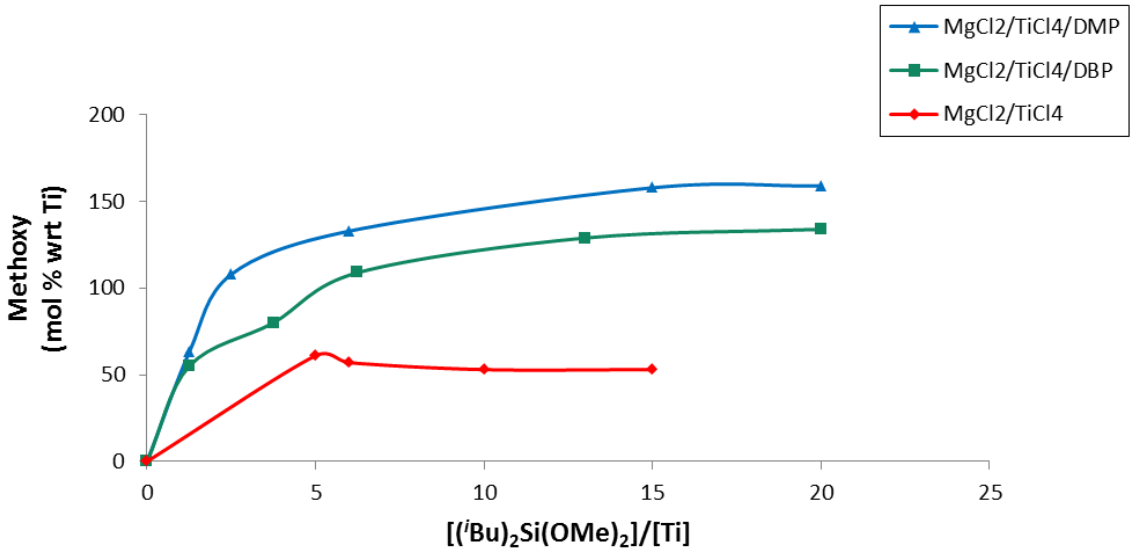

Figure 3.15. ^{1}H NMR quantification of methoxy groups in the solid phases recovered after the reaction of $MgCl_2/TiCl_4$, $MgCl_2/TiCl_4$/DBP, and $MgCl_2/TiCl_4$/DMP (DMP = diisobutyl-1,3-dimethoxypropane) with $^{i}Bu_2Si(OMe)_2$ in heptane solution at 70°C (data from Table 3.4).

Additional evidence in favor of our interpretation of the experimental findings is as follows:

i) Reversible Cl/OR metathesis was observed by ^{1}H NMR in hydrocarbon solutions of an alkoxysilane saturated with HCl(g) at room temperature

ii) No Cl/OR metathesis was observed when reacting neat 'activated' $MgCl_2$ samples with alkoxysilane heptane solutions in the XCM^{TM} platform under conditions otherwise identical to those used for the experiments in Table 3.4

iii) Unambiguous evidence of Cl/OR metathesis was obtained by means of 600 MHz High-Resolution Magic-Angle-Spinning (HR-MAS) ^{1}H NMR spectroscopy (at 30°C, 6 KHz spinning rate) for suspensions of $MgCl_2/TiCl_4$ in a cyclohexane-d_{12} solution of octadecylmethyldimethoxysilane (Figure 3.16).[18] Interestingly, only the dimethoxysilane turned out to chemisorb under the investigated conditions.

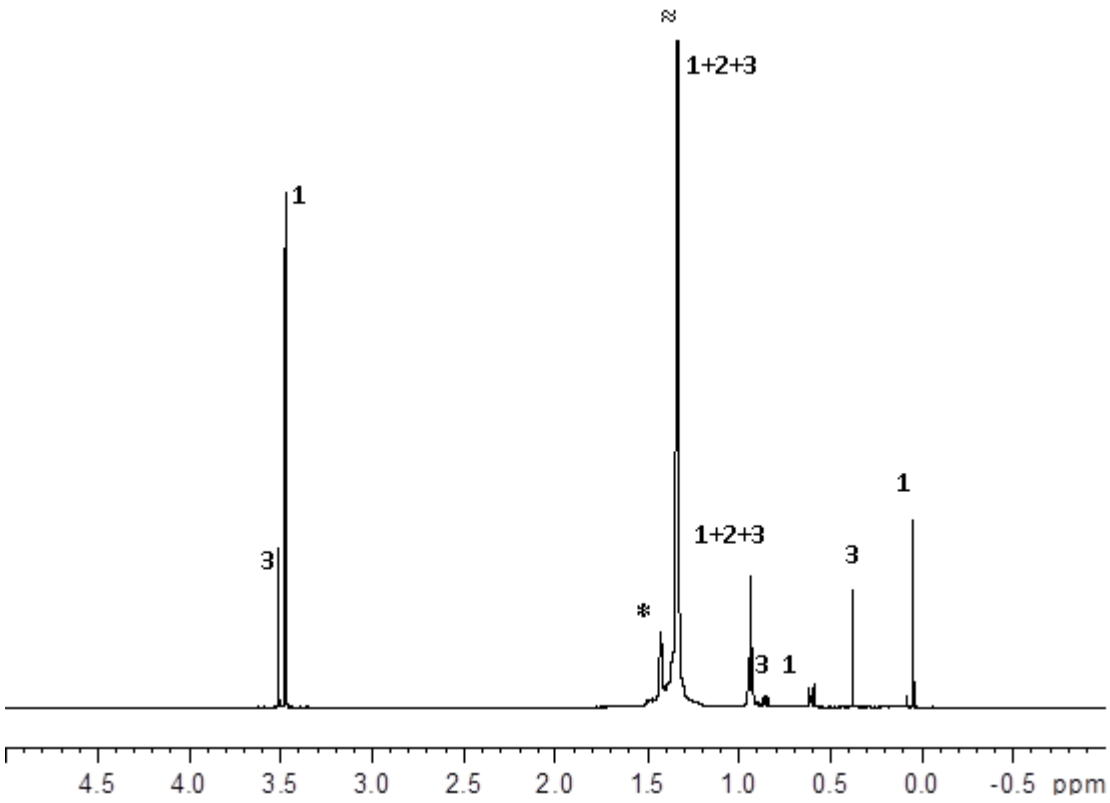

Figure 3.16. 600 MHz HR-MAS ^{1}H NMR spectrum (at 30°C, 6 KHz spinning rate) of $MgCl_2/TiCl_4$ suspended in a cyclohexane-d_{12} solution of octadecylmethyldimethoxysilane ([Mg]/[Si] = 30). Peaks numbered with **1**, **2**, **3** are due to 'free' and chemisorbed octadecylmethyldimethoxysilane, and 'free' octadecylmethylmethoxychlorosilane, respectively. From peak integration, the relative mol amounts of **1**, **2** and **3** can be estimated to be ca 50%, 30%, and 20%. The peak marked with an asterisk is due to the residual protons of cyclohexane.[18]

iv) No Cl/OR metathesis was ever observed when the same precatalysts were treated under similar experimental conditions with heptane solutions of R"Si(OR')$_2$/AlR$_3$, or of AlR$_3$ followed by R"Si(OR')$_2$.

We interpret the latter fact assuming that all terminal ('dangling') Cl atoms on Ti were 'stripped' by the strongly Lewis-acidic AlR$_3$[19], and as such were subtracted to the metathetical exchange of Scheme 3.2. *In line with said interpretation, we found that precatalysts treated with R"Si(OR')$_2$ prior to the alkylation/reduction step by AlR$_3$ cannot be changed into active catalysts.*

It is difficult to reconcile the above facts with the model of surface TiCl$_4$ species on MgCl$_2$(110) shown in Figure 3.5.[8] On the other hand, such a model agrees with a significant number of experimental and computational results (Chapter 1 and § 3.2). We recall at this stage that some years ago Parrinello proposed, for HY-ZNCs, the active Ti species of Figure 3.17-**2**, that he obtained by periodic Molecular Dynamics simulation as the kinetic product of TiCl$_4$ adsorption on MgCl$_2$(110).[20] This non-epitaxial, penta-coordinated (distorted-*tbp*), C_1-symmetric surface complex features two terminal ('dangling') Cl atoms and one coordination vacancy, and therefore matches all requirements to undergo the process of Scheme 3.2. According to Parrinello, it represents a local minimum which is 'only' 20-40 kJ/mol higher in energy than the absolute minimum corresponding to the epitaxial, C_2-symmetric, octahedral surface species of Figure 3.5 (and Figure 3.17-**1**). We propose that the two species can interconvert (vide infra), and the process of Scheme 2 takes place when the TiCl$_4$ adsorbates are temporarily in the form of Figure 3.17-**2**.

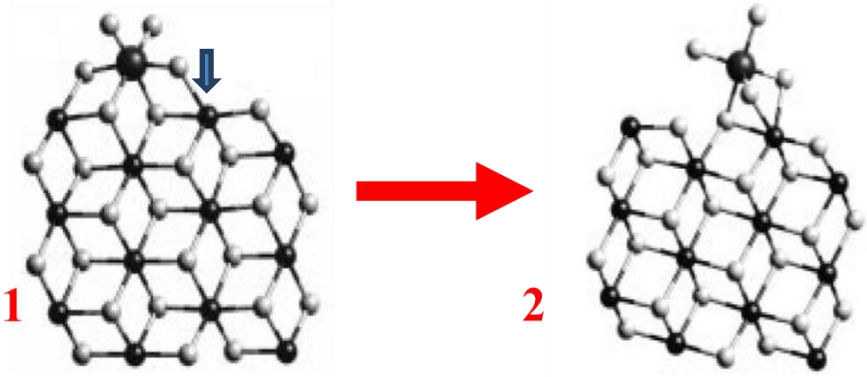

Figure 3.17. Hypothetical interconversion between an epitaxial surface TiCl$_4$ unit on MgCl$_2$(110) (**1**) into the non-epitaxial penta-coordinated one (**2**) proposed by Parrinello.[20] The process requires a surface vacancy adjacent to species **1**, indicated with an arrow (see text).

Although purely speculative at the present stage, our hypothesis may well-explain the lower propensity of simple $MgCl_2/TiCl_4$ precatalysts to undergo Cl/OR metathesis with alkoxysilanes, compared with $MgCl_2/TiCl_4$/ID ones (Figure 3.15). As a matter of fact, the postulated rearrangement of Figure 3.17 requires a surface Mg vacancy adjacent to the epitaxial species **1** (evidenced by an arrow in the figure), and in previous sections of this chapter we commented on the more compact coverage achievable for binary $MgCl_2/TiCl_4$ adducts on $MgCl_2$(110) compared with ternary $MgCl_2/TiCl_4$/ID adducts (see Figure 3.5 vs 3.2 and 3.4-right, and also compare the cartoon models of Figure 3.18 below).

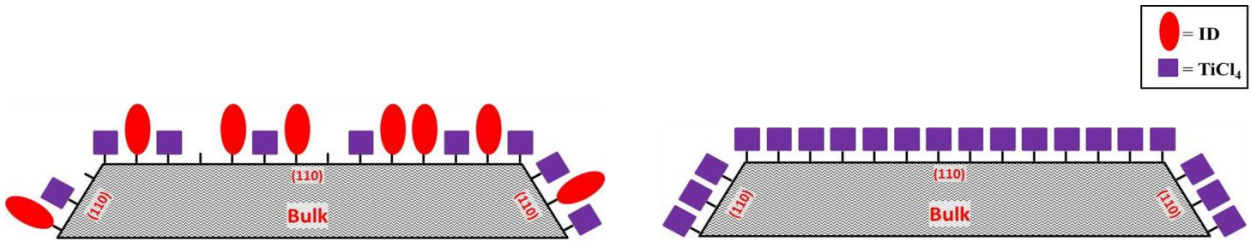

Figure 3.18. Cartoon models of $MgCl_2$(110) surfaces for $MgCl_2/TiCl_4$/ID (left) and $MgCl_2/TiCl_4$ (right) precatalysts.

3.3.3.4. *$MgCl_2/TiCl_4$(/ID) + (AlR_3/)ED*

As the last part of this surface study, we investigated 'full' catalyst formulations, that is combinations of $MgCl_2/TiCl_4$(/ID) precatalysts with AlR_3/ED solutions (the latter also in the variant without AlR_3, for comparative purposes). As usual, precatalyst aliquots were contacted in the XCM™, always at 70°C under magnetic stirring, for 30 min or – in some series of experiments – at variable time, with heptane solutions of AlR_3 (most typically $AlEt_3$, TEA) and a proper ED at variable [ED]/[Ti] ratio. After that, the solid phases were recovered, washed, dried, and characterized by means of ICP-OES for quantitative metal and donor analyses.

In Table 3.5 we report the ^{1}H NMR quantification of the ID and ED in the solid phases recovered after contacting $MgCl_2$/DBP/$TiCl_4$ with TEA/(^{i}Bu)$_2$Si(OMe)$_2$ and (^{i}Bu)$_2$Si(OMe)$_2$ alone in heptane at 70°C for 30 min. In the latter case (entries 1-6), we found that practically no DBP desorbed, and very low amounts of (^{i}Bu)$_2$Si(OMe)$_2$ adsorbed on the solid phase. In the presence of TEA (entries 7-12), on the

other hand, the ID was almost completely removed, and a roughly equimolar amount of $(^{i}Bu)_2Si(OMe)_2$ was adsorbed in its place, ending up with an almost constant total donor content throughout the explored range of [Si]/[Ti] molar ratios.

Table 3.5. Amounts of DBP (ID), $(^{i}Bu)_2Si(OMe)_2$ (ED), and total donor (ID+ED) in the solid phases recovered after reacting $MgCl_2/TiCl_4$/DBP with $(^{i}Bu)_2Si(OMe)_2$ and TEA/$(^{i}Bu)_2Si(OMe)_2$ in heptane at 70°C.

Entry	System	[Si]/[Ti]	ID [a]	ED [a]	Total Donor [a]
1	$MgCl_2/DBP/TiCl_4$ + $(^{i}Bu)_2Si(OMe)_2$	0	7.9	–	7.9
2		1.25	8.2	1.2	9.4
3		3.75	7.7	0.5	8.2
4		6.25	9.0	1.7	10.7
5		13.0	8.3	0.8	9.1
6		20.0	9.0	2.0	11.0
7	$MgCl_2/DBP/TiCl_4$ + TEA/$(^{i}Bu)_2Si(OMe)_2$	1.25	1.4	3.3	4.7
8		2.50	2.1	5.7	7.8
9		6.25	1.9	7.1	9.0
10		10.0	1.2	7.6	8.8
11		12.5	1.1	8.3	9.4
12		15.0	1.7	7.5	9.2

Reaction conditions: *T* = 70°C; heptane, 3.8 mL; precatalyst, 25mg; [Al]/[Ti] = 25; *t* = 30 min.
[a] mol% wrt Mg.

With the aim to highlight possible qualitative differences in the adsorption of $(^{i}Bu)_2Si(OMe)_2$ on $MgCl_2/DBP/TiCl_4$ treated with and without TEA, selected samples in the two sub-sets of Table 3.5 were re-prepared, and downstream to the reaction washed under more severe conditions (i.e. 3 times with heptane at 70°C) prior to the final drying step; the $(^{i}Bu)_2Si(OMe)_2$ contents were analysed by ^{1}H NMR, and compared with those of samples subjected to the standard protocol. As a matter of fact, the results, reported in Table 3.6, highlighted major differences: the binding of $(^{i}Bu)_2Si(OMe)_2$ turned out to be stronger in the sample treated with TEA, and therefore almost DBP-free (entries 4-6), whereas

the lower amounts found in samples still retaining DBP were only weakly adsorbed, and therefore were largely washed out at 70°C (entries 1-3).

Table 3.6. Amounts of $(^{i}Bu)_2Si(OMe)_2$ (ED) measured by ^{1}H NMR in the solid phases recovered after reacting $MgCl_2/TiCl_4$/DBP with TEA/$(^{i}Bu)_2Si(OMe)_2$ and $(^{i}Bu)_2Si(OMe)_2$ in heptane at 70°C, after two different washing protocols (see text). Reaction conditions were identical to those for Table 3.5.

Entry	System	[Si]/[Ti]	ED (mol% wrt Mg)	
			Standard washing	Thorough washing
1	$MgCl_2/DBP/TiCl_4$ + $(^{i}Bu)_2Si(OMe)_2$	1.25	1.2	0.1
2		6.25	1.7	0.1
3		13.0	0.8	0.3
4	$MgCl_2/DBP/TiCl_4$ + TEA/$(^{i}Bu)_2Si(OMe)_2$	1.25	7.7	4.2
5		2.5	5.7	5.8
6		6.25	6.8	6.4

Next, we investigated the kinetics of ID/ED exchange, by treating $MgCl_2/DBP/TiCl_4$ with TEA/$(^{i}Bu)_2Si(OMe)_2$ in heptane solution at 70°C under given conditions for different contact times, and analyzing the recovered solid phases. Figure 3.19 demonstrates that the exchange is rather fast, and reaches a steady state within 5 min. This agrees with the previous observation that the reactions of DBP with AlR_3 are fast already at room temperature (§ 3.3.3.2.), and confirms that the resulting DBP removal from the catalyst surface governs the chemisorption of the ED.

Importantly, we found that (within certain limits) the ID/ED exchange is basically independent of the specific alkoxysilane ED used in combination with AlR_3. This is shown in Figure 3.20, which refers to a set of 11 alkoxysilanes largely differing in chemical structure and steric demand, screened under the same conditions of Table 3.5 (the various EDs are identified with numerical codes only on Sabic's request, for intellectual protection reasons). The figure further confirms that the desorption of DBP is not assisted by the ED, and indicates that the molar uptake of a given catalyst sample as a result of the ID/ED exchange is only marginally dependent on the individual alkoxysilane ED (at least for the catalyst class investigated here and within certain prototypical molecular structures).

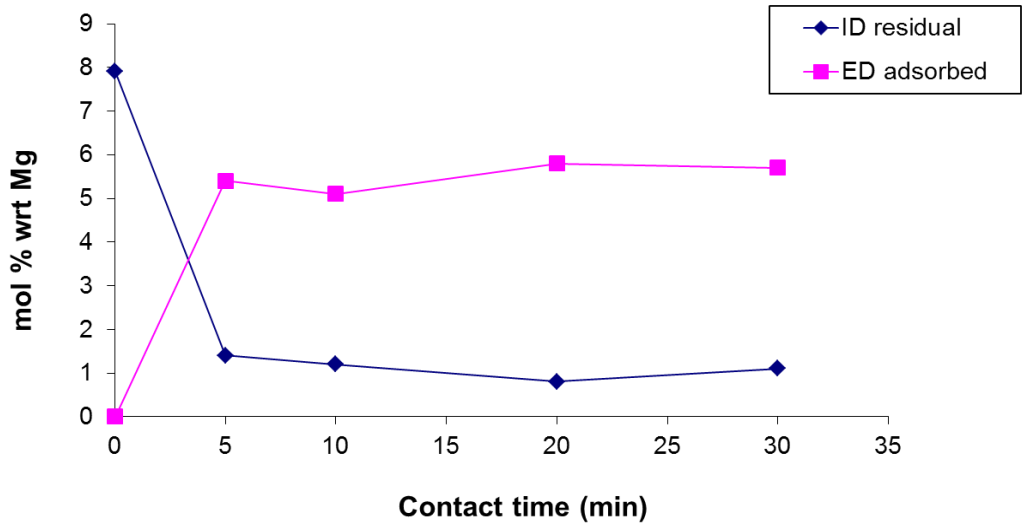

Figure 3.19. Kinetics of DBP (ID)/(^{i}Bu)$_2$Si(OMe)$_2$ (ED) exchange for $MgCl_2/TiCl_4$/DBP + $AlEt_3$/(^{i}Bu)$_2$Si(OMe)$_2$ in heptane at 70°C ([Al]/[Ti] = 25; [Si]/[Al] = 0.10).

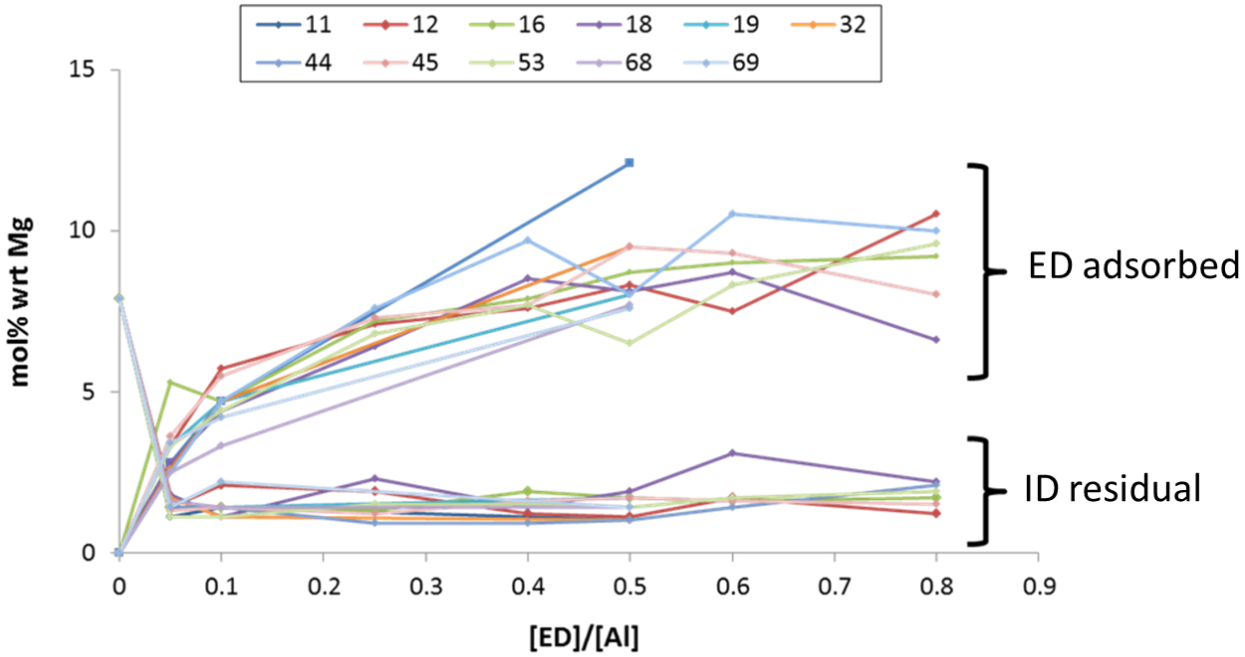

Figure 3.20. DBP (ID)/alkoxysilane (ED) exchange for $MgCl_2/TiCl_4$/DBP + $AlEt_3$/ED systems featuring 11 different EDs, reacted in heptane at 70°C under the same conditions of Table 3.5.

To make this important point more explicit, in Figure 3.21 we compare the quantified ID/ED exchange for the reaction of $MgCl_2/TiCl_4$/DBP in heptane (at 70°C for 30 min) with $AlEt_3/(^iBu)_2Si(OMe)_2$ and $AlEt_3/(Me)_2Si(OEt)_2$. Despite the largely different steric hindrance, these two EDs turned out to adsorb in the same molar amount (roughly corresponding to that of DBP in the original precatalyst removed by the Al-Alkyl) within the experimental error. Looking at the model of Figure 3.2, one can easily find a rationale for that, but also anticipate that the steric hindrance on the surface will be definitely different, and so will the modification of the co-adsorbed catalytic species and the resulting catalyst behavior. We will come back to this issue under § 3.4.

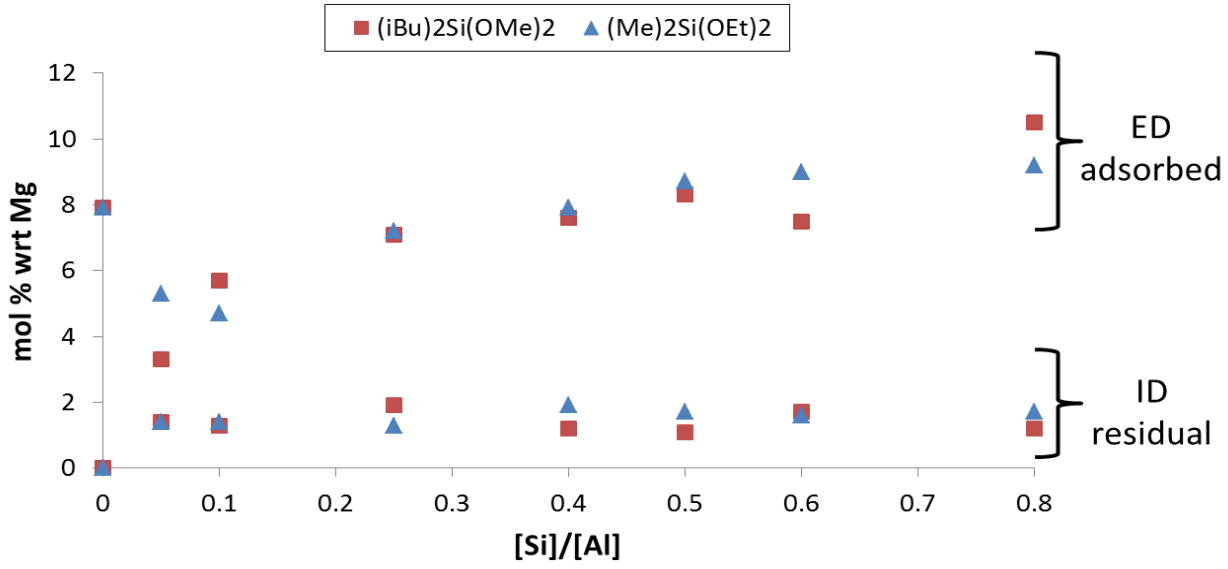

Figure 3.21. DBP (ID)/alkoxysilane (ED) exchange for $MgCl_2/TiCl_4$/DBP + $AlEt_3/(^iBu)_2Si(OMe)_2$ and $MgCl_2/TiCl_4$/DBP + $AlEt_3/(Me)_2Si(OEt)_2$, reacted in heptane at 70°C for 30 min under the same conditions of Table 3.5.

The hypothesis that the ED molecules can only chemisorb on $MgCl_2$ surfaces liberated by the ID was further probed by investigating the behavior of two precatalysts which are not expected to provide large amounts of ED-binding sites, namely $MgCl_2/TiCl_4$/2,2-diisobutyl-1,3-dimethoxypropane (DMP) and $MgCl_2/TiCl_4$. The former features an ID known to be unreactive toward AlR_3[9,10], whereas experimental and computational evidence suggests that the latter has mainly $MgCl_2$(110)

terminations with a close-to-full coverage by $TiCl_4$ (Figures 3.5 and 3.18-right). The two precatalysts were reacted at 70°C for 30 minutes with heptane solutions of $AlEt_3/(^iBu)_2Si(OMe)_2$ at variable [Si]/[Al] ratios, and the donor contents in the recovered solid phases were measured by ^1H NMR. In agreement with the starting hypothesis, $(^iBu)_2Si(OMe)_2$ adsorption on $MgCl_2/TiCl_4$ was almost negligible (Table 3.7, entries 1-6). On the other hand, a slightly larger incorporation was observed onto $MgCl_2/TiCl_4$/DMP (Table 3.7, entries 7-10), without any appreciable release of DMP. Tentatively, we trace the latter finding to the aforementioned looser coverage of $MgCl_2$ surfaces where large LB molecules and $TiCl_4$ units are co-adsorbed (Figure 3.18-left); this would explain, inter alia, the known fact that alkoxysilane EDs are still necessary for catalysts modified with 1,3-dimethoxypropane IDs to reach a high stereoselectivity.[9,10]

Table 3.7. Donor contents of $MgCl_2/TiCl_4$ and $MgCl_2/TiCl_4$/2,2-diisobutyl-1,3-dimethoxypropane (DMP) after reaction with $AlEt_3$(TEA)/$^iBu_2Si(OMe)_2$ (ED) in heptane at 70°C.

Entry	System	[Si]/[Al]	DMP (mol % wrt Mg)	ED (mol % wrt Mg)
1	$MgCl_2/TiCl_4$ + TEA/$(^iBu)_2Si(OMe)_2$	0	–	–
2		0.05	–	0.8
3		0.10	–	1.0
4		0.20	–	1.5
5		0.5	–	1.5
6		0.8	–	1.7
7	$MgCl_2/TiCl_4$/DMP + TEA/$(^iBu)_2Si(OMe)_2$	0	8.1	–
8		0.05	8.1	2.2
9		0.10	8.9	2.4
10		0.5	8.6	2.6

Reaction conditions: *T* = 70°C; heptane, 3.8 mL; precatalyst, 25 mg; [Al]/[Ti] = 25; *t* = 30 min.

In concluding this section, in Table 3.8 we summarize the overall picture for the two HY-ZNC precatalysts identified in § 3.1 as specially representative, namely $MgCl_2/TiCl_4$ and $MgCl_2/TiCl_4$/DBP. The table collects the amounts of Ti, Al, ID and ED (in mol% wrt Mg) found to cover the lateral

terminations of the $MgCl_2$ matrix after reacting said precatalysts with $AlEt_3/Me_2Si(OEt)_2$ in heptane at 70°C for 30 min.

Table 3.8. Typical compositions of the solid phases formed after reacting $MgCl_2/TiCl_4$ and $MgCl_2/TiCl_4$/DBP precatalysts with $AlEt_3$ (TEA) and $AlEt_3/Me_2Si(OEt)_2$ (ED) in heptane at 70°C.

Entry	Precatalys	Cocatalyst	Ti [a]	DBP [a]	ED [a]	Al [a]	Total [a]
1	$MgCl_2/TiCl_4$	–	3.8	–	–	–	3.8
2		TEA	3.5	–	–	3.4	6.9 [b]
3		TEA/$(Me)_2Si(OEt)_2$	3.5	–	0.8	3.4	7.6 [b]
4	$MgCl_2$/DBP/$TiCl_4$	–	7.5	7.9	–	–	15.7
5		TEA	5.6	1.3	–	18.8	24.9 [b]
6		TEA/$(Me)_2Si(OEt)_2$	5.6	1.3	7.6	12.1	26.5 [b]

Reaction conditions: *T* = 70°C; heptane, 3.8 mL; precatalyst, 25 mg; [Al]/[Ti] = 25; [Si]/[Al] = 0.10; *t* = 30 min.
[a] mol% wrt Mg. [b] Possible overlayer(s) formation

Our interpretation of the data in Table 3.8 is as follows:

- A binary $MgCl_2/TiCl_4$ precatalyst is able to achieve a high degree of surface coverage, due to the good match of epitaxial $TiCl_4$ adsorbates on $MgCl_2$(110) terminations (Figure 3.5). When treated with excess $AlEt_3$, Al-alkyl species adsorb in roughly equimolar amounts wrt to Ti; this most probably indicates the formation of Cl-bridged hetero-dinuclear adducts, and implies in turn that all the Ti species are exposed and accessible. EDs like alkoxysilanes find relatively few available (Mg) chemisorption sites, which explains the rather low incorporation and relatively poor effectiveness of their action of surface modification. As noted before, the primary crystallites in this system are not exceedingly small (roughly 10 nm along *a* and *c*), which is consistent with an overall Mg/adsorbate mole ratio of 20-30 (not considering over-layers).
- An $MgCl_2/TiCl_4$/DBP precatalyst differs from the previous one in at least two important respects: (a) along with $TiCl_4$, it contains a stronger and sterically demanding adsorbate, namely DBP, which results into smaller and more defective primary crystallites (as indicated by

the poorly defined powder X-ray diffraction profile[21]), and a less compact surface coverage leaving behind some Mg vacancies; and (b) DBP is rapidly removed by excess AlR_3, which liberates large amounts of $MgCl_2$ surface for the chemisorption of an ED (e.g., an alkoxysilane), and probably reaction products of AlR_3 with DBP (e.g., Al-alkoxides). This results into a massive incorporation of both, ending up with an overall Mg/adsorbate mol ratio (not considering overlayers) as low as ~5; such a value is not unusual in heterogeneous catalysis, and for $MgCl_2$ requires primary particles with average dimensions of ~6-7 nm along *a* and close to the monolayer state, which is what is typically claimed for such catalysts in the literature.[21]

3.4. Relationships with catalyst polymerization behavior

The experimental facts reported in the previous section and their tentative interpretation are important because they represent the basis for determining and hopefully controlling the behavior of the catalytic species in HY-ZNCs for iPP. Surface modification with LBs is key to modulate the steric (and to some extent the electronic) environment of the active Ti centers, similarly to what can be achieved by means of ancillary ligands in molecular catalysis. Therefore, correlating surface structure and analysis with observed propene polymerization trends is the necessary step to implement a working model of the catalysts, irrespective of the 'white-box' or 'black-box' character of such a model.

In this section, we will focus on rational elements, in line with the declared objective of the chapter. The polymerization experiments were carried out in the PPR48 platform, but were aimed to highlight fundamental trends, pinpointing structure/properties correlations that can be interpreted in light of descriptors with an immediate molecular significance; for this, a truly HTE approach was not necessary. The parallel HTE implementation of a large QSAR database functional to the construction of a 'black-box' model, on the other hand, will be the subject of Chapter 4.

A first simple set of polymerization experiments that were carried out and we like to comment here are summarized in Table 3.9.

Table 3.9. Results of propene polymerization experiments in heptane slurry at 70°C in the presence of $MgCl_2/TiCl_4$ and $MgCl_2/TiCl_4$/DBP in combination with $AlEt_3$(TEA) or $AlEt_3/(^iBu)_2Si(OMe)_2$, with and without H_2 as a chain transfer agent.

Entry	Catalyst	Cocatalyst	H_2	R_p [a]	I.I. (%)	M_n (KDa)	M_w (KDa)	M_w/M_n
1	$MgCl_2/TiCl_4$	TEA	No	12	29	44	925	21.1
2		$TEA/(^iBu)_2Si(OMe)_2$		5	72	84	1950	23.2
3		TEA	Yes [b]	22	40	18	82	4.5
4		$TEA/(^iBu)_2Si(OMe)_2$		6	75	17	121	7.1
5	$MgCl_2/TiCl_4$/DBP	TEA	No	16	79	80	582	7.2
6		$TEA/(^iBu)_2Si(OMe)_2$		23	96	75	536	7.1
7		TEA	Yes [b]	48	81	22	123	5.7
8		$TEA/(^iBu)_2Si(OMe)_2$		63	95	31	206	6.7

Polymerization conditions: T = 70°C; $p_{(C3H6)}$ = 4.4 bar; heptane, 5.0 mL; precatalyst, 0.10-1.0 mg; [Si]/[Al] = 0.20; [Al]/[Ti] ~ 200; reaction time, 20-60 min.
[a] g(PP) mg(Ti)$^{-1}$ h^{-1} bar^{-1} ; [b] p_{H2} = 0.2 bar

In our opinion, the strikingly different behavior of the two screened catalysts is in line with the hypotheses on their surfaces put forward in the previous section. In particular, adding the ED to the system with no ID caused a *drop in catalyst productivity,* and only a *moderate enhancement of stereoselectivity*, to be compared with a marked *increase in productivity* and a *large enhancement of stereoselectivity* for the ID-containing system. This provides a confirmation that in the former case the ED had limited access to the $MgCl_2$ surface, and therefore its action likely consisted in a partly selective poisoning of the less-stereoselective catalytic species, rather than their modification into more stereoselective ones. On the other hand, for both systems the addition of H_2 to regulate polymer molecular mass caused an increase in productivity, which can be related with the waking-up of 'dormant sites' (§ 1.3.6). The stronger H_2 response of the ID-free catalyst system is in line with its much lower regioselectivity.[22,23] On the other hand, the very broad molar mass distribution (MMD) of the polymer produced in the absence of H_2 is somewhat surprising; the strong narrowing produced by H_2 may indicate a correspondingly broad distribution of 'dormant' site character for the catalytic species, that the addition of H_2 largely levels-off.

Focusing now on the $MgCl_2/TiCl_4$/DBP precatalyst, Table 3.10 reports propene polymerization results in heptane slurry at 70°C when such a precatalyst was activated with $AlEt_3$ (TEA) alone, or $AlEt_3/(^iBu)_2Si(OMe)_2$ and $AlEt_3/(Me)_2Si(OEt)_2$ combinations.

Table 3.10. Results of propene polymerization experiments in heptane slurry at 70°C in the presence of $MgCl_2/TiCl_4$/DBP in combination with $AlEt_3$ (TEA), $AlEt_3/(^iBu)_2Si(OMe)_2$, and $AlEt_3/(Me)_2Si(OEt)_2$ combinations.

Entry	Cocatalyst	[Si]/[Al]	R_p [a]	[*mmmm*] [b]	M_n (KDa)	M_w (KDa)	M_w/M_n
1	TEA	-	14.4	0.73	42	290	6.9
2	TEA + $(^iBu)_2Si(OMe)_2$	0.50	8.0	0.91			
3		0.10	11.4	0.88	181	907	5.0
4		0.05	12.9	0.88	128	1050	8.2
5	TEA + $(Me)_2Si(OEt)_2$	0.50	7.9	0.77			
6		0.10	14.2		95	445	4.7
7		0.05	18.3	0.76	94	418	4.4

Polymerization conditions: T = 70°C; $p_{(C3H6)}$ = 4.4 bar; heptane, 5.0 mL; precatalyst, 0.10 mg; [Al]/[Ti] ~ 200; reaction time, 20 min.
[a] Productivity ($g_{(PP)}$ $mg_{(Ti)}^{-1}$ $h^{-1}$$bar^{-1}$). [b] Fraction of isotactic pentad, determined by ^{13}C NMR.

In Figure 3.21 we reported experimental results demonstrating that the ID/ED exchange for the two investigated $MgCl_2/TiCl_4$/DBP + $AlEt_3$/ED systems proceeds identically as a function of the [Si]/[Al] ratio, meaning in particular that equimolar amounts of the two EDs are chemisorbed on the surface in the place of DBP at a given [Si]/[Al] ratio. On the other hand, we noted before that $(^iBu)_2Si(OMe)_2$ and $Me_2Si(OEt)_2$ have largely different steric demands, and therefore the surface modification that they can cause at formally equal degree of coverage must be different. Indeed, Table 3.10 and Figure 3.22 demonstrate that only the bulkier $(^iBu)_2Si(OMe)_2$ is able to bring the catalyst to acceptable levels of stereoselectivity (which would further increase in case H_2 were used). Not unexpectedly, an even lower stereoselectivity was observed when no ED was added to replace DBP.

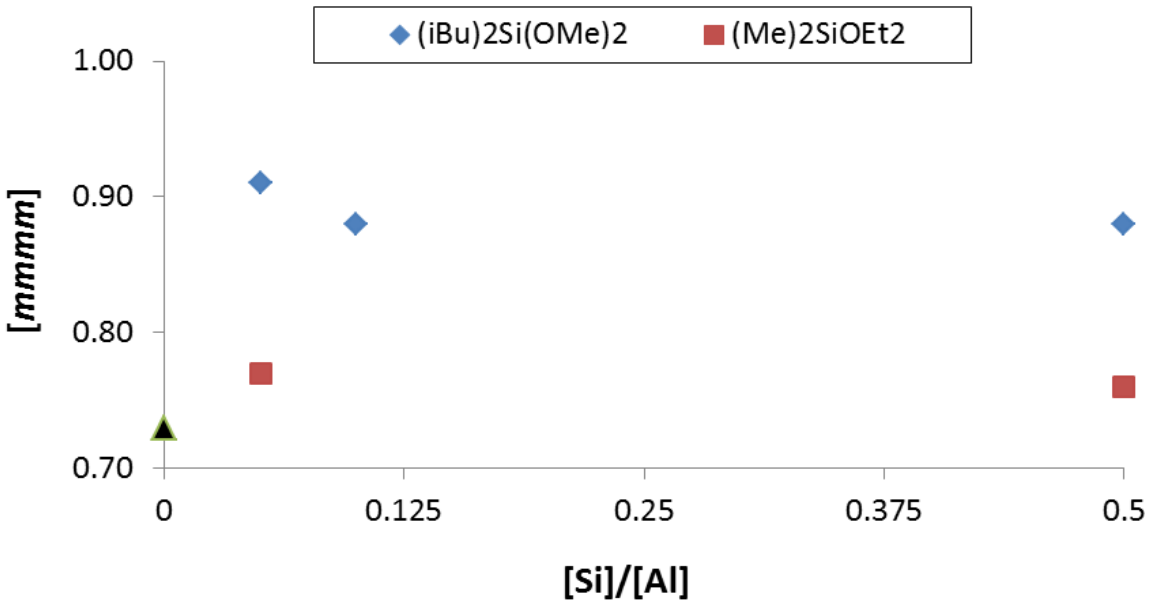

Figure 3.22. ^{13}C NMR fraction of isotactic pentad as function of [ED]/[Al] for PP samples obtained in the presence of catalyst systems $MgCl_2/TiCl_4$/DBP – $AlEt_3/(^iBu)_2Si(OMe)_2$, and $MgCl_2/TiCl_4$/DBP – $AlEt_3/(Me)_2Si(OEt)_2$ (data from Table 3.10).

That the action of modification by LB molecules at non-bonded contact of the active species on the surface of HY-ZNCs is exquisitely dependent on the molecular features of said molecules, more than their local concentration, finds an extreme confirmation in Figures 3.23 and 3.24. The former shows data of ID/ED exchange for $MgCl_2/TiCl_4$/DBP reacted at 70°C with heptane solutions of $AlEt_3/(^iBu)_2Si(OMe)_2$ and $AlEt_3$/2,6-dimethylpyridine; the latter belongs in a totally different class of EDs, and has a much lower steric demand compared with the alkoxysilane. Still, the ID/ED exchange for the two systems turned out to proceed almost identically. On the other hand, the results in terms of catalyst behavior were dramatically different, as Figure 3.24 indicates: the methyl region of the polymer produced with ED = $(^iBu)_2Si(OMe)_2$ is typical of an enantiomorphic-sites-controlled iPP sample with fairly high degree of stereoregularity, whereas that of the polymer made with ED = 2,6-dimethylpyridine reveals similar fractions of isotactic and syndiotactic sequences/blocks.[7,24,25]

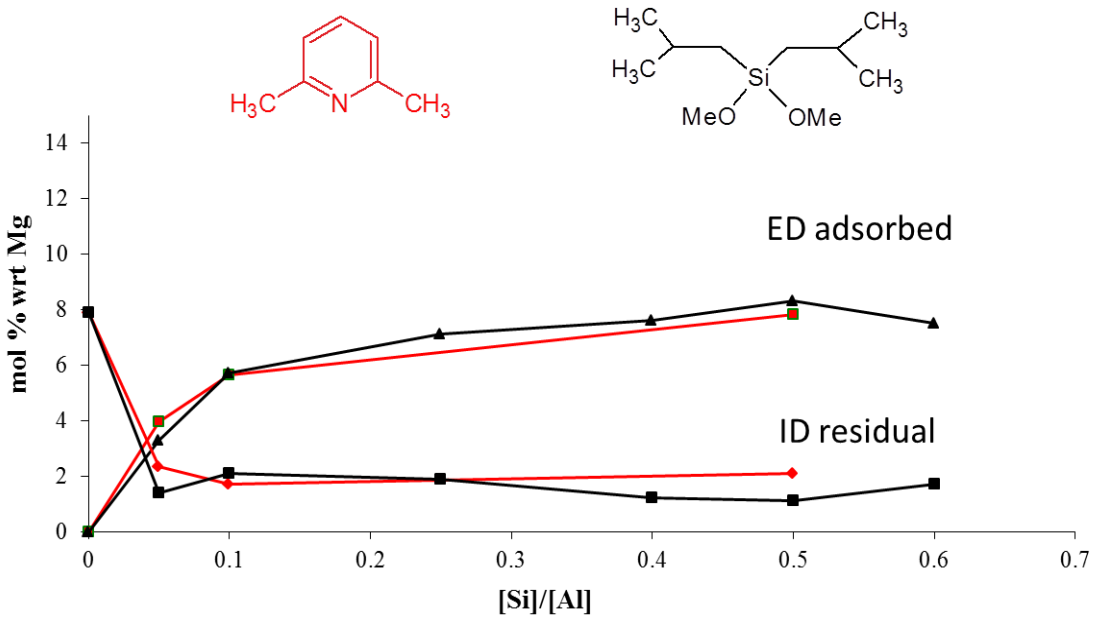

Figure 3.23. ID/ED exchange for $MgCl_2/TiCl_4$/DBP – $AlEt_3/(^{i}Bu)_2Si(OMe)_2$ and $MgCl_2/TiCl_4$/DBP – $AlEt_3$/2,6-dimethylpyridine catalyst systems in heptane slurry at 70°C ([Al]/[Ti] = 25).

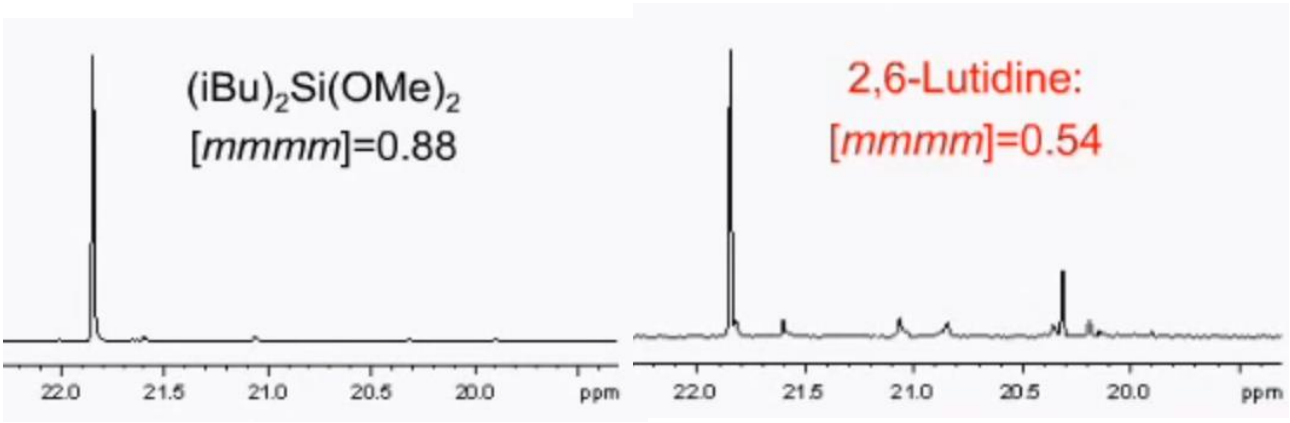

Figure 3.24. Methyl region of the ^{13}C NMR spectra of PP samples obtained in the presence of $MgCl_2/TiCl_4$/DBP – $AlEt_3/(^{i}Bu)_2Si(OMe)_2$ and $MgCl_2/TiCl_4$/DBP – $AlEt_3$/2,6-dimethylpyridine catalyst systems ([Al]/[ED] = 10) in heptane slurry at 70°C.

A possible interpretation of these results can be attempted in the framework of the 3-site model of active sites for HY-ZNCs illustrated in § 1.3.5 (Figure 1.15)[7,24]; in particular, the presence of bulky $(^{i}Bu)_2Si(OMe)_2$ molecules at non-bonded contact with a surface Ti species may result into the situation

of Figure 1.15-**C1**, whereas the small molecules of 2,6-dimethylpyridine may rather lead to a local environment closer to Figure 1.15-**C3**.

In concluding this section, we note that EDs are not the only tool to modulate an active HY-ZNC surface. In previous sections of this chapter, we have shown that large amounts of Al-alkyl species are chemisorbed on the solid catalyst along with LB molecules. Thus, it looked plausible to predict that the molecular features of the AlR_3 used to activate the precatalyst and scavenge the system can also impact on catalyst behavior. Indeed, this was confirmed by the data in Table 3.11, which refers to catalyst systems $MgCl_2/TiCl_4$/DBP – $AlR_3/(^{i}Bu)_2Si(OMe)_2$ featuring four different AlR_3, namely $AlMe_3$ (TMA), $AlEt_3$ (TEA), $Al(^{i}Bu)_3$ (TIBA) and $Al(^{t}Bu)_3$ (TTBA). As is well-known, the steric demand of the R groups on Al dramatically affects molecular behaviors: in aliphatic hydrocarbon solution at moderate temperatures, TMA and TEA are mainly in dimeric Al_2R_6 form, whereas TIBA and TTBA are monomeric.[26] Table 3.11 combines information on surface analysis obtained in the XCM™ platform with propene polymerization results in the PPR48; the overall picture clearly demonstrates that Al-alkyls can indeed affect the stereoselectivity of the active species in the investigated HY-ZNC.

Table 3.11. Results of surface analysis and propene polymerization for catalyst systems $MgCl_2/TiCl_4$/DBP – $AlR_3/^{i}Bu_2Si(OMe)_2$ with AlR_3 = TMA, TEA, TIBA, TTBA.

Entry	AlR_3	Surface analysis		Polymerization results	
		Ti final [a]	Al adsorbed [a]	R_p [b]	[*mmrrmm*] [c]
1	$AlMe_3$ (TMA)	5.6	13.3	28.3	0.36
2	$AlEt_3$ (TEA)	5.6	16.3	52.0	0.42
3	$Al(^{i}Bu)_3$ (TIBA)	5.5	10.6	29.2	0.52
4	$Al(^{t}Bu)_3$ (TTBA)	5.0	8.4	11.0	0.90

Precatalyst activation conditions: T = 70°C; heptane, 3.8 mL; precatalyst, 25 mg; [Al]/[Ti] = 25; [Si]/[Al] = 0.10; t = 30 min.
Polymerization conditions: T = 70°C; $p_{(C3H6)}$ = 4.4 bar; p_{H2} = 0.20 bar; heptane, 5.0 mL; precatalyst, 0.10-1.0 mg; [Al]/[Ti] ~ 200; reaction time, 20-40 min.
[a] mol% wrt Mg. [b] $g_{(PP)}\ mg_{(Ti)}^{-1}\ h^{-1}bar^{-1}$. [c] Determined by ^{13}C NMR.

Correlating the above results with the size of the Alkyl group on Al is not trivial, because many simultaneous effects must be considered. As noted before, AlR_3 species with bulky R groups are

monomeric, and therefore in principle more Lewis-acidic; on the other hand, the steric demand of R disfavors the tendency to form bridges with the surface Ti species, and may impede access to 'crowded' regions of the $MgCl_2$ surface. Tentatively, the comparatively low adsorption of Al species in the case of TMA can be traced to its strong tendency to be dimeric and as such remain in solution; on the other hand, once on the surface the $AlMe_3$ molecule can bind tightly to Ti, which may well be the reason for the low catalyst productivity observed with this Al-alkyl, and the high stereoselectivity as well in case sterically open catalytic species are blocked in preference. With bulky AlR_3 like TIBA and TTBA, on the other hand, the picture is less obvious. The low mol amount of chemisorbed Al species here does not necessarily correspond to a low surface occupation, due to the large steric demand of R; in all cases, these molecules feature a rather low ability to activate the precatalyst (i.e., low(er) productivity compared with TMA and TEA), and also to usefully modify the catalytic species (rather low polymer stereoregularity). All in all, the best compromise seems to be represented by TEA, which is in fact by far the preferred activator in industrial HY-ZNC formulations; that TEA is also the cheapest one certainly does not harm…

References

(1) Busico, V.; Causà, M.; Cipullo, R.; Credendino, R.; Cutillo, F.; Friederichs, N.; Lamanna, R.; Segre, A.; Van Axel Castelli, V. *J. Phys. Chem. C*, **2008**, *112*, 1081-1089.

(2) Credendino, R.; Busico, V.; Causà, M.; Barone, V.; Budzelaar, P. H. M.; Zicovich-Wilson, C. *PCCP* **2009**, *11*, 6525-6532.

(3) D'Amore, M.; Capone, F.; Budzelaar, P. H. M.; Busico, V., manuscript in preparation.

(4) Correa, A.; Piemontesi, F.; Morini, G.; Cavallo, L. *Macromolecules* **2007,** *40,* 9181-9189.

(5) D'Amore, M., to be published.

(6) Boero, M.; Parrinello, M.; Weiss, H.; Hüffer, S. *J. Phys. Chem. A* **2001**, *105*, 5096-5105.

(7) Busico, V.; Cipullo, R.; Monaco, G.; Talarico, G.; Vacatello, M.; Chadwick, J. C.; Segre, A. L.; Sudmeijer, O. *Macromolecules* **1999**, *32*, 4173-4182.

(8) D'Amore, M.; Credendino, R.; Budzelaar, P. H. M.; Causá, M.; Busico, V. *J. Catal.* **2012***, 286,* 103-110.

(9) Cecchin, G.; Morini G; Piemontesi, F. In *Encyclopedia of Chemical Technology*; John Wiley and Sons: New York (NY), 2006; Vol. 26, pp. 502-554.

(10) *Polypropylene Handbook: Polymerization, Characterization, Properties, Applications*; Moore, E.P. Jr., Ed.; Hanser Publishers: Munich, 1996.

(11) Busico, V.; Corradini, P.; De Martino, L.; Proto, A.; Savino, V.; Albizzati, E. *Makromol. Chem.* **1985**, *186*, 1279-1288.

(12) Giunchi, G.; Allegra, G. *J. Appl. Cryst.* **1984**, *17*, 172-178.

(13) Cutillo, F., unpublished results.

(14) Ehm, C., to be published.

(15) Vähäsarja, E.; Pakkanen, T. T.; Pakkanen, T. A.; Iiskola, E.; Sormunen, P. *J. Polym. Sci. A: Polym. Chem.* **1987**, *25*, 3241-3253.

(16) Busico, V.; Corradini, P.; De Martino, L.; Graziano, F.; Iadicicco, A. *Makromol. Chem.* **1991**, *192*, 49-57.

(17) See, e.g.: Barbè, P.C.; Cecchin, G.; Noristi, L. *Adv. Polym. Sci.* **1986**, *81*, 1-81, and refs. therein.

(18) Cutillo, F.; Busico, V.; Lamanna, R.; Van Axel Castelli, V.; Segre. A., manuscript in preparation.

(19) Ystenes reported IR evidence for this. See, e.g.: Bache, O.; Ystenes, M. Appl. Spectr. **1994**, *48*, 985-993, and refs. therein.

(20) (a) Boero, M.; Parrinello, M.; Terakura, K. *J. Am. Chem. Soc.* **1998**, *120*, 2746-2752. (b) Boero, M.; Parrinello, M.; Hüffer, S.; Weiss, H. *J. Am. Chem. Soc*. **2000**, *122*, 501-509.

(21) Zannetti, R.; Marega, C.; Marigo, A.; Martorana, A. *J. Polym. Sci. B: Polym. Phys.* **1988**, *26*, 2399-2412.

(22) Busico, V.; Cipullo, R.; Polzone, C.; Talarico, G.; Chadwick, J. C. *Macromolecules* **2003**, *36*, 2616-2622.

(23) Busico, V.; Chadwick, J. C.; Cipullo, R.; Ronca, S.; Talarico, G. *Macromolecules* **2004**, *37*, 7437-7443.

(24) Busico, V.; Cipullo, R. *Progr. Polym. Sci.* **2001**, *26*, 443-533.

(25) Macko, T.; Cutillo, F.; Busico, V.; Brüll, R. *Macromol. Symp.* **2010**, *298*, 182-190.

(26) Shreve, A. P.; Muelhaupt, R.; Fultz, W.; Calabrese, J.; Robbins, W.; Ittel, S. D. *Organometallics* **1988**, *7*, 409-416.

4. A 'Black-Box' QSAR Approach to HY-ZNCs

4.1. Introduction

There are at least two complex hyperspaces that need to be explored and mapped precisely in order to 'design' a HY-ZNC. One is the hyperspace of catalyst structure, with its numerous –mainly chemical– individual variables (namely, the support, the Ti precursor, the Internal Donor, the Al-alkyl, the External Donor(s)…), and partial or full combinations thereof. Chapter 1 and 3 of this thesis traced –we believe– a reasonably good low-definition map, able to provide some orientation for the navigation. The other, probably more complicated and featuring chemical, physical and process variables often wildly intertwined, is the hyperspace of (pre)catalyst preparation, meant to create the previous one, and define fundamental aspects related with morphology and physico-mechanical properties. In the present thesis, we did not even step into it; based on the literature[1], though, the impression is that of a labyrinth, where expert scouts are still useful to find the right path without first wondering in loops.

In view of the above, while confirming the ultimate objective of Chapter 3 to understand and 'design' HY-ZNCs, we decided to exploit in parallel the great potential of our HTE polyolefin workflow to generate an adequate experimental database for the implementation of a 'black-box' Quantitative Structure Activity Relationship (QSAR) model of catalyst behavior, able to predict the effects of surface modification by means of certain classes of LBs, and orient the synthesis and testing of novel ones, without needing or making assumptions on catalyst structure, behavior, and mechanism(s) of LB action.

It may be worth recalling that, according to the general definition, QSAR models are regression or classification models used in the chemical and biological sciences and engineering.[2-3] Like other regression models, QSAR regression models, in particular, relate a set of 'predictor' variables (X) to the potency of the response variable (Y). The predictors consist of physico-chemical properties or theoretical molecular descriptors of chemicals; the QSAR response-variable is typically some kind of activity of the chemicals. When physico-chemical properties or structures are expressed by numbers,

one can find a mathematical relationship – that is the QSAR – between the two. The mathematical expression, if properly validated, can then be used to predict the modeled response of other chemical structures, by carefully verifying the applicability domain. Since in most cases the mathematical expression is complex and makes use of a large number of descriptors, it is mandatory to build, train and validate the model on a large-enough high-quality input database, to reduce the error and avoid overfitting.

This chapter describes the implementation, validation and predictive use of a 'black-box' QSAR model whose applicability domain is the modification of the 'activity' of a specific HY-ZNC for iPP, i.e. $MgCl_2/TiCl_4$/DBP – $AlEt_3$/ED with ED = $R'_xR''_ySi(OR)_{4-x-y}$, by means of different $AlEt_3$/ED combinations. As we shall see, 'activity' here includes catalyst productivity, polymer molar mass distribution, Index of Isotacticity, and ^{13}C NMR fraction of isolated enantiomorphic-sites stereodefects.

The input database was built at LSP making use of its HTE infrastructure, and in particular the Freeslate PPR48 setup with integrated analytics (Chapter 2). A set of close to 100 alkoxysilane structures was provided by Sabic Europe and Sabic India. Last but not least, the QSAR models were implemented by Dr. Betty Coussens (DSM Resolve). The overall project is part of the program of an ongoing bilateral Research Collaboration Agreement between Sabic and LSP.

4.2. Model Description

4.2.1. Basic features

A 'black-box' QSAR model belongs in the wider class of 'Black-Boxes', representing any device, system, model, process or objects which converts a series of input into one or more outputs with no knowledge of its internal workings (Figure 4.1).[3]

Figure 4.1. Generic representation of a 'Black-Box'.

Whenever a thorough knowledge/understanding of a system to be investigated is not available, 'black-box' models, relying on an empirical/statistical basis, can represent the only option. Moreover, compared with 'white-box' models, usually they can be implemented in shorter times and with reduced costs. On the other hand, their application window is quite limited (due to the fact that they can be used only within the implemented domain), and rarely the outcome provides direct insight.

A schematic representation of the 'black-box' QSAR approach adopted in the present work is shown in Figure 4.2. For each alkoxysilane, a large set of molecular properties ('descriptors') was calculated, and mathematical equations expressing the relationship(s) between the experimental 'activity' and the chosen descriptors were identified. Such equations ('models') were tested and validated on the experimental data, and then used predictively for the in-silico screening of new structures.

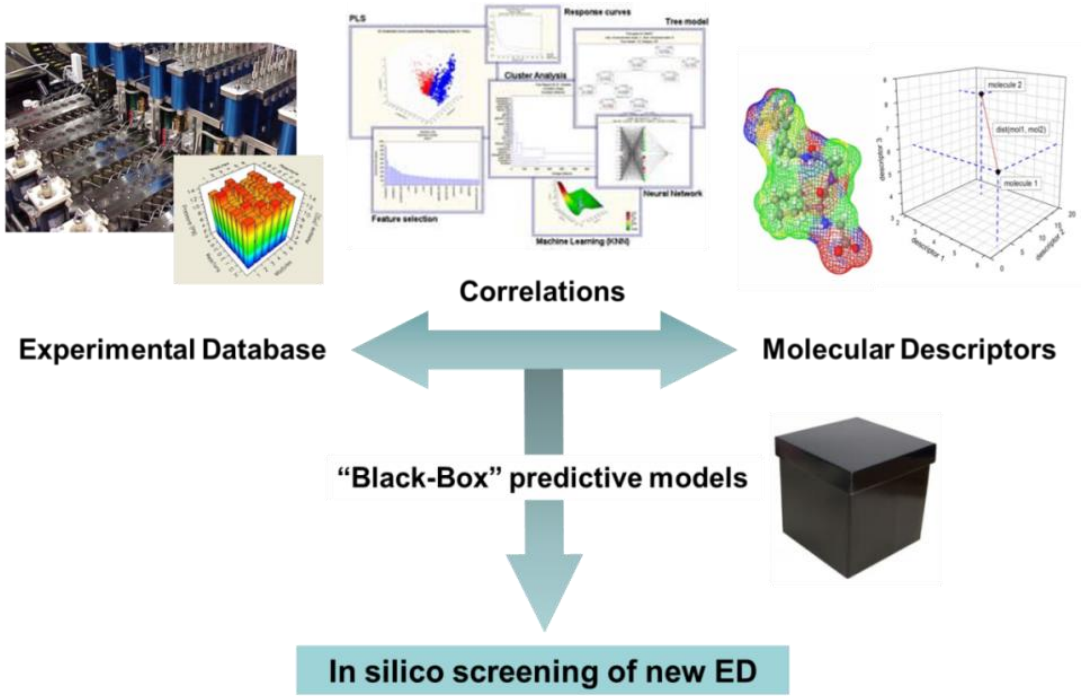

Figure 4.2. Schematic representation of the QSAR workflow implemented in this thesis.

The next sections describe the various steps (e.g. alkoxysilane selection, DoE for the experimental database construction, model implementation, etc) ultimately ending up with a predictive QSAR tool.

4.2.2. Alkoxysilane selection

The set of alkoxysilanes was limited to dimethoxy, trimethoxy, diethoxy and triethoxy structures with a maximum number of six C atoms in the alkyl fragment. This choice was based on perusal of the patent literature, and practical considerations. Out of ~330 structures that could be written on paper, 80 were chosen for experimental screening in the PPR48, to generate the input database, either because commercially available, or in view of the possibility to have the molecules synthesized at the Sabic Research Center of Baroda (India). On Sabic's request, for Intellectual Protection reasons, the molecular structures of these 80 alkoxysilanes will not be disclosed herein, and will be identified by a numerical code. In view of the 'black-box' character of the approach, and the methodological scope of this chapter, we saw no reasons to object.

4.2.3. Planning the experimental database

For each of the 80 EDs selected for the database, the 'activity' in propene polymerization of the resulting $MgCl_2/TiCl_4$/DBP – $AlEt_3$/ED catalyst system was evaluated in the Freeslate PPR48, and the polymers were characterized making use of the tools, methods and protocols thoroughly described in Chapter 2. The DoE for a typical PPR48 library is shown in Figure 4.3.

	1	2	3	4	5	6
A	STD	STD	STD	STD	STD	STD
B	ED1	ED1	ED1	ED2	ED2	ED2
C	ED3	ED3	ED3	ED4	ED4	ED4
D	ED5	ED5	ED5	ED6	ED6	ED6
E	ED7	ED7	ED7	ED8	ED8	ED8
F	ED9	ED9	ED9	ED10	ED10	ED10
G	ED11	ED11	ED11	ED12	ED12	ED12
H	tbd	tbd	tbd	tbd	tbd	tbd

Figure 4.3. DoE of a typical PPR48 library for the QSAR ED screening.

The experimental parameters that were selected to define ED 'activity' and feed the input database were:

(i) Average catalyst productivity, R_p, expressed as g(polymer) mg(Titanium)$^{-1}$ h^{-1} bar(propene)$^{-1}$

Each catalyst system (including a given ED) was normally tested in triplicate, to end up with a standard deviation (SD) on R_p ≤20% (within the specifications of the PPR48 setup). Despite the demonstrated high reliability and reproducibility of the tool (Chapter 2), we decided to include one reaction cell running a reference catalyst system with a known R_p value in each of the 6 PPR48 modules, and to refer the absolute R_p value of an unknown catalyst system to that of the standard system under the same set of reaction conditions, assumed by definition as R_p = 100%. This precaution is specially important in case of mishaps, like e.g. a wrong concentration of the catalyst slurry for whatever reason, or unusually high levels of contaminants in the solvents, monomers, or glove-box environment due to catalyst saturation in the purifiers.

(ii) Average molecular weights, M_n and M_w, and Polydispersity Index (PDI = M_w/M_n)

The SD on these values, usually measured on 1 or 2 replicas of a given sample, can be estimated as ≤20%, which is the 'physiological' value for the technique used to measure them, i.e. High-Temperature Gel Permeation Chromatography.[4] This was verified on sample replicas during a preliminary validation test.

(iii) Index of Isotacticity, I.I.

This represents the fraction by weight of 'isotactic' (that is high-melting) material in a given PP sample. In particular, in the context of the present screening we define I.I. the % by weight of polymer that is insoluble in boiling pentane after an exhaustive process of Kumagawa extraction. Empirically, the thus determined I.I. value is numerically close to (1-X.I.), where X.I. represents the amorphous polymer fraction, defined as the % by weight that does not re-precipitates from a hot xylene solution upon slow cooling to room temperature. The absolute error on I.I., usually measured in duplicate, turned out to be ±1%, which is higher than would be normal for the method, due to the small amount of polymer produced in the PPR cells and usable for the extraction. Considering that most screened EDs performed rather well with respect to this parameter, the said large error covered the subtle differences that would have been important to appreciate. An alternative, more accurate method to measure the I.I. is Crystallization Elution Fractionation (CEF); a Polymer Char setup[5] suited for the purpose was satisfactorily benchmarked, but most unfortunately was not available in time for the screening.

(iv) *^{13}C NMR fraction of isolated enantiomorphic-sites stereodefects in the 'isotactic' (boiling-pentane-insoluble) polymer fraction, numerically coincident with the normalized fraction of [mmrrmm] methyl heptad.*[6]

The accuracy of this measurement was very high, with an absolute error as low as ±0.02%.

From Figure 4.3 it can be seen that, under normal circumstances, one library of 48 PPR experiments was enough to screen 12 EDs in triplicate, each under one given set of conditions (T = 70°C, $p(C_3H_6)$ = 4.4 bar, $p(H_2)$ = 0.20 bar, [Al]/[Ti] ~ 300, [Al]/[Si] = 20, t = 20-40 min). Moreover, the DoE also included 6 'spare' cells in case of outliers, hardware or software malfunctions at individual cells, etc. **The actual database will be provided under § 4.3.**

4.2.4. Descriptor calculations

The selected QSAR approach was a chemical descriptor based one. In this approach, molecular descriptors quantifying various electronic, geometric, or steric properties are computed and used to develop the correlating models. The alkoxysilane structures for the descriptor calculations were obtained by performing DFT optimizations at the BP86-RI/SV(P) level with the Turbomole program.[7] In case of structures featuring more conformations, BP86-RI/SV(P) optimizations were carried out for the lowest energy conformations resulting from an MMFF conformational analysis with the Spartan 06 program. Based on this set of alkoxysilane structures, a first group of more than 100 descriptors was automatically generated via 'MS.QSAR' software (version 4.2) from Accelrys Materials Studio[8], and a number of others descriptors were manually added. Due to the lack of reliable information about the ED-precatalyst interaction, and considering the 'black-box' character of the QSAR approach, it was decided not to use any conformation dependent descriptor. Some representative descriptors[8] are reported in Table 4.1, where they are classified according to the following categories:

- *VAMP Descriptors.* The computation of descriptors according to VAMP electrostatics model was done by means of the semi-empirical molecular orbital code VAMP. Various Hamiltonians such as AM1, MNDO and PM3 can be employed, and properties can be obtained both from a single point energy calculation or geometry optimization.

- *Forcite Energetics.* This energetics model allows to calculate a variety of descriptors by means of the classical molecular mechanics code 'Forcite'. The descriptors can also be obtained from a single point energy calculation or a geometry optimization run.
- *'Fast' Descriptors.* This qualification refers to a set of efficient algorithms that enables the calculation of a variety of bidimensional molecular properties. They include topological, information-content, structural and thermodynamic descriptors.
- *Fragment-Counting Descriptors.* The fragment counting model determines various fragments within a structure using a pattern-matching algorithm which looks for matches based on topology, element type and hybridization without using bond information directly. The search can be customized (inclusion of hydrogens, allowance of atom overlapping, etc…).
- *Spatial Descriptors.* These include all the spatial properties of the molecules.
- *Periodic Descriptors.* The periodic model returns crystal-based properties as descriptors.
- *Atomic Descriptors.* These include all the atom-based properties.
- *JURS Descriptors.* These are descriptors based on the 'Solvent Accessible Surface' (SAS).

Table 4.1. Some of the alkoxysilane molecular descriptors used for the QSAR models.

VAMP Electrostatic	Forcite Energetics	"Fast"	Fragment Counting	Spatial	Periodic	Atomic	JURS
Total Energy	Total non-bond Energy	Wiener index	hydrocarbon fragments	Molecular Volume	Lattice Parameters	Atom count	SAS Area
Electronic Energy	Total valence Energy	Zagreb index	Counting for range of functional groups	Surface Area	Cell Volume	Total charge	Charge distribution on SAS
HOMO Energy		Kier & Hall molecular indices	Counting for a range of ring fragments	Molecular Density	Crystal Density	Element Counts	
LUMO Energy		# of rotatable bonds		Moments of inertia			
Dipole Moments		# of H-bond acceptors		Radius of gyration			
Quadrupole Moments		# of H-bond donors		Elipsoidal volume			
Octupole Moments		Molar refractivity		Molecular shadows indices			

4.2.5. QSAR model implementation and validation

The QSAR model implementation consisted in the identification of mathematical equations describing the response data Y (experimental data) as a function of explanatory variables X (descriptors). Models were built for a set of 65 EDs ('training set'), whereas 15 structures were selected to be used for validation ('test set'). The splitting of the full data set into said two sub-sets was made randomly. The starting point for deriving QSAR equations was the construction, for each experimental response (i.e. R_p, M_n, M_w, M_w/M_n, I.I., [*mmrrmm*]), of the so called 'study table' (Figure 4.4). This consists of a spreadsheet with ED structures across the rows, and molecular characteristics (response data Y, explanatory variables X) down the columns. Although in principle simple bivariate analysis could have been used (i.e., correlations with one descriptor only), no working one was identified and, in consequence, multivariate analysis had to be adopted. In mathematical sense, this meant that no single linear regressions (SLR of Table 4.2) could be established, but exclusively multiple linear regressions (MLR of Table 4.2).

Property of interest

Descriptors

ED	Y	D1	D2	D3	….	Dn
1	xx	xxx	xx	xx	…..	xx
2	xx	Xxxx	xx	xx	…….	xx
3	xx	Xxxx	xx	xx	…..	xx
4	xx	Xxxx	xx	xx	…..	xx
….	xx	Xxx	xx	xx	…..	…….
n	xx	xx	xx	xx	…..	xx

Figure 4.4. Representative starting worksheet for the implementation of the QSAR models.

Table 4.2. Possible linear regression for QSAR model implementations.

Regression type	Mathematical Expression
Single Linear (SLR)	$Y_i = b_0 + b_1 X_i$
Multiple linear (MLR)	$Y_i = b_0 + b_1 X_{1,i} + b_2 X_{2,i} + \ldots. + b_k X_{n,i}$

Just as an example, a functioning model for catalyst productivity is shown below:

Y = -0.042509828*X3 – 0.214584509*X6 – 0.027598381*X25 + 0.070036724*X35 + 0.014434016*X42 + 0.061500541*X45 + 0.201381616*X49 – 0.106766506*X54 – 0.345308332*X74 + 0.000422593*X84 + 0.014295276*X109 + 6.078951047

where *Y* is the log of R_p, and X3, X6, ...X109 are different descriptors in the pool. Similar models were found to correlate all the experimental data (R_p, M_w, M_n, PDI, I.I, [*mmrrmm*]) to sets of molecular descriptors.

The models established for the training set were subsequently validated on the test set. In simple words, the polymerization parameters predicted by the models were compared with the experimental values.

As an example, Figure 4.5 shows the correlation between QSAR-predicted activities and experimental ones for the 15 alkoxysilanes belonging in the test set. The clear diagonal correlation confirmed the goodness of model, which was at this point deemed ready to be used as a predictive tool.

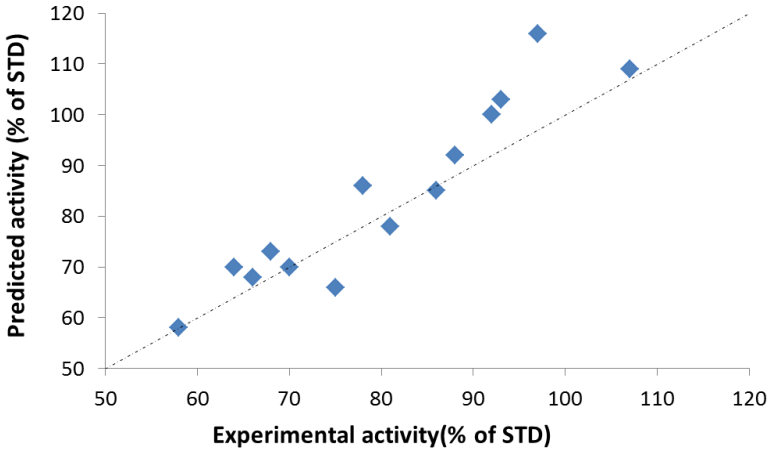

Figure 4.5. Correlation between QSAR-predicted productivities and experimental ones for the 15 alkoxysilanes belonging in the 'test set'.

4.3. The experimental database

The complete set of results collected throughout the HTE screening and assembled into the database is provided in Table 4.3. In particular, for each ED, R_p values in excess to triplicates were added whenever more than 3 cells were run for whatever reason (e.g., for poorly active systems, to accumulate the yields of more cells in order to reach the polymer amount necessary for all the characterizations). Measurements of M_n, M_w and [*mmrrmm*] were normally carried out in single, whereas I.I. values were measured in duplicate.

Table 4.3. The experimental ED screening database.

ED code	R_p (% of $R_{p\,av}$ STD)									M_n (KDa)	M_w (KDa)	M_w/M_n	I.I. (%)		[*mmrrmm*] (%)
	Cell								*Av.*				Value 1	Value 2	
	1	2	3	4	5	6	7	8							
1	68.6	81.5	70.0						73.4	50	184	3.7	96.0	94.9	0.39
2	76.4	77.3	74.8	70.1	76.7				75.1	37	186	5.0	94.9	95.1	0.50
3	56.6	64.8	64.0	64.6	56.1	55.7	72.6	60.2	61.8	32	188	5.9	96.9	95.6	0.43
4	58.4	71.8	59.1	61.1	53.0	65.4	72.5	61.9	62.9	34	176	5.2	97.9	97.9	0.49
5	55.5	56.4	61.7						57.9	35	160	4.5	92.1	92.4	0.70
6	59.1	70.5	77.5						69.0	42	183	4.4	95.0	95.0	0.50
7	94.8	90.8							92.8	38	171	4.5	94.9	93.7	0.47
8	45.2	44.7	42.2	56.5	44.2				46.5	35	203	5.8	96.7	96.2	0.35
9	72.0	60.1	67.1						66.4	50	245	4.9	98.8	97.3	0.51
10	49.0	70.0	56.9						58.6	26	122	4.7	94.8	93.6	0.81
11	49.4	60.1	48.3	51.5	65.0	50.1			54.1	39	203	5.1	95.1	96.1	0.62
12	94.3	92.2	79.9						88.8	39	172	4.4	96.6	96.3	0.42
13	82.4	83.4	73.3						79.7	44	154	3.5	94.9	95.5	0.41
14	49.0	45.6	50.4						48.3	48	220	4.6	98.0	97.5	0.59
15	64.6	73.7	90.4						76.2	34	133	3.9	96.7	96.4	0.59
16	44.5	49.0	47.5	46.2	38.9	42.5	41.4	52.4	45.3	28	128	4.5	89.8	88.2	1.00

17	60.6	62.7							61.7	31	161	5.2	94.8	94.4	0.63
18	76.7	71.4	71.9						73.3	53	264	5.0	97.4	97.7	0.37
19	61.0	65.8	57.7						61.5	44	224	5.1	96.5	96.1	0.64
20	58.7	57.9	48.5						55.0	39	234	6.0	93.6	96.4	0.45
21	74.7	75.8							75.3	28	132	4.7	94.8	93.0	0.60
22	67.4	81.9							74.7	53	202	3.8	97.7	96.9	0.37
23	112.3	99.8	90.8	110.5	104.1	95.9	102.5	106.6	102.8	47	269	5.7	95.8	95.7	0.31
24	64.4	70.8	70.6						68.6	37	184	4.9	95.6	96.6	0.73
25	68.8	65.8	65.6						66.7	42	212	5.0	97.2	98.0	0.30
26	74.1	69.6							71.8	34	170	5.0	96.6	96.9	0.31
27	73.7	64.8	76.8						71.8	31	133	4.3	92.8	93.6	0.54
28	67.3	75.5	64.2						69.0	27	171	6.4	93.3	95.5	0.56
29	54.7	73.6	84.7						71.0	29	170	5.8	93.2	95.4	0.34
30	56.6	34.5							45.6	29	186	6.4	96.2	96.4	0.40
31	72.5	70.0							71.3	29	151	5.2	93.4	93.0	0.77
32	64.2	72.2	85.3	79.7	68.8				74.0	47	171	3.6	92.7	94.6	0.95
33	77.4	79.6	83.6						80.2	34	192	5.6	98.1	98.0	0.37
34	104.7	73.3	94.9						90.9	36	176	4.9	95.5	94.7	0.42
35	80.4	106.1	107.1						97.9	44	218	4.9	98.0	97.8	0.32
36	97.6	95.3	93.8	92.8	89.0	91.0			93.2	48	232	4.8	96.1	96.1	0.34
37	94.7	81.8	80.1						85.5	35	225	6.4	96.0	95.1	0.30
38	92.2	99.6	85.3						92.4	40	166	4.1	93.9	94.5	0.39
39	83.6	76.9	77.3						79.3	29	149	5.2	95.4	93.6	0.52
40	77.0	77.5	81.8	66.1	95.5				79.6	53	258	4.9	94.8	96.8	0.35
41	92.6	103.6	102.3						99.5	34	194	5.7	95.5	94.9	0.30
42	118.1	122.5	125.3	105.1	100.5	127.0			116.4	41	197	4.8	98.1	97.4	0.68
43	121.2	101.5	124.8	122.2	100.6	86.0			109.4	31	175	5.6	97.0	97.5	0.43
44	103.6	107.5	120.0	112.6	102.3	126.9			112.2	44	248	5.7	96.0	96.0	0.38
45	74.7	78.9	87.3	57.0	85.8				76.7	34	153	4.4	95.6	97.2	0.99

46	57.4	68.4	75.0						66.9	28	155	5.4	95.6	95.7	0.46
47	49.3	47.9	66.5	56.3	54.4	53.1			54.6	34	149	4.3	96.0	98.4	0.64
48	52.5	61.1	67.7	71.9	63.4	66.9			63.9	31	169	5.4	95.5	94.8	0.55
49	68.2	52.2	55.3	64.1	60.7	73.6			62.4	34	179	5.2	96.0	94.8	0.42
50	74.1	74.2	78.3						75.5	32	212	6.7	95.5	95.9	0.51
51	62.2	60.4	68.3	72.0					65.7	22	104	4.6	98.0	96.5	0.74
52	62.0	64.9	63.7						63.5	26	125	4.8	94.7	95.5	0.79
53	82.8	88.5	70.7	81.9	84.9				81.8	35	172	4.9	96.9	97.5	0.32
54	60.7	59.7	53.3	60.5	54.8				57.8	33	160	4.9	96.8	94.9	0.54
55	67.0	77.4	98.0	82.8	92.9				83.6	45	192	4.2	94.0	96.4	0.65
56	89.7	81.7	76.6	73.3	82.0				80.7	35	194	5.5	96.0	95.7	0.90
57	58.2	65.5	58.6	72.5	61.9	67.0			64.0	36	181	5.1	95.5	95.1	0.52
58	20.2	23.6	20.4						21.4	38	200	5.2	94.6	94.9	0.70
59	79.3	79.9	65.6	78.3					75.8	30	147	4.9	96.9	97.3	0.52
60	83.2	91.9	81.0	74.3					82.6	41	187	4.7	97.5	96.7	0.64
61	77.4	82.6	75.6	69.5	74.4				75.9	36	176	4.9	95.8	93.2	0.39
62	79.5	75.5							77.5	37	171	4.6	96.9	97.4	0.21
63	63.4	62.4	71.3						65.7	27	147	5.5	91.7	94.5	0.81
64	61.6	56.4							59.0	25	105	4.2	97.5	97.6	0.73
65	65.5	80.6	67.8	69.7	73.1	66.0	68.4	81.3	71.5	36	167	4.6	94.2	96.0	0.54
66	53.5	62.3	69.7	49.3					58.7	34	160	4.6	95.8	94.5	0.58
67	59.2	67.2	57.8	60.9	53.8	59.8			59.8	28	145	5.2	95.5	94.5	0.57
68	54.5	58.2	76.6						63.1	38	175	4.6	95.8	96.6	0.49
69	73.7	80.9							77.3	31	133	4.3	95.2	95.4	0.43
70	73.8	59.8	62.6	71.8	51.8	67.3			64.5	37	166	4.5	95.7	95.5	0.80
71	67.0	52.1	62.8	64.4	56.9	62.4			60.9	31	161	5.2	95.7	96.0	0.77
72	58.9	56.8	60.6	60.6	56.9	64.5			59.7	35	176	5.1	95.4	94.6	1.15
73	34.9	31.7	34.7						33.8	21	120	5.7	95.8	95.7	0.48
74	13.9	16.2	16.6						15.6	26	113	4.3	95.5	94.6	0.40
75	83.4	77.0	88.2						82.9	33	155	4.7	94.5	94.2	0.38
76	73.9	85.0	91.2						83.4	33	161	4.8	96.0	95.3	0.50

77	53.9	52.1	47.7						51.3	20	94	4.7	97.8	96.5	0.81
78	86.9	59.4	80.1						75.4	20	183	9.0	90.2	92.1	0.36
79	49.2	47.6	47.9						48.2	18	131	7.0	89.0	91.3	0.74
80	64.7	75.2							69.9	26	174	6.6	96.3	95.1	0.29

4.4. Predictive use of the QSAR models

The validated QSAR model was then used to predict the performance of a set of new alkoxysilane EDs for the modification of the selected HY-ZNC for iPP (Figure 4.6).

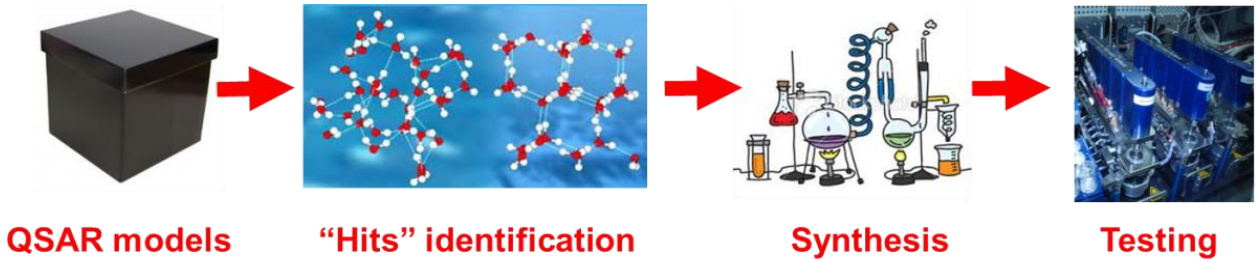

Figure 4.6. Predictive use of the validated QSAR model.

The set of novel alkoxysilanes subjected to a *virtual screening* based on the QSAR model consisted of ~250 molecules, structurally similar to those of the training set (i.e. dimethoxy, diethoxy, trimethoxy, triethoxy, and with a maximum of six C atoms in the alkyl fragments). For each experimental property (R_p, M_n, M_w, M_w/M_n, I.I., [*mmrrmm*]), a large number of models (from 20 to 50) was employed to predict the output value associated to each alkoxysilane. As an example, Figure 4.6 shows the virtual screening of 41 dimethoxysilanes wrt to the M_n value anticipated for the PP samples obtained. The overlapping of the models confirms their coherency.

The graphical outputs of the performance predictions were inspected, and a set of 16 alkoxysilanes was selected for further investigation. The selection was made according to criteria including, inter alia, a high productivity and stereoselectivity. Aspects such as commercial availability and ease of synthesis (both in terms of cost and time), were not taken into account in this phase.

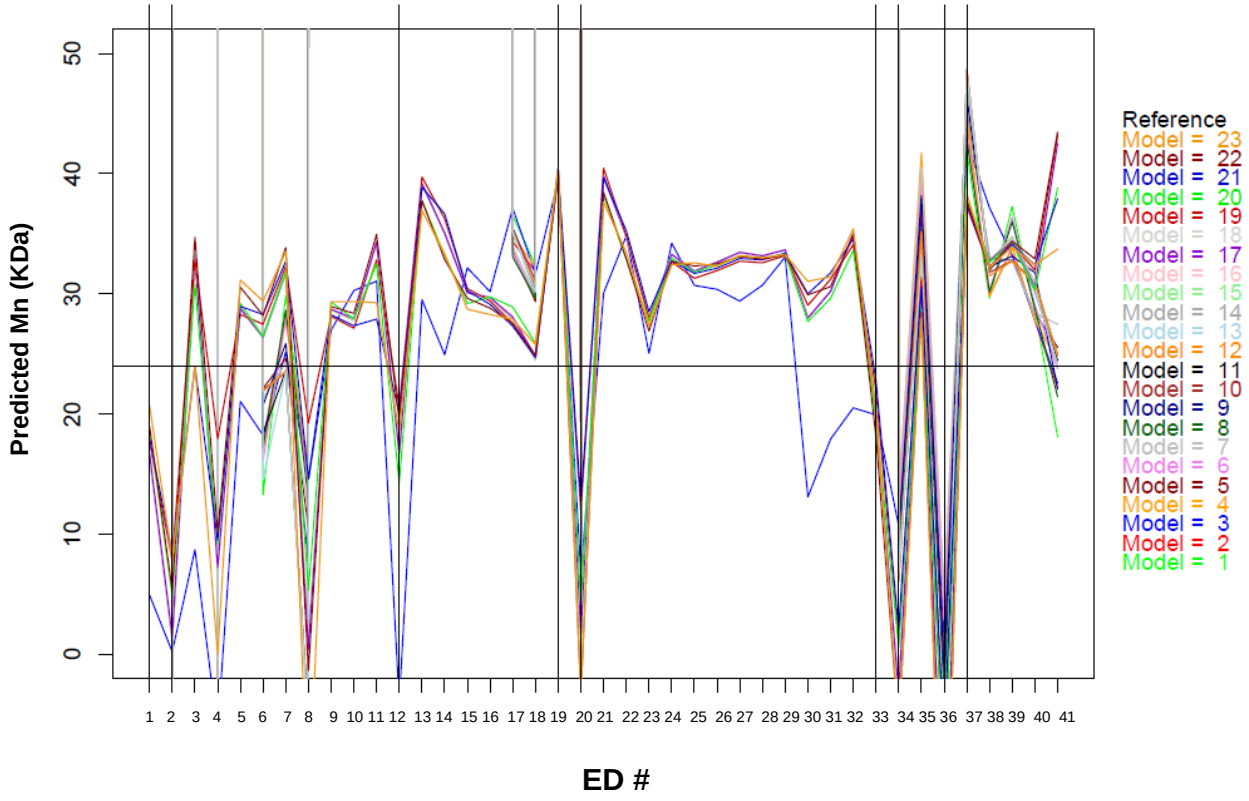

Figure 4.6. In silico QSAR screening of 41 dimethoxysilane EDs focusing on the predicted M_n value. Vertical lines mark the alkoxysilanes selected for experimental evaluation.

The 16 molecules were synthesized by Dr. J. B. Sainani, at the Sabic Research Center of Baroda (India), and tested at LSP in the PPR48. The experimental results obtained in propene polymerization are compared with the predicted ones in Table 4.4, whereas a visual correlation for R_p is shown in Figure 4.7.

Table 4.4. Experimental and QSAR-predicted results of propene polymerization in the presence of $MgCl_2/TiCl_4$/DBP – $AlEt_3$/ED systems, with 16 novel alkoxysilanes selected as the ED from the virtual screening.

	R_p (% of R_p STD)		M_w (KDa)		M_w/M_n		I.I. (%)	
ED #	Exp.	Pred.	Exp.	Pred.	Exp.	Pred.	Exp.	Pred.
1	83	92	161	120	4.8	4.5	95.7	95.1
2	83	85	208	107	5.3	3.9	88.4	92.1
3	77	82	220	104	4.0	4.0	94.0	93.8
4	89	108	183	142	4.6	5.3	96.8	95.2
5	91	116	226	155	5.3	4.8	96.2	94.1
6	67	69	137	82	6.0	8.6	95.0	91.0
7	103	113	198	128	5.6	2.7	97.1	94.7
8	87	97	260	110	8.7	3.8	97.6	82.0
9	62	73	191	112	4.6	8.5	88.5	90.3
10	68	93	192	162	4.0	4.8	95.5	92.2
11	62	73	176	140	4.7	6.8	94.5	94.8
12	65	74	166	98	4.8	3.6	94.4	94.7
13	56	59	229	150	6.2	12.3	96.4	97.8
14	68	71	160	94	4.1	3.6	94.5	97.1
15	75	91	191	119	5.4	4.4	97.0	96.6
16	71	72	229	130	5.6	8.5	95.9	98.1

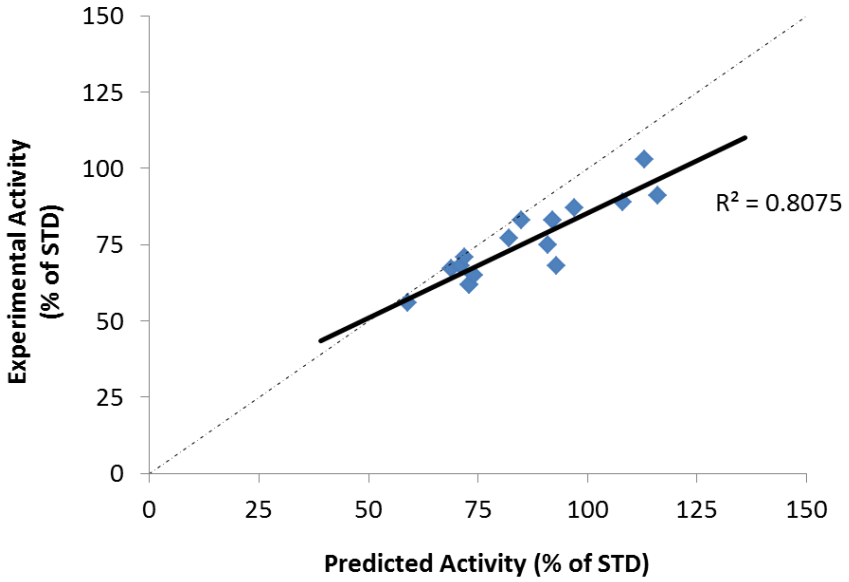

Figure 4.7. Correlation between QSAR-predicted productivities and experimental ones for the 16 novel alkoxysilane EDs (data from Table 4.4).

At least in the case of properties measurable with high accuracy in the HTE workflow (Chapter 2), such as catalyst productivity, the agreement between experimental and predicted data is notably good, as the diagonal correlation of Figure 4.7 demonstrates. Unfortunately, the model has not yet been extended to the prediction of chain microstructure (i.e., to the value of [*mmrrmm*]), which is the most accurate and one of the most significant parameters provided by the HTE screening.

On the other hand, some outliers can be spotted for properties affected by a larger experimental error (such as M_w and M_w/M_n). Moreover, we have already commented on the inadequacy of the experimental evaluation of I.I. for the catalyst of interest. An action of refinement on the HTE tools and methods is already in progress.

All in all, we believe that the outcome of this part of the work is very significant. In particular, to the best of our knowledge this is the first time that the productivity of HY-ZNCs for iPP can be *predicted* successfully based on a QSAR model. As soon as the model is fully implemented, its application will open the door to the *design* of catalysts and polymers with tunable properties.

References

(1) (a) Cecchin, G.; Morini G; Piemontesi, F. In *Encyclopedia of Chemical Technology*; John Wiley and Sons: New York (NY), 2006; Vol. 26, pp. 502-554. (b) *Polypropylene Handbook: Polymerization, Characterization, Properties, Applications*; Moore, E.P. Jr., Ed.; Hanser Publishers: Munich, 1996.

(2) A dedicated journal to QSAR is: http://onlinelibrary.wiley.com/journal/10.1002/(ISSN)1611-0218/issues

(3) Profeta, S. J. In *Encyclopedia of Chemical Technology*; John Wiley and Sons, 2005; Vol. 16, pp.724-768.

(4) D'Agnillo, L.; Soares, J. B. P.; Penlidis, A. *J. Polym. Sci. B: Polym. Phys.* **2002**, *40*, 905-921.

(5) http://www.polymerchar.com/cef

(6) Busico, V.; Cipullo, R. *Progr. Polym. Sci.* **2001**, *26*, 443-533.

(7) The contribution of Prof. P. H. M. Budzelaar is gratefully acknowledged.

(8) http://accelrys.com/products/datasheets/qsar-plus.pdf

Chapter 5. Concluding Remarks

This thesis focused on so-called High-Yield Ziegler-Natta Catalysts (HY-ZNCs) for the industrial production of isotactic polypropylene (iPP), the second largest volume synthetic polymer (after polyethylene), with a global installed capacity close to 60 MT/y. In extreme synthesis, HY-ZNCs are heterogeneous systems featuring a nano-crystalline $MgCl_2$ matrix, on which chiral Ti-based active species are co-adsorbed with organic electron donors which tailor the local environment of the transition metal, enforcing its regio- and stereoselectivity in propene insertion, similarly to the ancillary ligand of a molecular catalyst but according to far less understood mechanisms. In Chapter 1 we reviewed the literature on the subject, and could only conclude that, while several classes of electron donors are known able to do the job with remarkable efficiency, their identification was serendipitous, and until now no one could rightfully claim the ability to *design* a novel HY-ZNC with *pre-determined* behavior using any kind of white-box or black-box model.

Without over-emphasizing the results achieved in the present work, in Chapter 4 we were certainly pleased to report the first successful attempt to implement a QSAR model of HY-ZNC surface modification with predictive ability. Although admittedly of black-box character, and limited to one of the several industrial catalyst platforms, of composition $MgCl_2$/$TiCl_4$/diisobutyl-*ortho*-phthalate – $AlEt_3$/$R'_xR''_ySi(OR)_{4-x-y}$, our model was implemented thanks to the innovative application of state-of-the-art High Throughput Experimentation (HTE) tools and methods for the fast and thorough exploration of the complex variable hyperspace, as was explained in detail in Chapter 2. This represents the first case of HY-ZNC surface fine-tuning by means of alkoxysilane electron donors with an anticipated modifying action.

At the same time, a more traditional use of HTE for the thorough investigation of the adsorption/desorption processes that occur on the catalytic surfaces under conditions representative of real use, integrated with state-of-the-art periodic DFT-D studies, led us to formulate, if not yet a working white-box model of these systems, convincing and reasonably well-defined hypotheses on the structure of the active species and their non-bonded interactions with various adsorbates, including organic electron donors, Al-alkyls and –possibly– reaction products thereof. This part was covered in Chapter 3.

A most important question is why, at more than 60 years from the initial discovery of ZN catalysis, and after 40 years of application of HY-ZNCs for iPP, further investing in research would still be worth the effort. In our opinion, the main driver for the work carried out in the present project, and for its continuation, is the payback that a finer and (more) rational tuning of the catalytic surfaces can ensure. The aim is to combine well-known parameters, such as e.g. stereosequence and molecular mass distributions, in still unprecedented ways, so as to produce with high activity polymers with novel and tailored features for specific applications. In this respect, the key-word is 'control'; in other words, it's probably not necessary to step outside the standard ranges of individual polymer properties to achieve useful and original *combinations* thereof. On the other hand, pushing some properties (e.g. polydispersity, degree of chain stereoregularity etc) to the limits or even beyond is also an objective of potential value.

Working on a single catalyst platform, i.e. starting with the same precatalyst and elaborating on a given ED class (which was the case of the present work), obviously represents only one comparatively narrow case with respect to what can be achieved by means of fine-tuning. As a matter of fact, the HTE approach as implemented in this thesis can be iterated stepwise on different precatalysts (or ID classes), ED classes, and mixtures thereof, thus tremendously broadening the scope, and with it the catalyst and polymer properties envelop. There is nothing conceptually new in the proposed approach (after all, industry has always been doing that), but with the introduction of HTE, and HTC already on the way, the time frame for the identification of leads can be realistically reduced from decades to months.

This is our main take-away message in concluding this dissertation. Whether something closer to the definition of 'breakthrough' can also be expected, such as e.g. the controlled exploitation of surface dynamics for stereoblock homopolymerizations and block copolymerizations, remains to be seen.

Acknowledgments

I like to sincerely thank all the people who made it possible for me to achieve, if only in part, the ambitious targets of my project.

First of all, I wish to express my sincere and deep gratitude to my research advisor, Prof. Vincenzo Busico, not only for giving me the opportunity to carry out this PhD project in his group, but also for constantly helping me and stimulating my scientific growth, always conjugating competence with passion.

I am also grateful to Prof. Roberta Cipullo, for the competent NMR experiments and her continuous support, and Prof. Peter Budzelaar for so many valuable discussions and advise.

Thanks to Dr. Maddalena D'Amore, for letting me 'steal' precious computational results (even when still unpublished), adding a lot to the thesis.

Thanks also to all other LSP members, namely: Raffaele Bernardo, Emanuele Breuza, Pasquale Cacace, Angela D'Amora, Christian Ehm, Alessio Mingione, Alessia and Natascia Napolitano, Antonello Pastore, Enrica Villano and Yue Yu; they certainly helped with great technical and scientific assistance, but above all it was their personal support that I acknowledge and am grateful for.

I also like to extend my grateful thanks to Sabic, for the financial and 'logistic' support to this work, and in particular to Nic. Friederichs (our key reference in Geleen), and many more Sabic scientists and technologists (specially Klaas Remerie, J. B. Sainani, Aurora Batinas, Tom Schoffelen). Last but not least, thank you Betty Coussens, collaborating from DSM Resolve. With all of them I could enjoy, along with their great professional skills, the warm hospitality when visiting them in Geelen.

An important acknowledgement concerns the Freeslate team, for the constant and professional assistance on the High Throughput platforms. My special thanks are due in particular to Rob Rosen, who always energized me (and the rest of LSP) when helping with tools and protocols from his unreachable level of competence, and made me enjoy much more Naples and nearby places when enjoying together some time away from work.

A big thank-you to all of my friends who supported me throughout the difficulties encountered along the way.

I am more than grateful to my girlfriend Sabrina, for the (critical) help and the precious assistance and, above all, for choosing me as her daily co-traveller in the life journey.

Thanks to my sister Monica, my grand-mother “la nonna”, and my brother-in-law Salvatore: they demonstrated how the concept of ‘family’ truly applies to all those situations where there are people linked by deep and reciprocal love.

Finally, my deepest gratitude goes to my parents, for making me who I am (despite my imperfections and limitations); I am certain that their love and teachings will always accompany and guide me through the rest of my life.